

SRESA's International Journal of

LIFE CYCLE RELIABILITY AND SAFETY ENGINEERING

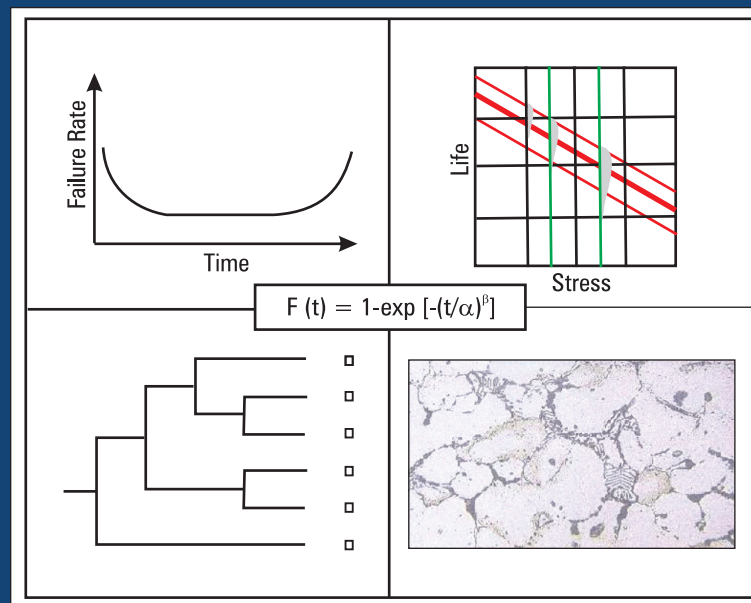
Vol.3

Issue No.1

Jan–March 2014

ISSN – 2250 0820

Special Issue :
On
“ Structural Reliability ”



Guest-Editors
Prof. Helmut WENZEL
Prof. G. R. Reddy

Chief-Editors
P.V. Varde
A.K. Verma
Michael G. Pecht



Society for Reliability and Safety

website : <http://www.sresa.org.in>

SRESA Journal of Life Cycle Reliability and Safety Engineering

Extensive work is being performed world over on assessment of Reliability and Safety for engineering systems in support of decisions. The increasing number of risk-based / risk-informed applications being developed world over is a testimony to the growth of this field. Here, along with probabilistic methods, deterministic methods including Physics-of-Failure based approach is playing an important role. The International Journal of Life Cycle Reliability and Safety Engineering provides a unique medium for researchers and academicians to contribute articles based on their R&D work, applied work and review work, in the area of Reliability, Safety and related fields. Articles based on technology development will also be published as Technical Notes. Review articles on Books published in the subject area of the journal will also form part of the publication.

Society for Reliability and Safety has been actively working for developing means and methods for improving system reliability. Publications of quarterly News Letters and this journal are some of the areas the society is vigorously pursuing for societal benefits. Manuscript in the subject areas can be communicated to the Chief Editors. Manuscript will be reviewed by the experts in the respective area of the work and comments will be communicated to the corresponding author. The reviewed final manuscript will be published and the author will be communicated the publication details. Instruction for preparing the manuscript has been given on inside page of the end cover page of each issue. The rights of publication rest with the Chief-Editors.

SCOPE OF JOURNAL

System Reliability analysis	Structural Reliability	Risk-based applications
Statistical tools and methods	Remaining life prediction	Technical specification optimization
Probabilistic Safety Assessment	Reliability based design	Risk-informed approach
Quantitative methods	Physics-of-Failure methods	Risk-based ISI
Human factor modeling	Probabilistic Fracture Mechanics	Risk-based maintenance
Common Cause Failure analysis	Passive system reliability	Risk-monitor
Life testing methods	Precursor event analysis	Prognostics & health management
Software reliability	Bayesian modeling	Severe accident management
Uncertainty modeling	Artificial intelligence in risk and reliability modeling	Risk-based Operator support systems
Dynamic reliability models	Design of Experiments	Role of risk-based approach in Regulatory reviews
Sensitivity analysis	Fuzzy approach in risk analysis	Advanced electronic systems reliability modeling
Decision support systems	Cognitive framework	Risk-informed asset management

SRESA AND ITS OBJECTIVES

- a) To promote and develop the science of reliability and safety.
- b) To encourage research in the area of reliability and safety engineering technology & allied fields.
- c) To hold meetings for presentation and discussion of scientific and technical issues related to safety and reliability.
- d) To evolve a unified standard code of practice in safety and reliability engineering for assurance of quality based professional engineering services.
- e) To publish journals, books, reports and other information, alone or in collaboration with other organizations, and to disseminate information, knowledge and practice of ensuring quality services in the field of Reliability and Safety.
- f) To organize reliability and safety engineering courses and / or services for any kind of energy systems like nuclear and thermal power plants, research reactors, other nuclear and radiation facilities, conventional process and chemical industries.
- g) To co-operate with government agencies, educational institutions and research organisations

SRESA's International Journal of

LIFE CYCLE RELIABILITY AND SAFETY ENGINEERING

Vol.3

Issue No.1

Jan–March 2014

ISSN – 2250 0820

Special Issue :
On
“ **Structural Reliability** ”

Guest-Editors

Prof. Helmut WENZEL
Prof. G. R. Reddy

Chief-Editors

P.V. Varde
A.K. Verma
Michael G. Pecht



SOCIETY FOR RELIABILITY AND SAFETY

Copyright 2014 SRESA. All rights reserved

Photocopying

Single photocopies of single article may be made for personnel use as allowed by national copyright laws. Permission of the publisher and payment of fee is required for all other photocopying, including multiple or systematic photocopying for advertising or promotional purpose, resale, and all forms of document delivery.

Derivative Works

Subscribers may reproduce table of contents or prepare list of articles including abstracts for internal circulation within their institutions. Permission of publishers is required for required for resale or distribution outside the institution.

Electronic Storage

Except as mentioned above, no part of this publication may be reproduced, stored in a retrieval system or transmitted in form or by any means electronic, mechanical, photocopying, recording or otherwise without prior permission of the publisher.

Notice

No responsibility is assumed by the publisher for any injury and /or damage, to persons or property as a matter of products liability, negligence or otherwise, or from any use or operation of any methods, products, instructions or ideas contained in the material herein.

Although all advertising material is expected to ethical (medical) standards, inclusion in this publication does not constitute a guarantee or endorsement of the quality or value of such product or of the claim made of it by its manufacturer.

Typeset & Printed

EBENEZER PRINTING HOUSE

Unit No. 5 & 11, 2nd Floor, Hind Services Industries,
Veer Savarkar Marg,
Dadar (west), Mumbai -28
Tel.: 2446 2632/ 3872
E-mail: outwork@gmail.com

CHIEF-EDITORS

P.V. Varde,

Professor, Homi Bhabha National Institute &
Head, SE&MTD Section, RRSD
Bhabha Atomic Research Centre, Mumbai 400 085
Email: Varde@barc.gov.in

A.K. Verma

Professor, Department of Electrical Engineering
Indian Institute of Technology, Bombay, Powai, Mumbai 400 076
Email: akvmanas@gmail.com

Michael G. Pecht

Director, CALCE Electronic Products and Systems
George Dieter Chair Professor of Mechanical Engineering
Professor of Applied Mathematics (Prognostics for Electronics)
University of Maryland, College Park, Maryland 20742, USA
(Email: pecht@calce.umd.edu)

Advisory Board

Prof. M. Modarres, University of Maryland, USA	Prof. V.N.A. Naikan, IIT, Kharagpur
Prof A. Srividya, IIT, Bombay, Mumbai	Prof. B.K. Dutta, Homi Bhabha National Institute, Mumbai
Prof. Achintya Halder, University of Arizona, USA	Prof. J. Knezevic, MIRCE Academy, UK
Prof. Hoang Pham, Rutgers University, USA	Dr. S.K. Gupta, Ex-AERB, Mumbai
Prof. Min Xie, University of Hongkong, Hongkong	Prof. P.S.V. Natraj, IIT Bombay, Mumbai
Prof. P.K. Kapur, University of Delhi, Delhi	Prof. Uday Kumar, Lulea University, Sweden
Prof. P.K. Kalra, IIT Jaipur	Prof. G. R. Reddy, HBNI, Mumbai
Prof. Manohar, IISc Bangalore	Prof. Kannan Iyer, IIT, Bombay
Prof. Carol Smidts, Ohio State University, USA	Prof. C. Putchu, California State University, Fullerton, USA
Prof. A. Dasgupta, University of Maryland, USA.	Prof. G. Chattopadhyay CQ University, Australia
Prof. Joseph Mathew, Australia	Prof. D.N.P. Murthy, Australia
Prof. D. Roy, IISc, Bangalore	Prof. S. Osaki Japan

Editorial Board

Dr. V.V.S Sanyasi Rao, BARC, Mumbai	Dr. Gopika Vinod, HBNI, Mumbai
Dr. N.K. Goyal, IIT Kharagpur	Dr. Senthil Kumar, SRI, Kalpakkam
Dr. A.K. Nayak, HBNI, Mumbai	Dr. Jorge Baron, Argentina
Dr. Diganta Das, University of Maryland, USA	Dr. Ompal Singh, IIT Kanpur, India
Dr. D. Damodaran, Center For Reliability, Chennai, India	Dr. Manoj Kumar, BARC, Mumbai
Dr. K. Durga Rao, PSI, Sweden	Dr. Alok Mishra, Westinghouse, India
Dr. Anita Topkar, BARC, Mumbai	Dr. D.Y. Lee, KAERI, South Korea
Dr. Oliver Straeter, Germany	Dr. Hur Seop, KAERI, South Korea
Dr. J.Y. Kim, KAERI, South Korea	Prof. P.S.V. Natraj, IIT Bombay, Mumbai
Prof. S.V. Sabnis, IIT Bombay	Dr. Tarapada Pyne, JSW- Ispat, Mumbai

Managing Editors

N.S. Joshi, BARC, Mumbai
Dr. Gopika Vinod, BARC, Mumbai
D. Mathur, BARC, Mumbai
Dr. Manoj Kumar, BARC, Mumbai

Editorial

Technologies enhancing industrial safety have been developed in the large European collaborative research project IRIS. During 4 years more than 300 researchers elaborated solutions ready for application in various industries. Some of the results are reported here, more can be found in the given references. The contributions cover both Life Cycle Reliability and safety engineering aspects. The works and development have reached a high technology readiness level already and found their way into practice.

The first paper concentrates on Life Cycle cost optimization of wind turbine structures with a focus on offshore applications. This important industrial sector requires efficient applications for operation of their wind turbine structures. Based on data from permanent monitoring systems, operating online and real-time, are used for Life Cycle Management of the assets. It is demonstrated that a significant expected operational benefit over the Life Cycle of an offshore structure can be achieved by the approach developed. The conceptual integration of structural monitoring techniques, structural reliability theory and reliability based inspection and repair planning is addressed.

The second paper reports about a massive shear wall testing campaign performed for the nuclear industry. During the IRIS project large scale shear wall testing of unprecedented size has been undertaken in the Joint Research Center (JRC) of the European Commission in Ispira, Italy. Consequences of Earthquakes have proven the need to study the shear mechanism of low rise reinforced concrete shear walls thoroughly. Because of the complexity of reinforced concrete behavior, generalized problem solutions are not readily available. Therefore an extensive experimental testing campaign has been performed to investigate these concrete elements. The contribution deals with cyclic shear testing of thick (0.40m wall thickness) reinforced concrete walls as typically found in structures of the nuclear industry. Analysis of the data obtained resulted in the determination of hysteresis characteristics, non-linear effects for shear, ultimate capacity and damping of the tested 5 specimens. Various strength assessments and comparison to test results is provided.

The third paper concentrates on the ageing behavior of structural components for integrated lifetime assessment and asset management. Managing assets is about making decisions. For the performance of Life Cycle costs studies (LLC) and in some cases Life Cycle benefit / cost analysis it becomes important to have standardized mathematical formulations of structural degradation. The presented paper provides the result of a standard activity called CEN Workshop 63. A standard document titled "Condition determination for integrated lifetime assessment of constructed facilities and components" has been accepted by the European Standardization Body (CEN). Subsequently this new standard has been accepted by standardization organization's in various countries on global level, like the USA (NIST), Canada, Russia, Japan, Germany (DIN), United Kingdom (BS) and a major number of other countries. This "Ageing Model" developed on basis of real data over 30 years of highway bridge inspection and assessment provides a unique breakthrough in this domain.

The fourth paper reports on the application of the IRIS risk paradigm in the assessment of a post tensioned containment structure. Structural elements like the post tensioning of a containment structure of a nuclear power plant are currently reviewed on 30 year old partly destructive approaches. A reliability based control approach has been developed and a proof of concept is described in the paper. The feasibility of applying the IRIS risk paradigm to establish a consistent approach for reliability based control, to be used in Life Cycle engineering aspects also, is shown at a post tension containment structure of a real plant.

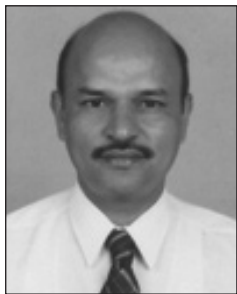
Typically in Probabilistic Safety Assessment (PSA) the time dependent frequency of an accident is not considered. Where as in actual practice failure probabilities of the systems changes with time due to random loading such as an earthquake and aging phenomenon. Time dependent PSA of nuclear power plants under seismic events is discussed in the fifth paper.

Depending on the nature of piping material, geometry and operating conditions, piping system is susceptible to Erosion-corrosion (EC) to different degrees. Reliability concept to determine the reliability of an elbow against EC at different times is explained in sixth paper. The usefulness of the concept developed in estimation of reliability of elbows against EC at different times is also demonstrated through example problems

Prof. Helmut WENZEL
Prof. G. R. Reddy



Prof. Wenzel has worked for large infrastructure projects in Europe and overseas for the first 15 years of his career. Driven by the demand for new technologies and practical applications in the construction industry he recognised the value of research and development and devoted his attention to national and international research projects. Since 1995 (in the BRITE-EURAM program of the European Commission) he took over the responsibility of coordinating large collaborative research projects (HARIS, CasCo, IMAC, OASYS, MOBILE, SAFEPIPES, IRIS, NERA) and organised dedicated international networks (SAMCO and I-SAMCO). Research and development has created a number of very successful applications grouped around the global brand BRIMOS (Bridge Monitoring System). This development brought him international recognition in the structural health monitoring community (2 books). The main objectives of recent projects concentrate on life cycle engineering issues which are supported by the demand of safe life extension of our European critical infrastructures. Dr. Wenzel is the author of 3 internationally well recognised books and has contributed with keynotes and papers to numerous initiatives of the scientific society. In his capacity as internationally well recognised expert he is performing evaluations of research programs, contributes to strategic research agenda and road maps and is engaged as technical and scientific advisor to major agencies and projects. Long standing international collaboration has been established with leading Universities and Research Institutes worldwide (i.e. University of Tokyo, Chinese Academy of Science, Stanford University, JRC, NCREE, NCSA, Drexel University, Rutgers University, BARC Mumbai, University of Ottawa, ETHZ, AUTH, Sheffield, KU Leuven, Porto,..)



Prof. G. R. Reddy, B.E, M.Tech, PhD(Japan) is heading Structural and Seismic Engineering section of Reactor Safety Division of Bhabha Atomic Research Centre and also serving as Professor, Homi Bhabha National Institute. In addition, he is a recognized guide for PhDs in Mumbai University and Christ University, Bangalore. He is holding honorary post of president of Association of Structural Rehabilitation (ASTR). Since 1984 he is working in the area of Structural Dynamics & Earthquake Engineering and analyzed, designed nuclear facility structures, equipment and piping systems. Made significant contribution in design of 500 MWe PHWRs and involved in the design of AHWR and structures for solar thermal power plants. Made contribution in the design of 30 M DSN antenna for Chandrayan project and recently completed the design of large size gamma ray telescope. Worked in the research areas like modeling techniques of complex structures, structure-equipment interaction due to earthquakes, stochastic methods of analysis, dynamic substructure techniques. Mastered seismic response control methods and involved in developing friction dampers, elasto-plastic dampers, Lead extrusion dampers, isolators and Tuned liquid dampers. Developed simple seismic design procedures for equipment and piping supported on hysteretic supports. As a part of developing more realistic design procedures, performed large number of experiments on beam-column joints, frames and piping systems till collapse. Simple method to evaluate the performance levels of structures and piping systems is developed. For the purpose of life extension of the existing facilities, evolved methods for performing seismic retrofitting of structures using dampers, FRP, steel jacketing. In addition to research in the area of earthquake engineering and structural dynamics, presently involved in research areas of structures subjected to fire and impact loads. He is also working as expert member to support the disaster management activities of Municipal Corporation of Greater Mumbai. He has guided several students for M.Tech and PhD. He has more than 360 publications to his credit.

Optimal Design of Monitoring Systems for Life Cycle Benefits: Application to an Offshore Wind Turbine Support Structure

Sebastian Thöns¹, Michael Havbro Faber¹, Werner Rucker²

¹DTU Civil Engineering, Technical University of Denmark, Kgs. Lyngby, Denmark

²Division VII.2 Buildings and Structures, BAM Federal Institute for Materials Research and Testing, Berlin, Germany

E-mail: sebt@byg.dtu.dk

Abstract

This paper contains recent research results in the field of Life Cycle cost optimized monitoring systems for wind turbines structures. The expected life costs for wind turbine structures are quantified that comprising the expected operation costs due to inspection, repair and monitoring actions and the structural risks. Approaches and findings on the characteristics of monitoring techniques and data within the framework of structural reliability are introduced and applied. The approaches are then utilized for a pre-posterior Bayesian decision analysis to determine the decision set consisting of the design parameters of a monitoring system namely the component set to monitor and the quality of the monitoring system. In this way the identification of a optimal design parameters in regard to the expected Life Cycle costs is facilitated. In a case study, an optimal monitoring system for a Multibrid M5000 offshore wind turbine prototype support structure is derived.

The essential finding of the research is that the efficiency of operation of wind turbine structures can be substantially supported by Life Cycle optimized monitoring systems. It is found that a significant expected operational benefit over the Life Cycle of a structure can be achieved by the developed approach, namely, the conceptual integration of structural monitoring techniques, structural reliability theory and reliability based inspection and repair planning.

Keywords: Off shore structures, monitoring, cost optimization, Life Cycle

1. Introduction

As more offshore wind parks are commissioned, the focus is shifting from a planning and construction focus to an operation, maintenance and investment

return focus. In the latter case, the efficient operation of wind parks is highly important.

In this study, a framework for the quantification of the expected Life Cycle Costs for wind turbine

structures is developed to facilitate and to support optimal decisions. The framework builds upon the approaches of structural reliability theory and Bayesian decision theory. The calculation of the Life Cycle Costs is performed utilizing an event tree which facilitates to assess the probabilities of events associated with consequences applying structural reliability theory. For the determination of the inspection and repair events, reliability based inspection and repair planning is utilized. Furthermore, the characteristics of monitoring data in a structural

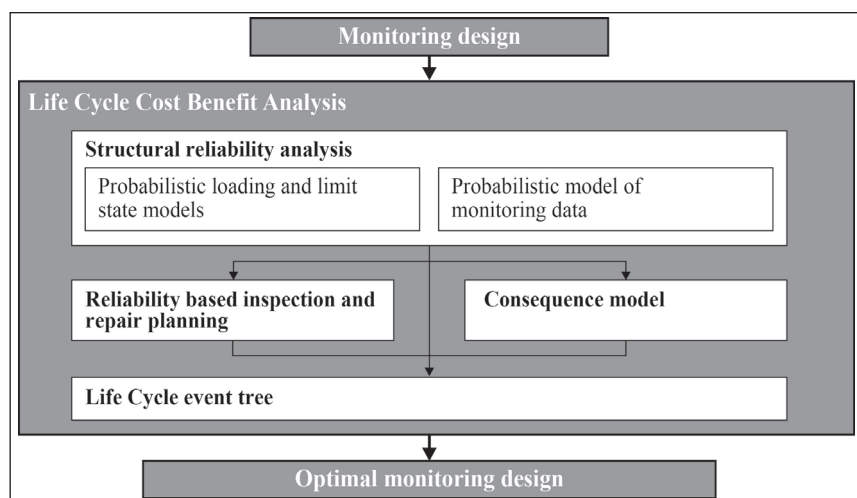


Figure 1: Framework for the quantification of Life Cycle Costs and its utilization for monitoring system design

reliability analysis are outlined and approaches for modeling monitoring data are introduced.

The framework given in Figure 1 illustrates how optimal decisions may be identified for the design and utilization of a monitoring system in the perspective of the Life Cycle of the structure. The decision analysis, namely, the analysis supporting the design of a monitoring system for a structure to be commissioned constitutes a Bayesian pre-posterior decision analysis. A pre-posterior analysis facilitates a decision analysis on the basis of not yet known data, i.e. not yet known monitoring data, which are modeled based on the developed monitoring system and data models. In this way the Life Cycle Costs associated with the utilization of a monitoring system are calculated.

In order to derive a Life Cycle optimal monitoring system, the expected Life Cycle Costs for various monitoring systems are calculated. On this basis the optimal monitoring systems are identified. A comprehensive description of the approaches and a case study is contained in the following sections.

Section 2 contains an approach for monitoring based condition assessment based on an uncertainty modeling of monitoring systems which is developed focusing on the measurement uncertainties. Furthermore, the characteristics of monitoring data in a structural reliability analysis are elaborated with focus on the model uncertainties.

In Section 3 the framework for a Life Cycle Cost-Benefit Analysis including the costs for monitoring is developed. Consecutively, the benefit associated with monitoring is defined. Within the framework of the Bayesian decision theory, a pre-posterior decision analysis is formulated to derive optimal design parameters for the design of a monitoring system.

Section 4 contains a case study of a Multibrid M5000 wind turbine support structure. Here, the results of a structural reliability analysis are summarized and the assumptions in regard to the reliability based inspection and repair planning, the consequences and the set of decision alternatives are described. The monitoring benefit with regard to the operation costs, structural risks and total Life Cycle Costs is quantified and the optimal decisions for different decision situations are derived. The article closes with the summary and conclusions in Section 5.

2. Monitoring Based Structural Condition Assessment

The utilization of monitoring data for the structural condition assessment (see e.g. [8] and [11])

facilitates reliability updating on the basis of temporal continuous information. This complex problem has recently gained significant interest in various fields of engineering (see e.g. [3], [14] and [15]). Monitoring data constitute time continuous measurement data. However, the modeling of all relevant uncertainties in a structural reliability analysis (as e.g. required by [9]) for what concerns monitoring data is mostly performed generically rather than on a systematic basis.

The thesis by the author [15] contributes to the modeling of monitoring uncertainty by suggesting an approach for the determination of the measurement uncertainty utilizing all available information which comprises information about the physical measurement process and observations of the measurement process (Section 2.1). Furthermore, with generic fatigue reliability analyses the characteristics of and the modeling of monitoring data in the context of structural reliability analyses are outlined (Section 2.2).

2.1 Monitoring Uncertainty Modeling

The approach for the determination of measurement uncertainties which is outlined in the following has been developed in [15]. The approach is based on the Bayesian definition of probability and builds upon the structural reliability analysis framework of the Joint Committee on Structural Safety (JCSS [9]) and the methods of the Guide to the Expression of Uncertainty in Measurement ([7]).

The measurement uncertainty is defined as the probability distribution function of a measurement quantity Y . The measurement quantity Y is per definition not directly measured and is calculated with the measurement equation g_m (Equation (1)). The measurement quantity is dependent on the random variables \mathbf{X} constituting the measured quantities and the random variable M_{g_m} which is defined as the measurement equation model uncertainty.

$$Y = g_m(M_{g_m}, \mathbf{X}) \quad (1)$$

The probability distribution function of the measurement quantity Y , i.e. the measurement uncertainty, can be determined on the basis of a process equation and on the basis of observations. These two types of measurement uncertainties differ in the way how the measured quantities \mathbf{X} are determined and can further differ in the formulation of the measurement equation g_m .

Taking a process equation as the basis for the determination of the measurement uncertainty, i.e. the distribution of the measured quantity Y_p , the measurement equation is defined as $g_{m,p}$ in dependency on the model uncertainty of the measurement equation $M_{g_{m,p}}$ as well as on the vector of the measured quantities $\mathbf{X}_{g_{m,p}}$. The probability distribution functions of the measured quantities $\mathbf{X}_{g_{m,p}}$ are here determined with a vector of process equations \mathbf{p} , with the random variables \mathbf{M}_p , i.e. the vector of process equation model uncertainties, and the random variables \mathbf{X}_p constituting the parameters of the process equations. The process equations model the physical measurement processes with probabilistic electrical, optical and/or mechanical models and thus facilitate the determination of the probabilistic model of the measured quantities \mathbf{X}_p .

On the basis of observations, the measurement quantity Y_o is calculated with the measurement equation $g_{m,o}$ dependent on the model uncertainty of the measurement equation $M_{g_{m,o}}$ and the vector of the measured quantities \mathbf{X}_o . Observations of the measured quantities $\mathbf{x}_{g_{m,o}}$ are utilized for the determination of the vector of the probability distribution functions \mathbf{F} of the measured quantities. Here, the measured quantities \mathbf{X}_o are probabilistically modeled for given observations of the physical measurement processes under defined conditions.

The measurement uncertainty determined on the basis of the probabilistic process equation is defined as the prior measurement uncertainty. This definition takes basis in an informative approach to the prior measurement uncertainty (e.g. in contrast to [12]) constituting the physical relations which facilitate to

conduct a measurement. The likelihood function is then the probability density function of measurement quantity determined on the basis of observations, i.e. $L(\mathbf{x}_{g_{m,o}} | Y_p) \sim f_{Y_o}(Y_o)$. With these definitions the posterior measurement uncertainty, i.e. the posterior probability density function of the measurement quantity $f''(Y | \mathbf{x}_{g_{m,o}})$, is calculated by Bayesian updating (Figure 2, with the constant c).

The introduced approach in this general formulation facilitates the quantification of the measurement uncertainty for various measurement technologies. The approach is further applied for the quantification of the monitoring uncertainty as a part of the probabilistic models in a structural reliability analysis.

2.2 Structural Reliability Analyses and Monitoring Data

A structural reliability analysis can be based on design data, i.e. on the data available before a structure is commissioned, and on the basis of monitoring data, i.e. on measurement data from the commissioned structure. Both design and monitoring data require specific modeling principles which are elaborated here (on the basis of [15]) to show the characteristics of monitoring data in a structural reliability analysis.

Considering monitoring data as strain measurements from components of a structural system, monitoring data can be assigned to either the loading model $S_{des/m}$ or the resistance model R taking basis in the generic format of a limit state equation g for a structural component (Equation (2)). The assignment of monitoring data to the resistance model constitutes the approach of proof loading ([18]).

$$g = R - S_{des/m} \tag{2}$$

Assuming that the strain measurements are interpreted as loading model information, the probabilistic model of the loading S_m can be formulated as the multiplication of the model uncertainty B_m , the measurement uncertainty U , and the loading S (Equation (3)). The measurement uncertainty U is quantified with the introduced approach in Section 2.1.

$$S_m = B_m \cdot U \cdot S \tag{3}$$

The probabilistic model for the determination of the loading model utilizing design data S_{des} may be expressed in terms of the model uncertainty B_{des} and the loading S .

$$S_{des} = B_{des} S \tag{4}$$

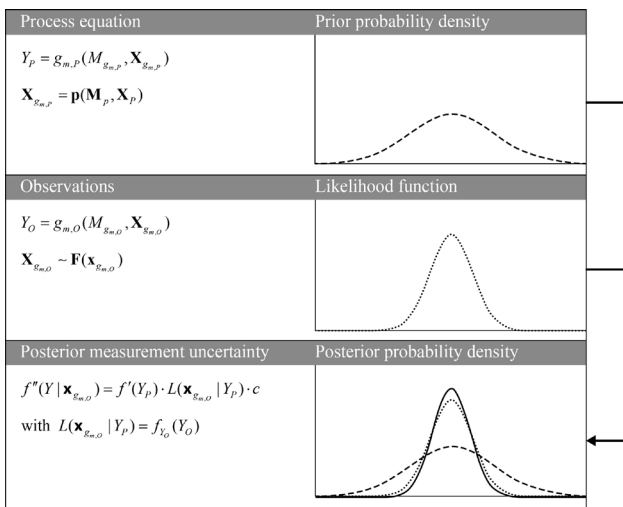


Figure 2: Approach for the determination of the measurement uncertainty

When design data are utilized for the reliability calculation, the calculation of the strains and stresses of a structural component requires a rather complex (Finite Element) model of the structure. These complex models are associated with the model uncertainty B_{des} , which can be modeled following e.g. the Probabilistic Model Code JCSS [9].

In contrast, the model uncertainty in a reliability analysis utilizing monitoring data B_m can be rather low as models with low complexities are applied. However, additional uncertainties like the measurement uncertainty U (Section 2.1) have to be considered.

The outlined characteristics of monitoring and design data in regard to the uncertainty modeling can lead to the situation that the monitoring data are more certain than design data. The structural reliability of a component can then be higher when monitoring data are utilized taking basis in the same distribution of the loading S . For instance, a significant higher fatigue reliability for a hot spot due to the reduction of the model uncertainties in combination with relatively low measurement uncertainties for strain gauge measurements is quantified in [15].

3. Approach for the Optimization of the Expected Life Costs by Monitoring Systems

The structural condition assessment based on information on structural reliability and risks constitutes an essential part of the operation of structures. Monitoring can be used for the structural condition assessment and can contribute to the structural reliability by more certain information on the condition of the structure, as described in Section 2 and [15]. However, monitoring systems can be further utilized aiming at the minimization of the expected operation costs and risks. In order to proceed in this direction the generic design decision for a monitoring system is formulated within the framework of the Bayesian decision theory utilizing a Life Cycle Cost-Benefit Analysis.

3.1 Life Cycle Modeling and Definition of a Monitoring Benefit

A Life Cycle Cost-Benefit Analysis for the management of structural integrity of a steel structure comprises the assessment of the expected values of the costs associated with inspection, repair and failure (e.g. [13]). A Life Cycle Cost-Benefit Analysis necessitates the formulation of various probabilistic and deterministic models such as degradation models,

inspection models, repair models and a structural event tree model.

The expected value of the total Life Cycle Costs $E[C_T]$ is the sum of the expected value of failure costs $E[C_F]$ and the expected operation costs of a structure $E[C_{OPEX}]$ which consists of the expected inspection costs $E[C_I]$ and the expected repair costs $E[C_R]$ (see Equation (5)). The dependency on inspection quality, repair policy and service life is suppressed here for clarity.

$$E[C_T] = E[C_F] + E[C_{OPEX}] \quad \text{with}$$

$$E[C_{OPEX}] = E[C_I] + E[C_R] \quad (5)$$

When a monitoring system is applied, the expected value of operation costs $E[C_{OPEX}^M]$ is calculated on the basis of modified expected inspection and repair costs ($E[C_I^M]$ and $E[C_R^M]$) and additionally with the expected value of monitoring operation costs $E[C_M]$ (Equation (6)). The expected value of the monitoring costs $E[C_M]$ is calculated from the number of sensors dependent (or channel (k) dependent) costs of the system $C_{Sys}^M(k)$ the costs of the installation of the system $C_{Inst}^M(k)$ as well as the costs of the operation of the system C_{Op}^M (Equation (7)). The monitoring system operation costs are discounted to the present value dependent on the time of the cash flow t and are multiplied by the yearly probability of no failure $(1 - \Delta p_F)$.

$$E[C_{OPEX}^M] = E[C_I^M] + E[C_R^M] + E[C_M] \quad (6)$$

$$E[C_M] = C_{Sys}^M(k) + C_{Inst}^M(k) + (1 - \Delta p_F) C_{Op}^M \frac{1}{(1 - i_r)^t} \quad (7)$$

The expected value of the benefit associated with monitoring $E[B_M]$ is defined as the expected total Life Cycle Costs $E[C_T]$ minus the expected total Life Cycle Costs associated with the application of a monitoring system $E[C_T^M]$ (Equation (8)).

$$E[B_M] = E[C_T] - E[C_T^M] \quad (8)$$

The outlined approach facilitates the calculation of the expected value of benefit associated with monitoring including the expected value of the costs for monitoring. The calculation of the expected monitoring benefit is dependent on various models and parameters. In order to quantify the effect of certain parameters on the expected value of the

benefit associated with monitoring the Bayesian decision analysis (see [10]) is utilized. The Bayesian decision theory defines decision situations with given information (prior decision analysis), with additional information (posterior decision analysis) and with unknown, i.e. not yet available, information (pre-posterior decision analysis). For these decision situations expected costs are calculated and optimized in dependency of decision variables, i.e. certain parameters of the utilized models.

Based on a pre-posterior Bayesian decision analysis, the expected value of the benefit of monitoring can be optimized in dependency of yet unknown monitoring information. This information can be modeled by the approaches of the structural reliability accounting for the measurement uncertainty and its effect on the structural reliability (see Section 2). Further, decision variables \mathbf{D} can be introduced which define the design of the monitoring system (Equation (9)).

$$E[B_M] = \arg \max (E[C_T] - E[C_T^M(\mathbf{D})]) \quad (9)$$

The probabilistic models which are utilized for the optimization of the expected value of the benefit of monitoring $E[B_M]$ are indicated in

Figure 3. The individual structural events no failure, failure, inspection and repair are modeled through a structural event tree for each service year. The probabilities of the events of no failure and of failure are calculated through structural system reliability analyses which require probabilistic models for loading, resistances and limit state models (Figure 3). The inspection events are accounted for using the approaches of reliability based inspection planning which themselves build upon structural reliability analyses and necessitate that inspection and repair strategies are defined and that the annual target probability of failure is defined. The consequence model accounts for the costs of the structural events in the event tree.

The event tree as depicted in the lower part of Figure 3 is taken as the basis for the following analyses additionally considering the costs of monitoring which apply for the case of survival of the structure in each year of the service life (see Equation (6)). An important characteristic of the event tree is the assumption of the simplification rule which is associated with the behavior of a repaired element; that is a repaired component behaves like a new component ([13], see Figure 3).

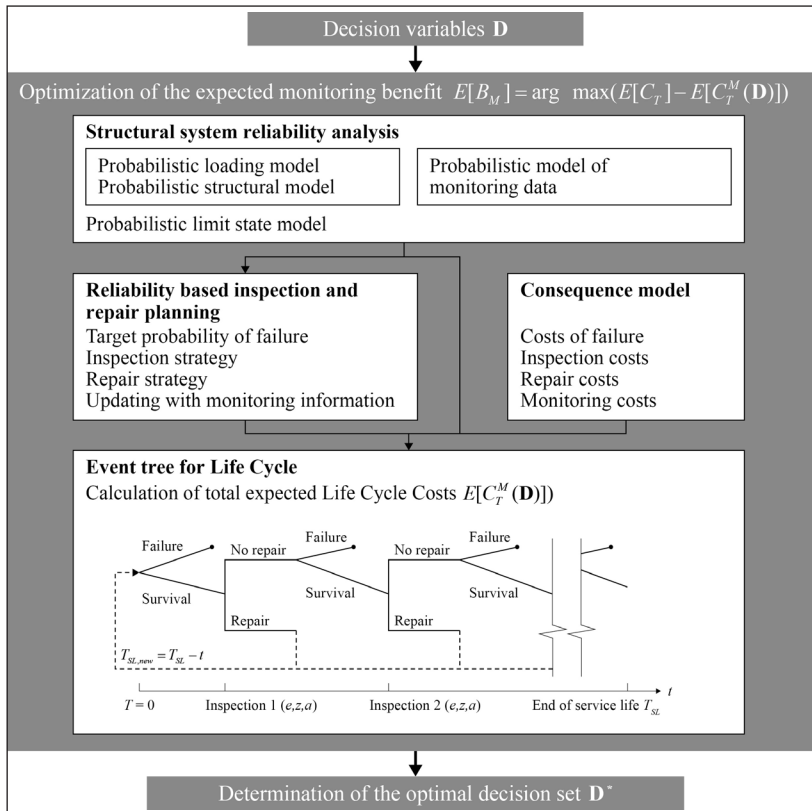


Figure 3: Utilized model for the optimization of the expected monitoring benefit with an event tree from [13].

3.2 Definition of Decision Variables

Monitoring is only sensible when a decision set can be found which leads to a positive monitoring benefit $E[B_M]$. The underlying decision, denoted with D_1 , is thus the decision whether to monitor or not to monitor (Equation (10)).

$$D_1 = \{M, \bar{M}\}, \quad (10)$$

The decision to monitor depends on the decision which components to monitor and which type of monitoring system should be applied. The decision set D_2 contains the monitored hot spot set (Equation(11)) consisting of n_2 monitored hot spot sets c_{HS} . The monitored hot spot set influences the monitoring system investment and installation costs (see Equation (7)) because $k = 3$ channels are assumed to monitor one hot spot.

$$D_2 = \{c_{HS,1}, c_{HS,2}, \dots, c_{HS,n_2}\}, \quad (11)$$

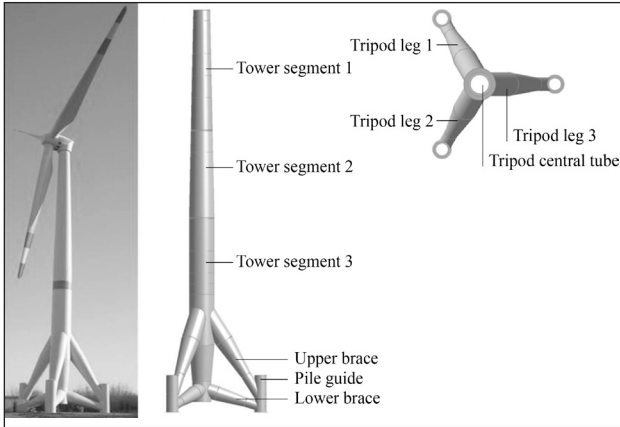


Figure 4: Prototype of a Multibrad M5000 off shore wind turbine and support structure with the structural parts

The decision set D_3 models the type of the monitoring system in terms of its precision. D_3 contains n_3 variables δ which describe the uncertainty reduction due to monitoring (Equation (12) and see Section 2.2). However, in Section 2.2 the underlying assumption is that the probabilistic loading model S is the same for the design data and for monitoring data which must not necessarily be given in a practical situation. Then, the uncertainty reduction factor δ describes the combination of the different probabilistic loading models in combination with the probabilistic model uncertainty and measurement uncertainty models.

$$D_3 = \{\delta_1, \delta_2, \dots, \delta_{n_3}\} \quad (12)$$

4. Case Study

The case study contains the Life Cycle Cost-Benefit Analysis investigating various monitoring solutions for the support structure of a Multibrad M5000 offshore wind turbine prototype as depicted in Figure 4.

The support structure of the wind energy converter consists of a tower divided in segments by ring flanges, the tripod consisting of upper braces, lower braces, the pile guide as well as the foundation, which consists

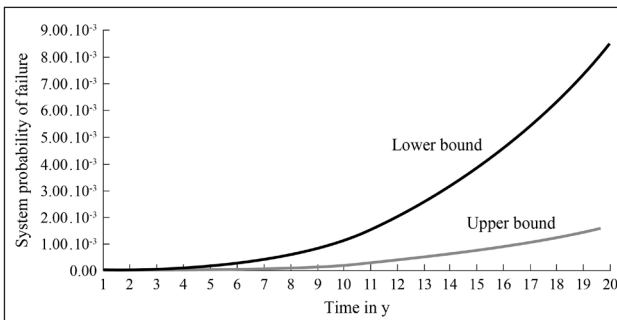


Figure 5: Support structure system probability of failure for a service life of 20 years

of circular reinforced concrete slabs attached to a pile group. The support structure involves 11 tower components assigned to three tower segments and 24 tripod components as parts of the tripod legs and central tube as well as their connections. For this case study a reliability analysis [17] on the basis of a developed model basis was performed.

4.1 Results of the Structural Reliability Analysis

The structural reliability analysis builds upon probabilistic structural, loading and limit state models comprising design, production and construction data. This model basis is derived by analyzing various aspects of the developed structural, loading and limit state models and on the basis of the results of a sensitivity study in conjunction with the developed probabilistic models ([19] and [20]). The complexity of the individual models dictates an efficient solution scheme for the reliability analysis. Such an algorithm is developed consisting of an adaptive response surface algorithm and an importance sampling Monte-Carlo algorithm in [17].

The calculation of the probabilities of fatigue failure involves the connections of all tower and tripod components with an SN limit state model. The probability that a fatigue failure occurs can be calculated with the simple bounds of system reliability theory (see e.g. [2]) based on a serial system. Then the probability that fatigue failure occurs results at the end of the service life for the tower in the bounds of 1.66×10^{-3} and 5.15×10^{-3} , for the tripod in the bounds of 9.28×10^{-4} and 3.30×10^{-3} and for the support structure in the bounds of 1.66×10^{-3} and 8.43×10^{-3} (Figure 5).

The calculated probabilities of failure should be in accordance with acceptance criteria such as target probabilities of failure given for components in the [1] and for structural systems in the Probabilistic Model Code [9]. A detailed analysis in [17] has shown that these requirements are fulfilled or not contradicted.

4.2 Reliability Based Inspection and Repair Planning

The inspection strategy builds upon the approaches of the reliability inspection planning and is based on the models in [13] utilizing the documented database. A magnetic particle inspection (MPI) is assumed as the inspection technology (see [13] and [22]). A typical probability of failure threshold $\Delta p_{F_2}^T = 1.00 \times 10^{-4}$ is assumed. The repair event is defined on the basis of a measured crack size during an inspection (see [13]).

The inspection plans are modified in dependency of the variable δ in the decision set D_3 which models the uncertainty reduction due to monitoring and consequently the reduction of the probability of failure of the hot spot. The modification of the inspection plans follows the approach described in [13] based on the calculation of a fictive installation year at the modification time (which here equals the monitoring system installation time plus one year) for which the inspection plan is then derived. This approach accounts for the properties of the underlying fracture mechanics model. The new inspection plan for the remaining service life is derived in combination with the original inspection plan considering already performed inspections before the modification time.

4.3 Consequence Model

The consequence model takes a structural failure associated with the loss of the structure and with the loss of the monitoring system (when applied) into account. For survival of the structure the consequences are inspections and repair (according to the reliability based inspection and repair planning) as well as the monitoring system operation.

The cost model consists of generic and normalized values for the failure costs ($C_F = 1$), the inspection costs ($C_I = 10^{-3}$) and the repair costs ($C_R = 10^{-2}$) per component and an interest rate of $i_r = 5\%$ (see [13]). In relation to this cost model, a monitoring cost model for the reference case is introduced. The costs of the monitoring system are assumed to $C_{Sys}^M(k) = 1.33 \cdot 10^{-4}$ per channel, where three channels (i.e. sensors) are used with the monitoring of one hot spot. The costs of installation are assumed to $C_{Inst}^M(k) = 1.33 \cdot 10^{-4}$ per channel and the operation costs are assumed to $C_{Op}^M = 6.67 \cdot 10^{-4}$ per year. As an example for the cost model the reference case is

Table 1: Consequence for the case study

Type of costs	Value
Failure costs C_F	7,500,000 €
Inspection costs per component C_I	7,500 €
Repair costs per component C_R	75,000 €
Costs of monitoring system per channel $C_{Sys}^M(k)$	1,000 €/k
Costs of system installation per channel $C_{Inst}^M(k)$	1,000 €/k
Cost of system operation per year C_{Op}^M	5,000 €/a

considered assuming generic costs of 1,500,000 € per megawatt [5]. The resulting costs for the reference case are summarized in Table 1.

4.4 Decision Set Definition

The decision set D_2 contains $n_2 = 20$ hot spot sets C_{HS} . The hot spot set is determined beginning with the hot spot with the highest probability of failure. Consecutively, the hot spot with the second lowest probability of failure is added to the set. The 20 hot spot sets cover the relevant hot spots for the calculation of the system probability of failure (see Section 4.1 and [15]). The decision set D_3 consists of $n_3 = 11$ variables with δ in the range of 1.0 to 1.5 modeling the reduction of the probability of failure by a monitoring system. The factor is generically assumed based on the results of a generic fatigue reliability analysis in [15].

4.5 Expected Total Life Cycle Costs and Calculation of the Monitoring Benefit

The total expected Life Cycle Costs for the support structure, as designed (see Equation (5)), of the wind turbine structure are calculated utilizing the cost model and the results of the structural reliability analysis (Section 4.1). The total expected Life Cycle Costs amount to 4.88×10^2 with 3.85×10^2 expected cost for the operation (inspection and repair) and with 1.03×10^2 expected failure costs (risks).

The monitoring benefit is calculated separately in relation to expected failure costs, i.e. in regard to the risks ($E[B_{M,F}]$ see Equation (13)), in regard to the expected operation costs ($E[B_{M,OPEX}]$ see Equation (14)) and in regard to the total Life Cycle Costs $E[B_M]$ (Equation (9)).

$$E[B_{M,F}] = E[C_F] - E[C_F^M(D)] \quad (13)$$

$$E[B_{M,OPEX}] = E[C_{OPEX}] - E[C_{OPEX}^M(D)] \quad (14)$$

The monitoring benefit in regard to the risks $E[B_{M,F}]$ is positive ranging from 0.0 to 3.4×10^3 (Figure 6 left) which corresponds to 0.0 to 33.0% of the expected failure costs. The higher the number of monitored hot spots (decision set D_2), the higher the expected monitoring benefit $E[B_{M,F}]$. The same applies to a higher uncertainty reduction factor for monitoring (decision set D_3). The monitoring benefit in regard to the risks increases more for a higher number of monitored hot spots and for a higher uncertainty reduction factor.

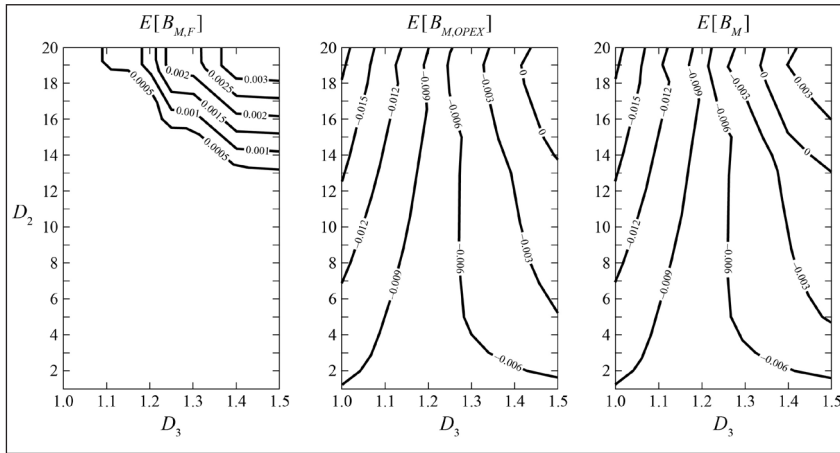


Figure 6: Expected monitoring benefit with regard to the risks $E[B_{M,F}]$ (left) and with regard to the expected operation costs $E[B_{M,OPEX}]$ (middle) and with regard to the total Life Cycle Costs $E[B_M]$ (right)

The monitoring benefit in regard to the operation costs $E[B_{M,OPEX}]$ ranges from -8.9×10^{-3} to 1.5×10^{-3} which is -23.1% to 3.90% of the expected operational costs (Figure 6 middle). The monitoring benefit is positive for high uncertainty reduction factors due to monitoring (decision set D_3) and at the same time monitoring at least the 14 hot spots with the highest probabilities of failure (decision set D_2).

The influence of the monitoring uncertainty reduction factor (decision set D_3) is more pronounced in comparison to the number of monitored hot spots (decision set D_2) for the monitoring benefit in regard to the operation costs. The reason here is that the monitoring uncertainty reduction factor does not affect the costs of monitoring.

The expected monitoring benefit in regard to the total Life Cycle Costs $E[B_M]$ is the sum of the expected monitoring benefit in regard to the risks $E[B_{M,F}]$ and in regard to the operation costs $E[B_{M,OPEX}]$. The expected monitoring benefit $E[B_M]$ ranges from -8.9×10^{-3} to 5.3×10^{-3} (-18.2% to 10.9% of the total Life Cycle Costs, see Figure 6).

The optimal decisions for the monitoring benefit in regard to the risks, the expected operational costs and the expected total Life Cycle Costs are shown in Table 2. For the utilization of monitoring systems to reduce risks optimal decision sets D_2^* and D_3^* can be found for which the monitoring benefit $E[B_{M,F}]$ is maximized. The optimal decision sets D_2^* and D_3^* are the maximum number of monitored hot spots ($c_{HS,20} = 20$) and a monitoring system possessing the maximum (considered) uncertainty reduction factor of $\delta = 1.5$, respectively (Table

2). Each element of D_2^* and D_3^* leads to a positive benefit in this case study. It follows that the decision is to monitor for risk reduction, i.e. $D_1^* = \{M\}$.

The maximization of the monitoring benefit for the operational costs $E[B_{M,OPEX}]$ also leads to the decision that a monitoring system should be applied ($D_1^* = \{M\}$) because a positive benefit can be achieved. However, only certain combinations of the decision variables lead to a positive monitoring benefit. The optimal decision is to monitor $c_{HS,19} = 19$ hot spots with a monitoring system possessing the maximum uncertainty reduction factor of $\delta = 1.5$. The same result is found for the maximization of the total Life Cycle Costs monitoring benefit $E[B]$ (Table 2).

5. Summary and Conclusions

One of the major challenges in the field of renewable energies represents the development of large scale offshore wind parks as this has been the research focus in the last decade. By the time the IRIS project is completed the commissioning of the first German commercial wind parks has started in significant water depths. In preparation for the next step, namely, the

Table 2: Optimal decision sets for the individual decision analyses

Decision situation	Decision set D_1	Decision set D_2	Decision set D_3
Risk reduction	$D_1^* = \{M\}$	$D_2^* = \max \{c_{HS}\}$	$D_3^* = \max \{\delta\}$
Operational cost reduction	$D_1^* = \{M\}$	$D_2^* = \{c_{HS,19} = 19\}$	$D_3^* = \max \{\delta\}$
Total life cycle cost reduction	$D_1^* = \{M\}$	$D_2^* = \{c_{HS,19} = 19\}$	$D_3^* = \max \{\delta\}$

operation of offshore wind parks, this research work contains conceptual and applied research results on Life Cycle Cost optimized monitoring systems of offshore wind turbine structures.

The essential finding of the research is that the operation efficiency of wind turbine structures can be substantially supported by Life Cycle Optimized Monitoring Systems. It is found that an expected benefit for the operation, the risks and the total Life Cycle Costs can be achieved by the conceptual integration of structural monitoring techniques, the structural reliability theory and the reliability based inspection and repair planning. The integration should be bidirectional in the sense that the generic design decisions for structural monitoring systems are based on Life Cycle Cost-Benefit Analysis and that simultaneously a possible reduction of the uncertainty associated with the condition is utilized for the structural reliability assessment and thus for the inspection and maintenance planning.

With this research it is shown on the basis of a pre-posterior decision analysis how an increase of information and knowledge (here by monitoring data) for the implementation of optimal decisions (monitoring systems, inspection, repair and risks) can and should be utilized.

In a broader sense the introduced approach facilitates the quantification of the value of monitoring information based on the difference between the Life Cycle Costs applying monitoring or not. The introduced approach thus constitutes the starting point for the development of a general approach for the quantification of the value of structural health monitoring (SHM) as recently published in [16] and [6].

The research results contribute to the aims of the European Strategic Energy Technology Plan (SET-Plan: [4]) focusing on the improvement of the competitiveness of the wind energy production. In this way the research results also support the German and European Union energy politics aiming at the establishment of renewable energies as a major component of future energy production.

5.1 Conclusions with regard to the IRIS Objectives

The achievements of the research contribute directly to the objectives of the IRIS project [21]:

I. Integrated Methodologies for Pioneering Risk Assessment and Management

The developed approaches pioneer structural condition assessment on the basis of monitoring data. This facilitates the quantification of risks for the Life Cycle of a wind turbine support structure.

II. Knowledge and Technologies for Risk Identification and Reduction

The conceptual developments of the monitoring based condition assessment constitute a knowledge progress and facilitate the utilization of monitoring technologies for risk identification and risk reduction. The risk reduction is achieved by the lower uncertainties of measurement data in comparison to design data of a structure. This fact has been quantified for the first time in the context of the structural reliability theory.

III. Online Monitoring with Decision Support Systems

The decision support is achieved by the explicit decision theoretical formulation facilitating an optimization of the expected Life Cycle Costs of an offshore wind turbine support structure. In this way the monitoring system design decisions are based upon a Life Cycle Cost-Benefit Optimization.

References

1. DIN 2010. Eurocode: Basis of structural design. DIN EN 1990.
2. Ditlevsen, O. 1979. Narrow Reliability Bounds for Structural Systems. *Journal of Structural Mechanics* 7(4): 453-472.
3. Enright, M. P., Hudak, S. J., McClung, R. C. and Millwater, H. R. 2006. "Application of Probabilistic Fracture Mechanics to Prognosis of Aircraft Engine Components". *AIAA JOURNAL* 44(2): 311-316.
4. European Union 2010. The European Strategic Energy Technology Plan: SET-Plan.
5. European Wind Energy Association (EWEA) 2009. The Economics of Wind Energy.
6. Faber, M.H. and Thöns, S., 2013, "On the Value of Structural Health Monitoring", ESREL 2013, Amsterdam, The Netherlands.
7. ISO 2008. Part 3: Guide to the Expression of Uncertainty in Measurement (GUM:1995). ISO/IEC Guide 98-3.
8. JCSS 2001. Probabilistic Assessment of Existing Structures. A publication of the Joint Committee on Structural Safety, RILEM Publications S.A.R.L.
9. JCSS 2006. Probabilistic Model Code, JCSS Joint Committee on Structural Safety.
10. Raiffa, H. and Schlaifer, R. 1961. "Applied statistical decision theory", New York, Wiley (2000).
11. Rucker, W., Hille, F. and Rohrmann, R. G. 2006 "Guideline for the assessment of existing structures". SAMCO F08a.
12. Sommer, K.-D., Kühn, O., León, F. P. and Siebert, B. R. L. 2009, "A Bayesian approach to information fusion for

- evaluating the measurement uncertainty", *Robotics and Autonomous Systems* 57(3): 339-344.
13. Straub, D. 2004, "Generic Approaches to Risk Based Inspection Planning for Steel Structures", PhD. thesis. Chair of Risk and Safety, Institute of Structural Engineering. ETH Zürich.
 14. Straub, D. 2011, "Reliability updating with equality information" *Probabilistic Engineering Mechanics* 26(2): 254-258.
 15. Thöns, S. 2012, "Monitoring Based Condition Assessment of Offshore Wind Turbine Structures" Institute of Structural Engineering, ETH Zurich, IBK Report 345, e-collection. library.ethz.ch/eserv/eth:6828/eth-6828-01.pdf, VdF Hochschulverlag AG, Zürich.
 16. Thöns, S. and Faber, M. H. 2013, "Assessing the Value of Structural Health Monitoring" 11th International Conference on Structural Safety & Reliability (ICOSSAR 2013). New York, USA.
 17. Thöns, S., Faber, M. H. and Rücker, W. 2010, "Support Structure Reliability of Offshore Wind Turbines Utilizing an Adaptive Response Surface Method" 29th International Conference on Ocean, Offshore and Arctic Engineering (OMAE 2010). Shanghai, China.
 18. Thöns, S., Faber, M. H. and Rücker, W. 2011, "On the utilization of monitoring data in an ultimate limit state reliability analysis" 11th International Conference on Applications of Statistics and Probability in Civil Engineering (ICASP). Zurich. Switzerland.
 19. Thöns, S., Faber, M. H. and Rücker, W. 2012a, "Fatigue and Serviceability Limit State Model Basis for Assessment of Offshore Wind Energy Converters", *Journal of Offshore Mechanics and Arctic Engineering (JOMAE)* 134(3): 031905.
 20. Thöns, S., Faber, M. H. and Rücker, W. 2012b, "Ultimate Limit State Model Basis for Assessment of Offshore Wind Energy Converters," *Journal of Offshore Mechanics and Arctic Engineering (JOMAE)* 134(3): 031904.
 21. VCE 2011. IRIS Integrated European Industrial Risk Reduction System (CP-IP 213968-2), Description of Work V21.
 22. Visser Consultancy Limited 2000. POD/POS curves for non-destructive examination. Offshore technology report. Offshore Technology Report 2000/018.

Massive Shear Wall Testing for Nuclear Industry

Adrian Bekö¹, Helmut Wenzel¹, Peter Rosko²

¹VCE Vienna Consulting Engineers ZT GmbH

²Vienna University of Technology, Center of Mechanics and Structural Dynamics

E-mail: beko@vce.at

Abstract

Consequences of earthquakes have proven the need to study the shear mechanism of low-rise reinforced concrete shear walls thoroughly. Because of the complexity of reinforced concrete behavior generalized problem solutions are not readily available. Experimental testing remains essential for investigating concrete elements. The contribution deals with cyclic shear testing of thick low-rise reinforced concrete walls. Analysis of the data obtained resulted in the determination of hysteresis characteristics, nonlinear effects for shear, ultimate capacity and damping of the tested specimens. Various strength assessments and comparison to test results is given. The experimental investigation provides valuable results applicable in monitoring and design of structures.

Keywords : *Thick low-rise shear wall, failure test, quasi-static cyclic load, pure shear, hysteretic damping*

1. Introduction

Reinforced concrete shear walls are frequently used in civil engineering as structural elements resisting horizontal forces in the plane of the wall. The stiffness of the shear wall has to keep drifts within reasonable limits. During past earthquakes around the world many structures (among them also reinforced concrete walls) collapsed suddenly and led to catastrophic failures which occurred due to dynamic shear loading. Consequences of such earthquakes have proven the need to study thoroughly the shear mechanism of reinforced concrete walls. Therefore the scientific research in this area is very intensive and has resulted in many experimental and numerical tests in the past years.

Because of the parameter variability, each experimental or numerical research is but a contribution to the knowledge base. The applicability of results is limited by the type of wall and parameter subspace. A number of failure modes can occur depending on parameters such as the type of cross-section, reinforcement detailing and quantities, properties of reinforcing steel, concrete compressive strength and boundary conditions. Complex destructive phenomena include concrete cracking, interaction effects between steel and concrete, steel yielding and concrete crushing in compression. It is not simple to generalize any given experimental or numerical test because of reasons mentioned above. When a test studies a specific type

of structure and well defined loading, the outcome is of great interest.

Generally, shear walls are divided into two groups based on their geometry: high-rise or tall and low-rise or squat/short shear walls. High-rise shear walls are governed by flexural behavior similar to a cantilever beam. The flexural behavior of reinforced concrete walls has been examined and it is theoretically described. The behavior of low-rise shear walls is governed mainly by shear behavior. Although there has been considerable activity directed towards low-rise shear walls this area of research is still in progress. One of the reasons is that low-rise shear walls are frequently used in nuclear power plants. Investigations presented here are focused on a low-rise wall specifically a more massive specimen which could be classified as a thick shear wall. Here we presented the results of a joint research activity to study a full scale shear wall with a thickness of 400mm.

The research work presented here builds on the contemporary knowledge in the field. Historical development of the research into reinforced concrete shear walls can be outlined by certain milestones.

Some of the first test results of shear walls under static loads are available in the literature of the fifties by Galletly(1952) [1]. Advancing the subject were Benjamin and Williams (1957, 1960)[2],[3] with significant experimental research. During the 1960s most experimental research aimed at understanding the

behavior of reinforced concrete elements was directed towards moment resisting frames. Later in the 1970s the interest in the seismic behavior grew and induced the experimental investigation of reinforced concrete walls. Paulay(1975) [4] presented design aspects of shear walls for seismic areas. Studies of Barda (1972) [5] led to the improved wall design provisions in ACI 318-71, including seismic requirements. Research in the field has been active till the present. Experimental shear-dominated response of reinforced shear walls with design implication was presented by Lopes (2001)[6],[7]. Salonikios et al. (2002) [8] carried out an experimental investigation of the validity of the design provisions of EC8 for walls of height to length ratios of 1.0 and 1.5. On the base of experimental testing Brun et al (2003)[9] presented a simple shear wall model with stiffness degradation. Thomson et al (2009)[10] studied the pinching effect and damage of squat reinforced concrete shear walls. Brun, Labbe et al (2011)[11] carried out pseudo-dynamic tests on low-shear walls and proposed a simplified model based on the structural frequency drift.

The currently applicable codes treat the problem in a variety of ways. Some of the more modern codes like the Eurocode[12] or the New Zealand code aims specifically at preventing shear failure by the use of capacity design. However low-rise shear wall design with intended use in nuclear facilities where a shearing failure is the only mode is not addressed by the Eurocode. The design of RC shear walls in the US is governed by ACI 318[13]. No special seismic provision for wall design was available in ACI 318 until the 1970s. Since then, significant changes have been implemented to improve the behavior of structural walls under earthquake loading. For example, requirements for wall boundary regions were included for the first time in 1971 and seismic provisions for shear design were placed in 1983. The current ACI 318-11 provisions call for a displacement-based seismic design procedure, where the wall boundaries are designed and detailed to achieve the expected response of the structure in a ductile manner. The complementary code for nuclear facilities is the ACI319 which follows the same design principles.

2. Experimental Testing of Shear Walls

The ability to accurately predict and model shear wall behavior is of the utmost importance. The reason for testing the specimens to complete failure was that there is not much data on complete failure tests. As the intention was to investigate a more massive or

so-called thick wall, experimental testing remains the only accurate means of assessment of shear response and capacity. The two main distinctive features of the tests were, first the thickness of the wall which was robust enough not to let the wall go into buckling and second the top of the wall was kept horizontal to load the wall predominantly in shear as much as it was possible to achieve (with corresponding axial load).

2.1 Specimen

The specimens were designed by Vienna Consulting Engineers (VCE) based on the suggestions of Électricité de France (EDF) and commissioned by VCE. The loading system was designed at the European Commission's Joint Research Centre (JRC) in cooperation with VCE and commissioned by VCE. The lab tests were carried out by the European Laboratory for Structural Assessment (ELSA) at JRC at their facilities in Ispra, Italy. The specimens were tested by a cyclic quasi-static load.

The reinforced concrete specimen comprises three parts. The wall part which is 3m long, 1.2m high and 0.4m thick is lined with two beams at the bottom and the top with a cross section of 1.25x0.8m. The beams are cantilevered 0.5m on either side of the wall which results in the 4.0m total length of the specimen. The design of the reinforcement and principal dimensions

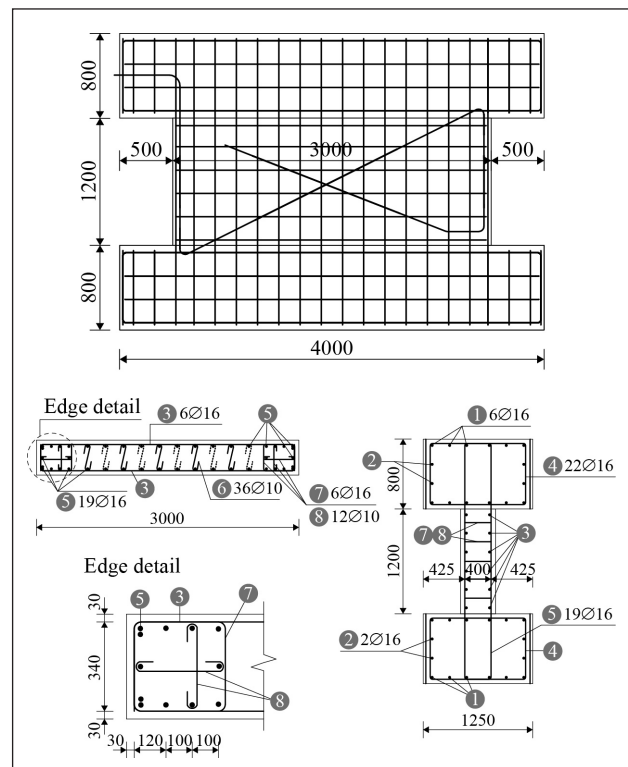


Figure 1: Details of reinforcement.

are shown in Figure 1. Figure 2 shows the picture of the wall and beams.

The reinforcement of the specimens was designed as standard for this type of structural element. The edges of the wall were strengthened with concentrated reinforcement to take the bending moment occurring in the wall. The mesh of vertical and horizontal (shear) reinforcement was designed based on structural principles and suggestions by EDF to represent an actual wall as used in nuclear power plants. As the wall is short direct load transfer is possible and engagement of shear reinforcement for force transfer was not foreseen. Vertical reinforcement runs from the bottom of the bottom beam through the wall to the top of the top beam creating a solid connection of the segments.

The specimens were concreted in their vertical positions to reduce inhomogeneities along the height of the wall. The concrete cubic strength was 54MPa. The reinforcement yield strength was 500MPa. The loading frequency was small and no notable increase in the strength of the materials was expected.

An important aspect of the specimen design and manufacture was the load transfer from the loading

system to the concrete wall. The wall was not loaded directly but through the upper and lower containment beams. The solution used was a pair of 3cm thick steel plates on both sides of the beams which were connected to the concrete through connecting studs and later casting.

The force from the loading machine to the steel plates of the specimen was to be transferred by steel to steel friction. A large enough normal force was required to allow for the transmission of the total shear force. This was achieved by means of transverse prestressing (see Figure 3).

2.2 Apparatus and Instrumentation

Due to the robustness of the wall to be tested the required forces to carry the specimen to failure could have damaged the reaction wall at the ELSA laboratory. For this reason the shear testing was conceived in a self-equilibrating manner. The complete loading system consisted of three parts: the main loading system, a system controlling the rotations at the end of the actuators and a restraining system that controlled the lateral motion.

The main loading system, a four part jaw-like steel frame, was designed to be placed around the specimen on the lower and upper beams. The frame had been conceived so that the load was applied at the height of the centerline of the wall as not to introduce additional bending of the specimen. The load was equally distributed to the lower and upper beams. This type of loading does result in a moment acting on the system as a whole that would induce rotation. It had been analyzed whether the self-weight of the entire system is sufficient to suppress uplift. It had been shown that uplift on one side would occur and so the lower part of the steel section was anchored. The steel frame was optimized to maximize stiffness while minimizing plate thickness.

The horizontal actuators were placed between the upper and lower jaw of the steel frame. These were fixed to the lower part of the main loading frame and pushed against the plates of the upper part of the system. The four 300 ton actuators were unidirectional devices capable of pushing in positive and negative direction. All four actuators worked in a synchronized fashion to exert the required loads. When the wall was being sheared in a given direction the two actuators on one end would apply forces to the external plates of the upper jaws while the two actuators at the other end would apply the same load to the inner plates

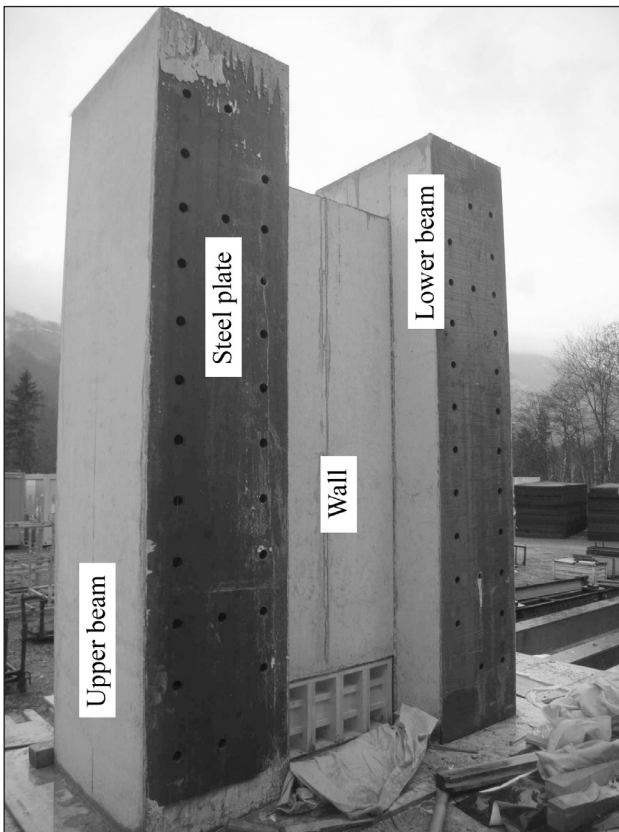


Figure 2: Photo of concreted specimen with steel plates.

of the upper frame. Once maximum load has been reached the actuators are driven back until contact with the original plates is lost and next they are driven in the other direction as first contact with the reverse plates is made and finally load application in the opposite direction can advance. From the nature of the load application it follows that actuation was not continuous.

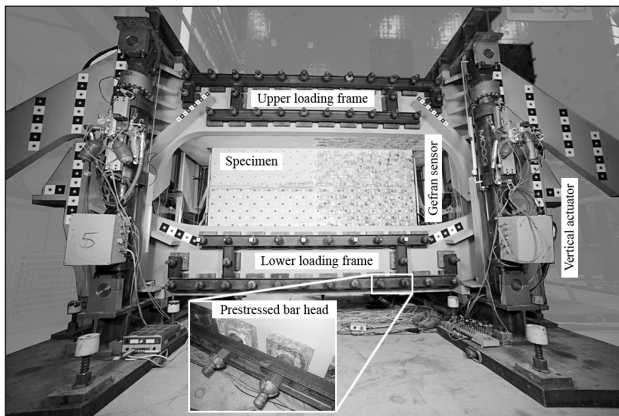


Figure 3: Prepared and instrumented setup.

The shearing of the wall translates also to vertical displacements and rotations at the point of load application to the frame which might exceed the shear or bending capacity of the acting rod. Moreover, the specimen was anticipated to elongate due to crack opening which could introduce additional spurious vertical forces. In order to protect the actuators a sliding and a rotation protective system has been devised.

To stabilize the wall laterally and to prevent out of plane spurious distortions the top section of the main loading system was on one side braced against the reaction wall by means of two steel bars capable of resisting 550kN buckling load.

To force the specimen in shear mode as much as possible considerable effort was devoted to keeping the top of the specimen horizontal. Four additional actuators were placed around the specimen vertically. These were fixed to the ground and connected to the top of the loading frame by transversal beams. These actuators operated in a push-pull mode, thus being able to exert forces in both directions. These jacks were also used to simulate the additional vertical load on the structure. The control of these actuators was made in such a way that equilibrium of forces was to be maintained diagonally, i.e. assuming notation according to Figure 4: $F_1 + F_4 = 0$ and $F_2 + F_3 = 0$ or actually for non-zero vertical forces the sum of

each couple had to equal half of the required vertical load. Also, in-plane and out-of-plane rotation was controlled by the condition posed upon displacements $u_1 = u_4$ and $u_2 = u_3$.

The objective was to follow the behavior of the stiff wall in cyclic shear loading up to its failure. For measuring the shear displacement four transducers were mounted at the top and bottom of the wall on each end. These Heidenhain sensors (H5-H8) were actually fixed to the containment beams close to the wall since failure of the wall could render them useless. For measuring the horizontal motion four Temposonic transducers were mounted on the horizontal actuators. These sensors recorded cumulative displacements.

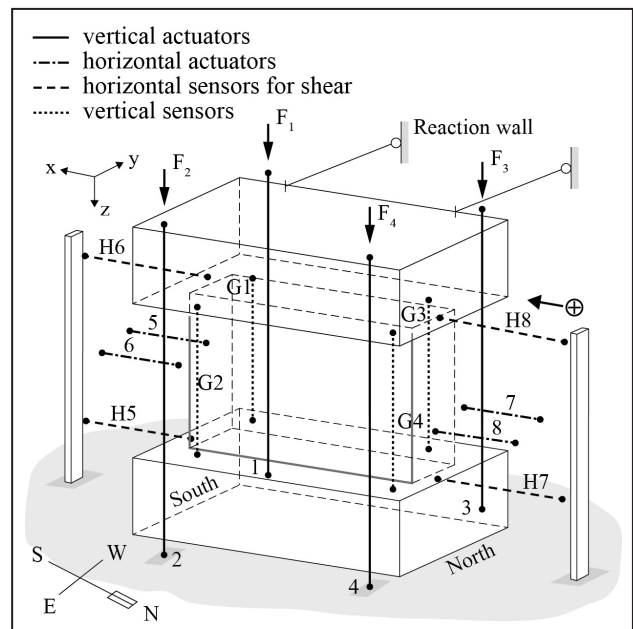


Figure 4: Main instrumentation on the specimen.

The measurement of displacements in the vertical direction was serviced by four Heidenhain transducers each next to the vertical actuators. These were connected to support plates welded onto the main loading system. It was assumed the deformations of the loading system were small and there was no sliding between the loading system and the wall. Additionally there were four Gefran transducers (G1-G4) mounted at the four corners of the wall between the upper and lower containment beams. These measured the displacements of the wall directly.

2.3. Testing and Output

Four specimens were tested in a similar way. Each wall was subjected to a combination of constant vertical load applied at the top of the shear wall and

variably increasing horizontal load. Generally on all tested walls ten initial cycles of 500kN were performed. For monotonic cases the load was increased in steps of 500kN to 1000kN and two cycles were performed at each load level until failure. A load cycle was defined as reaching the target load in one direction then retracting the actuators and subsequently pushing the wall in the opposite direction until target load has been reached. On the second cycle only the recorded maximum displacement corresponding to the target load on the first cycle was followed up.

After each main half-cycle a small loading loop of 500kN was carried out to allow for assessment of residual stiffness for smaller load levels after a certain state of damage had been reached.

2.3.1. Load-Displacement Curves

The plots show the performance of the wall in the main parameters, i.e. horizontal load, shear displacement, vertical displacement. Major points of interest have been marked in the data.

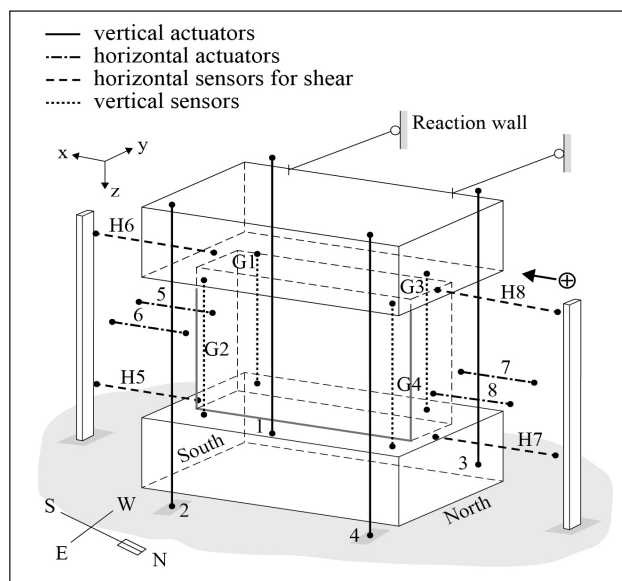


Figure 5: Horizontal load, shear displacement and vertical displacements of wall 4.

The moment of the first major crack appearing is defined as the point when the vertical displacements start to accumulate. This occurs when the two surfaces slide enough with respect to each other and aggregate interlocking prevents perfect closure in the crack. The onset of yielding in the reinforcement is difficult to accurately determine due to lacking direct instrumentation on the reinforcing bars. Nonetheless, the section of the data after which the effect of steel

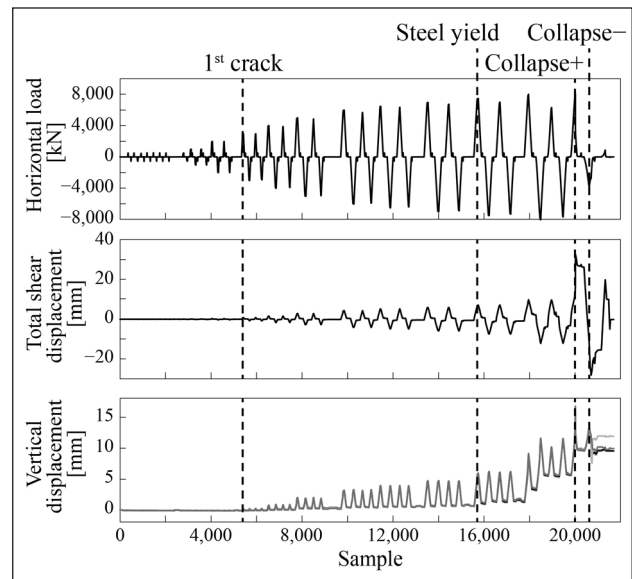


Figure 6: Load-displacement curve of wall 4.

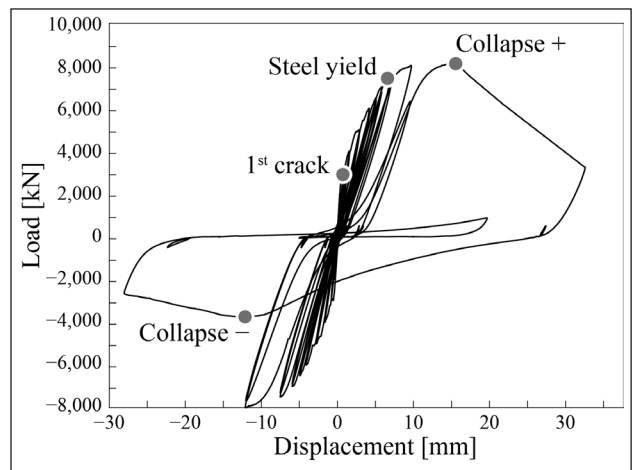


Figure 7: Shear displacement vs. cumulative vertical displacement (sensors G1-G4) of wall 4.

yielding is apparent in the form of a significant step of vertical displacements. This corresponds to about 3.75‰ vertical elongation and 2.3‰ shear distortion. Also the pinching around the origin becomes more pronounced after this point. To clearly differentiate which bars are under yielding is unreasonable; nonetheless judging from the deformation of the wall the reinforcement in the direction of shearing is not the one under excessive strain. The point of collapse is well defined by the sudden drop of the horizontal load, which in this case also indicates the failure was due to crushing of the concrete.

By the end of the test the specimens had developed a well-defined pattern of parallel diagonal cracks in both directions provoked by load reversals (see Figure 9).

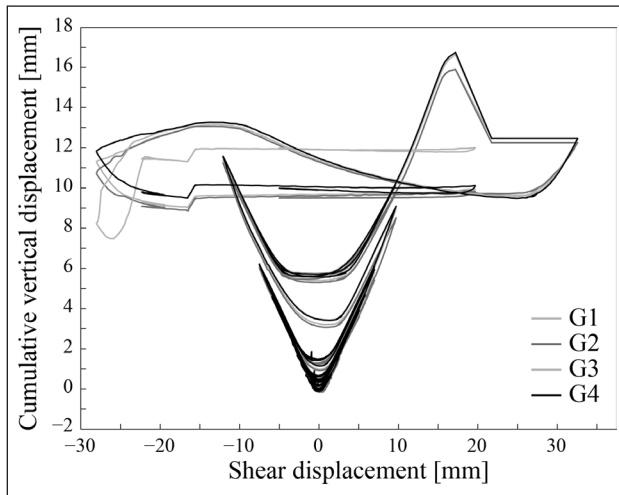


Figure 8: Load-displacement curve of wall 4 (a) and wall 2 (b) colored by cycles.

3. Results and Discussion

The behavior of a reinforced concrete shear wall cannot be separated into distinct linear and non-linear regions because concrete has an inherently plastic behavior. Although steel has a defined yield point, concrete is non-linear from initial loading and so the specimen as a whole shows a composite behavior. The hystereses presented in the previous section show well the cyclic strength degradation as the second cycle on a damaged specimen does not reach the set load level at an equal horizontal displacement, which was the controlled variable. Progressive degrading phenomena occur, starting with concrete cracking, trough reinforcement yielding until the specimen fails by concrete crushing in the middle region of the wall. The different load histories of the two presented walls did not result in noteworthy differences in their global behavior. Judging from the points of interest in the work diagrams the behavior of the wall does not significantly depend on the load history. Load levels for each feature are very similar including the ultimate load and the failure mechanism is the same.

According to damage mechanics the behavior of the shear wall specimen can be characterized as unidirectional. During the cyclic loading of the wall to specific directions of the shearing two distinctive sets of shear cracks form in the wall (see Figure 9). When the shear force changes sign one set of cracks tends to close and its presence has a reduced effect in the wall behavior while the other set of cracks tends to open and becomes the dominant stiffness reduction phenomenon. During opening and closing of existing cracks the reinforcement in the disturbed areas is activated.

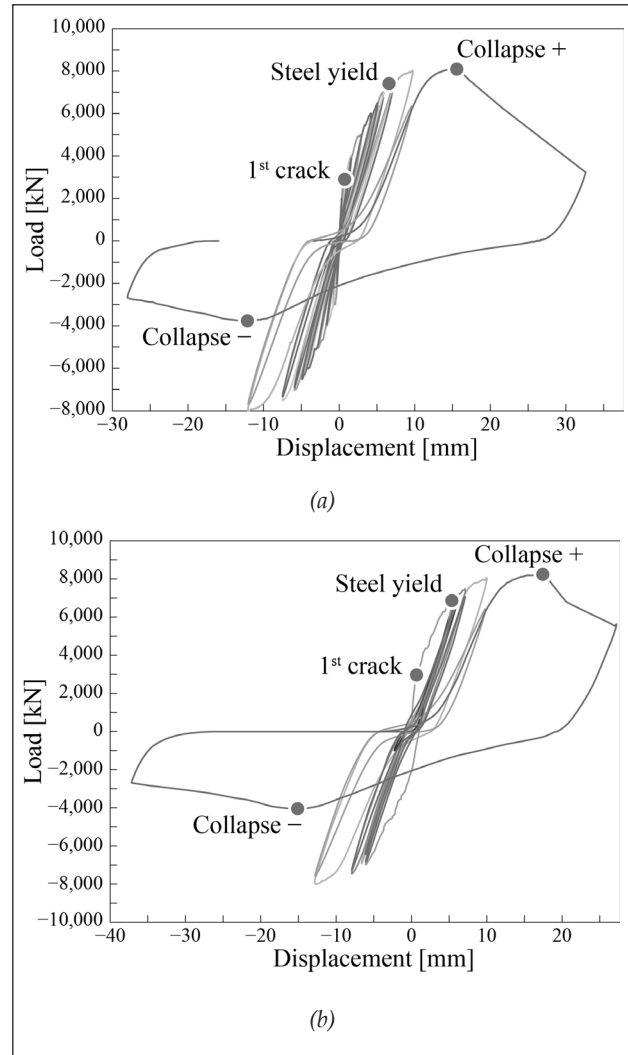


Figure 9: Crack pattern at the end of the test of wall 2 (penultimate and ultimate cycles).

In the load-displacement curves of the test in Figure 8 pinching around the origin can be seen. The phenomenon of pinching is due to sliding between the already cracked surfaces of concrete before they come in full contact. This can be observed in the hysteresis curves where the sign of the shear force changes upon load reversal. This action of sliding across a shear crack can be explained in terms of Coulomb friction. Under extensive shear load a crack has been formed in the wall. As the load is reduced to zero the crack remains partially open. Once the load is applied in the opposite direction friction across the crack is small initially but as the crack begins to close friction gradually increases which translates into increased resistance of sliding. Furthermore, if reinforcement yielding has occurred upon the crack opening, it is evident that in order to close the crack completely the reinforcement must yield in compression. An interaction between two

phenomena exists here: sliding across the shear cracks and yielding of the reinforcement. Both mechanisms contribute to the plastic behavior of the wall. The features related to these phenomena are observable in the load displacement plots in Figure 7 and Figure 8. Next, damping and shear properties for the selected specimens are calculated and discussed.

3.1. Damping

Damping is a fundamental property of any structure, and a crucial one for dynamic applications, which can be difficult to assess realistically. Raggett[14] proposed a practical way of predicting damping for real structures. Essentially, it is based on fundamental mechanics of energy dissipation in viscous damping of an SDOF system (see Chopra [15]). A condensed description is given here.

Considering an SDOF system in a steady-state motion with harmonic excitation the energy dissipated by viscous damping can be expressed as

$$E_D = \int_0^T (c\dot{d})\dot{d}dt = \pi c\omega D^2 = 2\pi\zeta \frac{\omega}{\omega_n} kD^2 \quad (1)$$

where T is the period, c is the damping coefficient, $d(t)$, $\dot{d}(t)$ are displacement and velocity respectively, k is the stiffness, ζ is the damping ratio and D is the maximum displacement in the cycle. The energy dissipated is proportional to the square of the amplitude of motion. Analogously the elastic energy belonging to the spring of the system is related to the maximum amplitude of the cycle as

$$E_S = \int_0^T (k\dot{d})\dot{d}dt = \frac{1}{2}kD^2 \quad (2)$$

The damping force is defined as

$$f_D = c\dot{d}(t) = c\omega\sqrt{D^2 - d(t)^2} \quad (3)$$

which can be rewritten as an equation of an ellipse

$$\left(\frac{d}{D}\right)^2 + \left(\frac{f_D}{c\omega D}\right)^2 = 1 \quad (4)$$

As the $f_D - d$ curve is a hysteresis loop the area enclosed by the ellipse, which equals $\pi c\omega D^2$, gives the dissipated energy. Now the damping force can be calculated based on the energy of a cycle as

$$f_D = \frac{E_D}{\pi D^2} \sqrt{D^2 - d^2} \quad (5)$$

Finally, the equivalent viscous damping is commonly defined by equating the energy dissipated in a vibration cycle of an actual structure with that of the equivalent SDOF viscous system. The energy dissipated in the actual structure in a hysteresis loop is the area enclosed by this loop and for discretized data can be computed using the trapezoidal rule

$$E_D = \sum_1^{N-1} f_{av,n}(d_n - d_{n+1}) \quad (6)$$

where N is the number of data points in the record and $f_{av,n}$ is the average force at step n . Placing this equal to the energy dissipated in viscous damping yields

$$\zeta_{eq} = \frac{1}{4\pi} \frac{E_D}{E_S} \text{ for } \omega = \omega_n \quad (7)$$

The elastic energy of the system is required next, and here we must realize that the total force measured in an experiment is the sum of the elastic and damping forces

$$f^M = f_S + f_D = kd + c\omega\sqrt{D^2 - d^2} \quad (8)$$

which then allows for the extraction of the elastic force f_S once f_D is known. Eventually, to calculate the elastic energy of the cycle E_S we need an equivalent stiffness for the entire hysteresis loop. This can be achieved by applying a linear regression of f_s over the cycle as

$$k = \frac{N\sum(df_s) - \sum d\sum f_s}{N\sum d^2 - (\sum d)^2} \quad (9)$$

As an alternative, for the sake of comparison, Igarashi's modification of Jacobsen's approach was also implemented. The easiest explanation of the method is a graphical one depicted in Figure 10.

Based on the methods described above the equivalent damping ratios for each test cycle were computed and are presented in Figure 11. The ultimate "cycle" in which failure occurred is omitted. The final values of equivalent damping by Raggett's method were computed for an average equivalent stiffness based on various stiffness estimates by linear regression and slope calculation between the centers of mass of the positive and negative segments of the loop. The resulting damping ratios are thought to represent material damping. For wall 4 the first eight cycles (at 0.5MN) show a more or less constant damping. The same is true for the first ten cycles

of wall 2. As the load increases the damping ratio decreases on average. Reviewing the energy plots in Figure 12 one can see that the proportion of the dissipated and elastic energies changes in favor of the elastic energy which means long and narrow cycles, mostly as an effect of pinching. This means that in general the damping ratio decreases with increased pinching in large deformation cycles. For such cycles the dissipated energy can get lower in proportion to the spring energy.

In case of wall 4 it should be noted that the first cycle to a defined load level always has a higher damping ratio than the subsequent cycle which reached a lower maximum load level. Looking at the result for wall 2 a similar trend is not visible for the lower level load cycles after the major cycle 11 (at 7.0MN). Only when loads are driven above the 7.0MN level does the damping ratio increase again and show the drop in value on the second repetition cycle for a given load level. The notable exception are cycles 33, 34 which can be classified as small displacement cycles meaning a low amount of pinching. Based on these outcomes it may be proposed that damping in the specimens is highly dependent on the current state of the composite material and its history. Given a cycle when a higher load is reached then the previous maximum, that is to say the material is pushed beyond its previous limit, a higher damping is realized. The element vibrating within its previously established limits can be expected to exhibit lower amounts of damping. Moreover, more pinching yields lower damping. Generally, equivalent damping is an equivalent to all mechanisms of energy dissipation involved. In our case the damping ratios computed

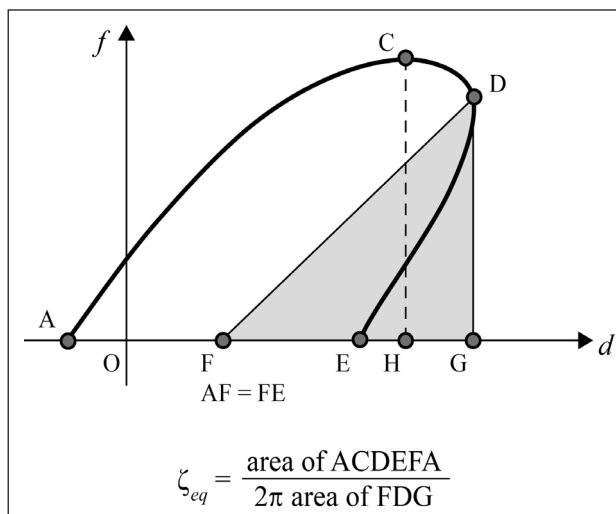


Figure 10: Method to evaluate equivalent damping according to Igarashi.

are assumed equivalent to the material damping in the hysteresis loops since no significant energy loss was possible through the boundary conditions also due to the slow rate of the tests. Since reinforced concrete is a composite material and it gradually deteriorates, slippage and friction bonding along the cracks occurs, the material damping manifests itself rather in the character of structural damping.

3.2. Shear Capacity

The final capacity of wall 4 in the negative direction, the direction the experiment started in, was 8117kN. It is useful to compare this with values calculated using various standards. Details are given below.

Eurocode 2, Clause 6.2.5

As the Eurocode 8 does not have specific provisions for low-rise shear walls the shear-friction concept is taken. The shear resistance of the wall connection plate at its bottom is to be calculated as

$$v_{Rdi} = cf_{ctd} + \mu\sigma_n + \rho f_{yd}(\mu \sin \alpha + \cos \alpha) \leq 0.5v f_{cd} \quad (10)$$

where c and μ are factors depending on the roughness of the interface, $f_{ctd} = \alpha_{ct} f_{ctd,0.05} / \gamma_c$, σ_n is the stress per unit area caused by the normal force, $\rho = A_s / A_i$, A_s is the area of the reinforcement crossing the interface, A_i is the area of the interface, α is the angle between the shear friction reinforcement and shear plane. On the right-hand side v is the reduction factor for concrete cracked in shear and f_{cd} is the design compressive strength of concrete. According to the code only the first term is factored with the material safety factor for concrete while the second term is taken at full value and the third term constituting the reinforcement is factored with γ_s . The shear capacity of the wall according to the EC2 equation is 5655kN, (without safety factors equals 5805kN).

US code ACI 349, Clause 11.7

Design provisions are given in ACI 318 for regular structures and ACI 349 for nuclear structures. This approach may be applied when shear transfer across a given plane is warranted. The nominal shear force is taken as

$$V_n = A_{vf} f_y (\mu \sin \alpha + \cos \alpha) \quad (11)$$

where μ is the coefficient of friction, A_{vf} is the area of reinforcement in the shear plane, f_y is the

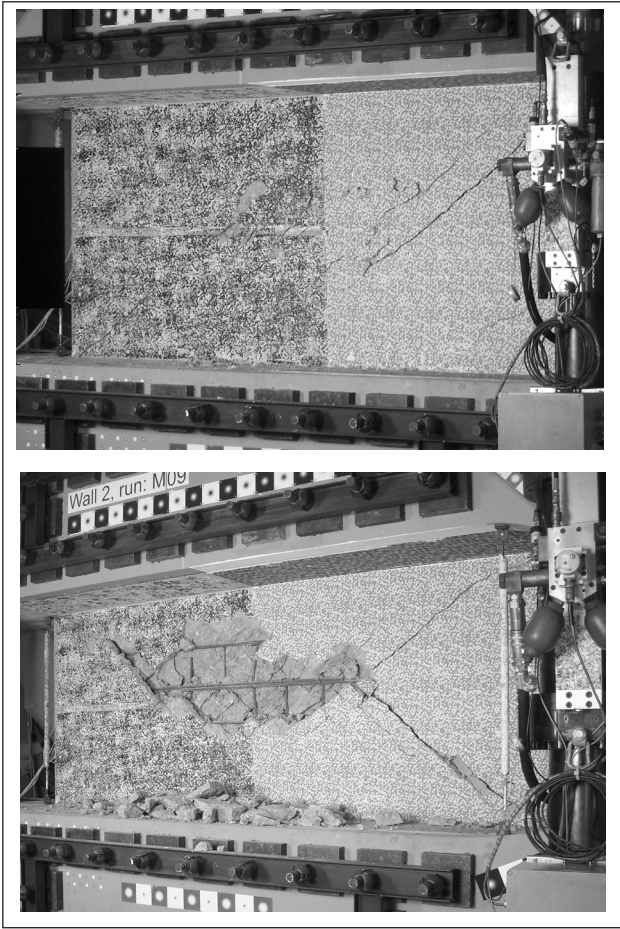


Figure 11: Equivalent damping estimates for each test cycle by both methods for wall 4 (a) and wall 2 (b).

yield strength of the reinforcement and α is the angle between reinforcement resisting shear and the shear plane. The value of V_n is limited between $0.2f_c A_c$ and $5.5A_c$. In this code the safety factor is not material but rather behavioral. For shear phenomena the factor is $\phi = 0.75$. Although the above equation does include a term for normal pressure the ACI 349 permits to add it to $A_{vf} f_y$ when calculating the required A_{vf} . The shear capacity of the wall including the effect of the axial force and applying the given safety factor is 4087kN, while without the safety factor capacity equals to 5450kN.

US code ACI 349, Clause 11.10

A special provision is given for shear transfer in case of walls. In term of shear stresses the capacity is given as follows

$$v_f = 0.75(0.216\sqrt{f_c} + 0.2\sigma_u + 0.8\rho_t f_y) \quad (12)$$

where f_c is the concrete strength in compression, σ_u is the normal stress pre unit area and ρ_t is the ratio of reinforcement resisting shear. Based on

this formula the wall strength is evaluated at 4340kN.

US code ACI 349, Clause 21.7.4

A special clause is given for low-rise shear walls with aspect ratio $H/L \leq 1.5$. The factored capacity per unit area is given by

$$v_f = 0.75(0.25\sqrt{f_c} + \rho_t f_y) \quad (13)$$

where ρ_t is the ratio of reinforcement resisting shear. The wall capacity according to this equation is 5137kN.

A commonly used approach for checking the shear capacity of walls applied in many cases over the years is Hirosawa's formula which is presented here

$$V_{ult} = \left(\frac{0.0679\rho_t^{0.23}(f_c + 1.76)}{\sqrt{\frac{M}{VL} + 0.12}} + 0.845\sqrt{f_{wh}\rho_{wh}} + 0.1\sigma_0 \right) t j \quad (14)$$

where ρ_t is the effective tensile reinforcement ratio as percentage equal to $(100A_{st})/t(L - a_l/2)$, A_{st} is the area of the longitudinal reinforcement in the tension side boundary region, $M/(VL)$ is the shear span to depth ratio, M is the moment at the base of the wall, V is the base shear at the wall, ρ_{wh} is horizontal wall reinforcement ratio, f_{wh} is the yield stress of the horizontal reinforcement, t is the thickness of the wall section, σ_0 is the average axial stress per unit area, $j = 7/8(L - a_l/2)$, L is the length of the wall and a_l is the length of the boundary wall edge region usually taken as 10% of wall length. The shear span M/V calculated in an elastic calculation is $\lambda=0.912$. The ultimate shear capacity of the tested wall according to Hirosawa's formula excluding all safety factors is 5553kN.

Table 1: Shear capacity of wall specimen as predicted by various formulae.

	w/o safety factors[kN]	factored for safety[kN]
EN 1992	5805	5655
US 349 - 11.7	5450	4087
US 349 - 11.10	5787	4340
US 349 - 21.7	6849	5137
Hirosawa's formula	5553	

Table 1 sums up the capacity predictions of the multiple approaches presented. The ultimate

shear loads from the tests were $P_{W1} = 8053\text{kN}$, $P_{W2} = 8279\text{kN}$, $P_{W3} = 8117\text{kN}$, $P_{W4} = 7997\text{kN}$. The actual bearing capacity of the wall in shear proved to be significantly higher than the values predicted by codes. The reason that can be given for this is the failure mechanism in which the wall eventually failed. All walls failed in shear compression, i.e. by crushing concrete in the center region of the wall whereas the codes treat the shear walls in general and in nuclear facilities by way of a friction concept which is an estimate of the joint strength seen as a weak point.

To assess the strength of a shear wall realistically a more elaborate analysis must be undertaken. Based on a strut and tie model the strength of the wall specimen can be estimated to be close to 8000kN which is much more in line with the outcome of the tests.

4. Summary

Thick short shear walls have been tested in a novel way where shearing was the dominant mode of behavior all the way to failure. The shear wall had a thickness of 40cm to closer represent a structural part existent in nuclear facilities. A special loading device was constructed allowing a symmetrical closed system loading. An elaborate displacement and rotation control was needed at the load transfer point. Additionally, the top of the specimen was held horizontal to promote shear behavior. The quasi-static loading was administered in cycles of preconceived load levels. The unilateral response of the wall was monitored by a group of horizontal and vertical transducers. On the resulting load displacement curves features of degradation are identifiable. Data for wall 2 and wall 4 were primarily processed. Points of interest have been identified in the data and it was established that the load history does not affect yield force significantly at the rate the test were conducted. It does, however influence the displacement at which the yield force is reached. A higher number of smaller cycles leaves the concrete more cracked and yield force is reached at higher displacement in a major cycle (wall 4) as opposed to the case when a major cycle was administered right away (wall 2).

The failure loads in the initial loading direction were closely matched around the 8110kN average. The mechanism of the failure was identical in all cases specifically the concrete was crushed in the middle of the wall. The experimental strength was rather high compared to various design checks based on different codes. Differences based on these comparisons ranged from 43% to 98%. It is well to be noted though, that

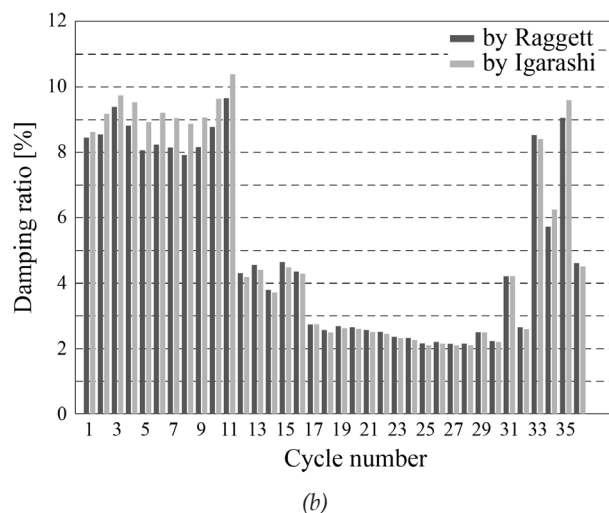
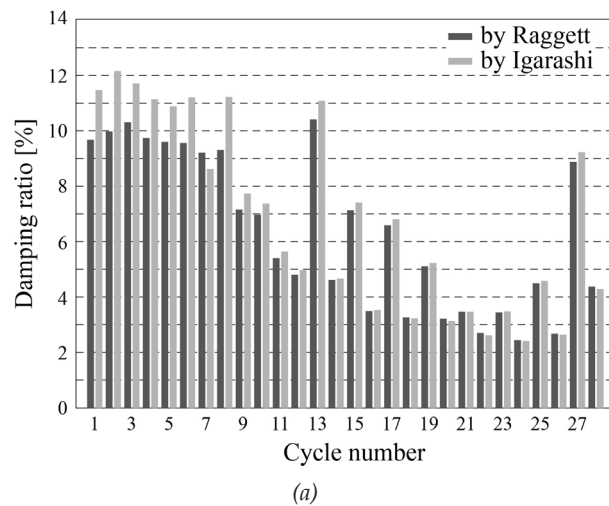


Figure 12: Energy dissipated in each cycle and elastic energy by Raggett and Igarashi for wall 4 (a) and wall 2 (b).

the failure mechanisms in the case of the experiment versus the codes are not comparable. However, when a more matching failure mechanism is reflected, the analysis of the shear wall resulted in a more closely matched estimate of its strength. The data was further investigated to assess hysteretic damping. The resulting damping ratios, calculated by two methods, range from values significantly higher than assumed by design to about half of those, yet remain relatively high on average. This should be viewed positively as the damping values essentially reflect available material damping only.

References

1. Galletly G.D., 1952, "Behavior of reinforced concrete shear walls under static load", Department of Civil and Sanitary Engineering, MIT Cambridge, MA.
2. Benjamin J.R., Williams H.A., 1957, "The behavior of one-storey reinforced concrete shear walls", Journal of the Structural Division, ASCE, 83:1-49.

3. Benjamin J.R., Williams, H.A., 1960, "Reinforced concrete shear walls assemblies", *Journal of the Structural Division, ASCE*, 86 (8):1-32
4. Paulay T., 1975, "Design aspects of shear walls for seismic areas", *Canadian Journal of Civil Engineering*, 2(3):321-344.
5. Barda, F., 1972, "Shear strength of low-rise walls with boundary elements", PhD dissertation, Lehigh University.
6. Lopes M.S., 2001, "Experimental shear-dominated response of RC walls", Part I: Objectives, methodology and results. *Engineering Structures*, 23:229-239.
7. Lopes M.S., 2001, "Experimental shear-dominated response of RC walls", Part II: Discussion of results and design implications. *Engineering Structures*, 23:564-574
8. Salonikios T.N., 2002, "Shear strength and deformation patterns of R/C walls with aspect ratio 1.0 and 1.5 designed to Eurocode 8 (EC8)", *Engineering Structures*, 24:39-49.
9. Brun M., Reynouard J.M., Jezequel L., 2003, "A simple shear wall model taking into account stiffness degradation", *Engineering Structures*, 25:1-9
10. Thomson E.D., Perdomo M.E., Picón R., Maranteb M.E., Flórez-López J., 2009, "Simplified model for damage in squat RC shear walls", *Engineering Structures*, 31:2215-2223.
11. Brun M., Labbe P., Bertrand D., Courtois A., 2011, "Pseudo-dynamic tests on low-shear walls and simplified model based on the structural frequency drift", *Engineering Structures*, 33:769-812
12. Eurocode 8, 2010, "Design provisions for earthquake resistance of structures", Part 1-3: General rules - Specific rules for various materials and elements. CEN: European Committee for Standardization, Bruxelles.
13. ACI Committee, 2011, "Building code requirements for reinforced concrete (ACI 318)", American Concrete Institute, Michigan.
14. Raggett J. D., 1975, "Estimating damping of real structures", *ASCE Technical Publication*, :1823-1835.
15. Chopra, A.K., 2007, "Dynamics of structures", Prentice Hall, 3rd edition.
16. Igarashi K., 2000, "Damping characteristics of RC shear wall in the weak nonlinear range", 12th World Conference in Earthquake Engineering.

Ageing Behaviour of Structural Components for Integrated Lifetime Assessment and Asset Management

Robert Veit-Egerer, Helmut Wenzel, Rui Lima
VCE Vienna Consulting Engineers ZT GmbH
E-mail: veit-egerer@vce.at

Abstract

Degradation of structural components is a fact. In order to apply these changes over lifetime in precise cost models a standardized degradation law is desired. Standardization particularly helps in a competitive environment like construction to apply innovative technologies.

In CEN-workshop 63 "Condition, Determination for Integrated Lifetime Assessment of Constructed Facilities and Components" a generic degradation law has been developed. It serves to determine the design life or the residual life of existing structures, helps to assess the real degradation process and enables the development of optimized maintenance plans.

Keywords: *Degradation law, lifetime assessment, codes and standards, asset management*

1. Introduction

Managing assets is about making decisions. From this it follows that Life Cycle Cost (LCC) and in some cases Life Cycle Benefit/Cost Analysis is a critical concept for making investment decisions, and therefore should be incorporated in the engineering and management routines of infrastructure systems.

However, several important questions remain before one may conduct a meaningful LCC analysis. These relate to the determination of the Life Cycle of a new, maintained, rehabilitated or retrofitted structure and its expected performance along the Life Cycle regarding the limit states. The impacts of uncertainty in estimating the risk involved in establishing appropriate demand envelopes for various limit events are significant for LCC analysis in design and in maintenance management.

The present article was prepared by CEN Workshop 63 "Condition Determination for Integrated Lifetime Assessment of constructed facilities and Components" the secretariat of which is held by ASI. It was developed through close collaboration with experts from the IRIS project "Integrated European Industrial Risk Reduction System", supported by the European Union's Seventh Framework Programme. Work in this project was organized in eight work projects.

In the course of the IRIS project methodologies for Life Cycle Management of constructed infrastructure were developed. In order to meet the infrastructure

owner's governing requirements regarding safety, operability and durability, the present article addresses the following major aspects:

1. The determination/estimation of the design life of new structures
2. The determination/estimation of the residual life of existing structures
3. Assessment criteria whether the real degradation process - determined by proper technologies - corresponds with the assumed and applied Life Cycle Model, in order to take corrective measures in cases of accelerated ageing
4. Maintenance instructions to ensure the intended service life

In IRIS WP 3 and WP 7 and CEN Workshop 63 experts from universities, consultancies, public authorities and standardization bodies contributed to the work. The present article has received the support of representatives of these sectors.

2. Scope

2.1 Ageing Model

The objective of the article is to elaborate a standard framework for the results of the IRIS Project, while it is recognized that there cannot be one extensive methodology fit for all specific industries.

There is a simple basic model with considerable uncertainties, which is improved step by step through introduction and evaluation of new

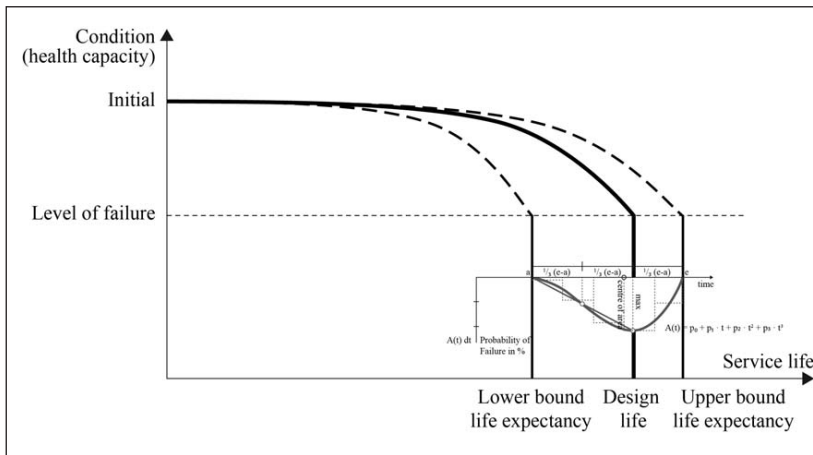


Figure 1 – General concept of structural ageing

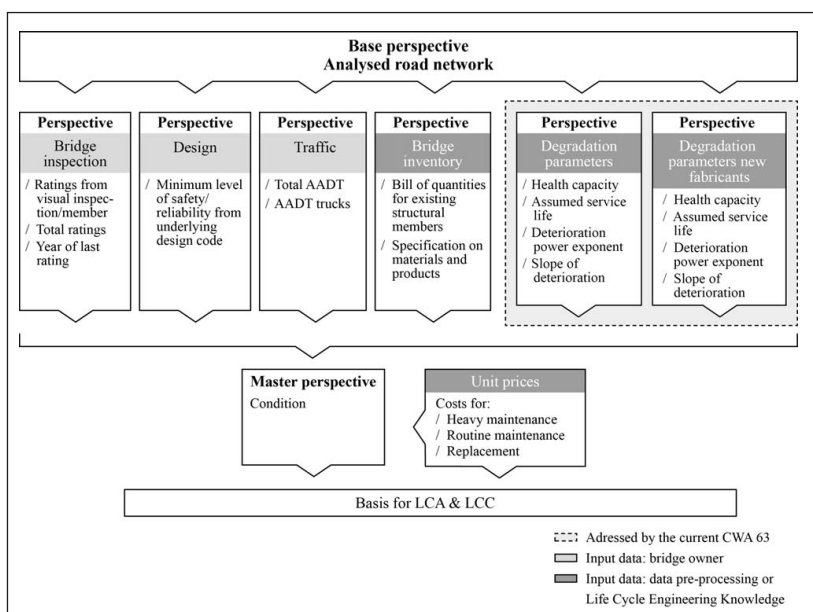


Figure 2 – Input data with regard to Life Cycle Analysis (LCA) and Life Cycle Cost Analysis (LCCA)

knowledge gained about a structure. The ideal result is a precise assessment of the condition with reasonable margins of uncertainty. The model is able to show the successive impact during the long-term deterioration process as well as the effect of sudden changes in condition (retrofit actions or local failure). It is recognized that the individual results from visual inspection and assessment will influence the quality of the prediction. Nevertheless after a number of assessments these uncertainties will be reduced to reasonable levels.

It is acknowledged that the basic model shall be kept simple and transparent for the end-users. In return the background computation is expected to become more and more complex with every new knowledge and methodology developed.

Therefore the concept is to give a common understanding on structural ageing in general, which can be incorporated into different industrial applications and adapted regarding the industry-specific demands.

In further consequence the focus of the chapter is on the area of bridge infrastructure, as there the most mature status within the IRIS Project has been reached.

The aspect of acceptance of structural failure and accidents is always depending on the involved individual society. The current document already reflects the current situation in Austria, Germany, the Netherlands and the USA.

2.2 Background – Asset Management

In the following an overall assessment scheme for asset management on the network level is described very briefly. The scheme is divided in two main processes:

- Flowchart 1: Input data with regard to Life Cycle Analysis (LCA) and Life Cycle Cost Analysis (LCCA) (as shown in Figure 2)
- Flowchart 2: LCA and LCCA itself, addressing the determination of

maintenance schedules (composed by individual treatments) and linked to budget category-related optimization (as shown in Figure 3).

In both flowcharts those parts, being explicitly covered by the current chapter are highlighted (yellow marking) and are discussed in full detail in the following chapters.

It is to be pointed out, that the shown assessment scheme utilizes conventional ratings (from structural inspection), which are usually available for every structure or can easily be provided. Neither the assessment scheme itself or the underlying rating process are intended to be standardized – but the curve describing structural ageing (Lifeline). Thus the intention of this article is to improve the current practice of maintenance budget planning based on

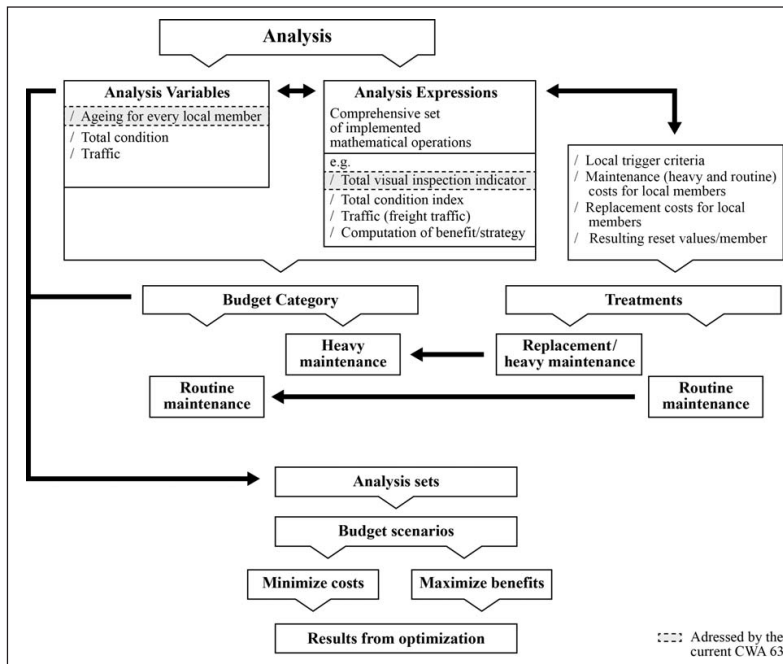


Figure 3 – Life Cycle Analysis (LCA) and Life Cycle Cost Analysis (LCCA)

ratings. The given ratings are transformed into health indices and incorporated into comprehensive Life Cycle Calculations. By this means the gap between rating and service life considerations is bridged.

Previous activities and work of other groups worldwide have already produced a basic set of standards. The most sophisticated procedure is established in Germany, where based on existing DIN-standards, specific rules for application in different industries are being developed by VDI (Verein Deutscher Ingenieure). A dense network of certification agencies (managed by TÜV) takes care of sound and safe procedures. Nevertheless the current practice does not take account of the typical end of life situation with assessment of lifetime extension.

In terms of standards, there are no referenced documents being indispensable for the application of this document. Certain relevant literature and a list of standards giving an overview on the related activities have been added to the bibliography.

3. Terms and Definitions

For the purposes of this document, the following terms and definitions apply.

Ageing

Degradation due to long-term influence of operational conditions related to use

Assessment

Set of activities performed to verify the reliability of an existing structure for future use

Asset

Whole building or structure or unit of construction works, or a system or component or part thereof

Capacity

Capacity to perform

Capacity describes the resistance of a member or component, or a cross-section of a member or component of a structure to actions without mechanical failure e.g. bending resistance, buckling resistance, tension resistance.

Condition; Health

Characteristic of a structure, system

or component which can be observed, measured or trended to infer or directly indicate the current and future ability of the structure, system or component to function within acceptance criteria

Degradation

Process whereby an action on an item causes a deterioration of one or more properties

Properties affected may be, for example, physical, mechanical or electrical.

Demand

Requirement for functionality

Design Life

Service life intended by the designer

Design life is also referred to as intended service life or expected service life.

Deterioration

Process which adversely affects the structural performance, including the reliability over time

Durability

Capability of a structure or its parts to perform its required function over a specified period of time under the influence of the agents anticipated in service

Failure

Loss of the ability of a structure or its parts to perform a specified function

Inspection

Regular observation, noting and reporting of structures and components

Life Cycle

All phases through which a structure passes from its manufacturing to the time it ceases to exist

It involves all levels of engineering work, including design, construction, inspection, management, repair, improvement and demolition

Life Cycle Cost (LCC)

Cost of an asset or its parts throughout its Life Cycle, while fulfilling its performance requirements

Lifeline

Numeric progression of the introduced health index over time

Limit state

Set of performance criteria beyond which the structure no longer fulfils the relevant design criteria

This reference state must be met by a structure under factored loading.

Maintenance

Combination of all technical and associated administrative actions during the service life to retain a structure or its parts in a state in which it can perform its required functions

Operability; functionality

Suitability or usefulness required by users or other stakeholders for a specific purpose or activity

Operability limit states correspond to conditions beyond which specified service requirements for a structure or structural member are no longer met.

Performance

Behaviour in service of a facility for a specified use

Perspective

Database-appropriate tables governing predefined relevant information for asset management on network level

Process

Set of interrelated or interacting activities that transforms inputs into outputs

Rating

Result of a classification process of determining the serviceability of a constructed asset

Rehabilitation

Work required to repair or upgrade an existing structure

Replacement

Changing of parts of an existing item to regain its functionality

Retrofit

Modifying existing structures with additional or new components or members in order to enhance their condition

Risk

Likelihood of the occurrence of an event or failure and the consequences or impact of that event or failure

Safety

Condition of a structure being protected against failure, damage, error, accidents or harm, in both causing and exposure

Service Life

Period of time after installation during which a facility, or its component parts, meets or exceeds the performance requirements

Service Life Prediction

Generic methodology which, for a particular or any appropriate performance requirement, facilitates a prediction of the service life distribution of a structure or its parts for the use in a particular or in any appropriate environment

Structural Member

Physically distinguishable part of a structure, e.g. a bearing, a beam, railing

Treatment

Maintenance measure

Uncertainty

Lack of certain, deterministic values for the variable inputs used in an LCC analysis of an asset

4 Performance of Bridge Components

4.1 General

All important Key Performance Indicators (KPIs) which influence the performance or durability of a structural member are to be acquired. These datasets are usually implemented into a probabilistic model for service life calculations of the individual items. The reason is to cover occurring uncertainties which have to be considered within the established maintenance plans in terms of lower and upper bound of service life expectancy.

The starting point of the bridge member's service life is mainly based on the applied design code and the underlying safety consideration in the course of the static calculations, while the ageing process in general depends on certain major sources of impact:

- year of construction (generation of the structural manufacturing),
- static system,
- material,
- cross section.

To describe the individual deterioration process properly the following additional aspects are of relevance with regard to structural performance over time:

- direct loading frequency (e.g. freight traffic volume),
- direct loading intensity (level of freight traffic impact),
- quality in manufacturing,
- environment influences (temperature, radiation, frost action),
- chemical exposure.

4.2 Service Life Expectancy vs. Prognosis on Remaining Service Life

4.2.1 Service Life Expectancy

The basis for local Life Cycle Considerations is expressed in terms of structural condition. To represent common practice in bridge engineering the set of ratings – according to the national guideline for visual inspections – is utilized. Usually these ratings are available for every bridge component (superstructure, substructure, expansion joints, bearings, pavement, edge beam, guard rail and railings, dewatering and miscellaneous facilities).

After being put into operation, each member's range of ratings represents the available (total) capacity, which is consumed over time during the entire service life. Due to that idea these ratings are converted into so-called health indices, which can be done freely, as long as this single component is analysed individually and independently from its relevance within the whole structure.

The proposed ageing law used for Life Cycle Analysis is introduced briefly. It is built on suggestions from [3] and was adapted regarding the used terms as well as the further utilization - addressing prognosis on remaining service life. In principle it covers all the major sources of deterioration.

It is to be emphasised, that the following equations are intended to describe the lifeline-progression within a stated service life expectancy. The so-called deterioration capacity $C_i(t)$ for an analysed bridge component is determined by the following formula expression:

$$C_i(t) = C_I + a_n \times (S_i - S_I)^c \quad (1)$$

with

$$a_n = (C_F - C_I) / (S_F - S_I)^c \quad (2)$$

where

C_I initial condition

a_n slope of deterioration

S_i current year of service life

S_I initial year of service life

c deterioration power exponent; empirical, constant value derived from sensitivity analysis; for bridge components $c = 3$ is established

C_F final condition (early-warning level)

S_F final (assumed) year of service life

The ranges for service life expectancy and the total deterioration capacity are of course to be known in advance. An example can be studied in chapter 4 (example 1). Certain details on the input data for different types of structural members, materials and product types can be taken from [4]. They are based on literature, bridge owner databases and long-term expert experience (generic approach). The tables elaborated in [4] address certain infrastructure only (bridges, gantries). As the approach is generic the methodology could be adapted (mainly with regard to c and a_n) and transferred to other infrastructure.

The following visualization, Figure 4, corresponds with the previous formula expressions. The given

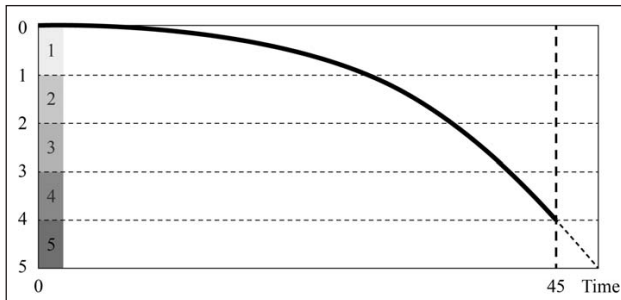


Figure 4 – Superstructure life expectancy “do-nothing-strategy”

lifeline can be understood as a reference progression for a continuous observation process during operation with regard to corrective measures in order to ensure the intended service life timeframe. In cases that certain bridge components reach the stage of being rated with 4, bridge operators are usually forced to take action with regard to maintenance measures. As the preparation and performance of these measures can still take some time (even years) in practice, the end of rating 4 is defined to be the end of service life. Rating 5 is equivalent to the level of failure and is not accepted in the context of long-term maintenance planning (as this rating reflects a stage, where the structure or component cannot be operated anymore).

4.2.2 Prognosis on Remaining Service Life

When performing Life Cycle Prognosis, the deterioration capacity $C_i(t)$ which has been used so far, is still the guiding parameter, although the introduced formula expressions are to be adapted:

$$C_i(t) = a_n \cdot \left(\sqrt[c]{\frac{C_{i-1}}{a_n}} + 1 \right)^c \quad (3)$$

Equations (1) and (3) represent the deterioration capacity $C_i(t)$ and are quite similar. However, one is intended to be used to follow the stepwise lifeline progression within a process, which is defined in terms of service life expectancy of a certain structural member (equation 1). The other (equation 3) supports prognosis on remaining service life with regard to threshold analysis and corresponding decision making. The main difference between the two equations is the fact, that the derived prognosis-equation also incorporates the deterioration capacity from the previous year in order to compute the remaining capacity for a current year of service life.

The starting point for local Life Cycle Calculation is linked to the latest rating according to the national guideline for visual inspections. Usually it is available for every bridge component (superstructure,

substructure, expansion joints, bearings, pavement, edge beam, guard rail and railings, dewatering and miscellaneous facilities). These ratings are again converted into so called health indices. Based on the calculated health index for each bridge component and its underlying inspection year a first deterministic lifeline prognosis is performed. This lifeline considers all available information at the time of investigation and assumes the so-called “do-nothing-strategy” (unrestricted deterioration) during the entire service life.

Consequently the derived lifeline is used as the basis for the elaboration of the maintenance schedules. During the progression of the analysed lifelines (annual analysis variables) routine or heavy maintenance interventions and finally replacement measures of the analysed structural member can be triggered. The introduction of trigger mechanisms is linked with stages, when the structural members are appearing e.g. in the range of rating 3 (maintenance works) or in the range of rating 4 (retrofit, replacement).

The trigger mechanisms, deciding about maintenance and replacement, are defined by deterioration analysis on every single structural component, leading to an entry in the maintenance plan to be scheduled. For further details see chapter 5.

5 Lifeline Calculation

5.1 Example 1: Life Expectancy

In order to follow the service life expectancy of a certain member it is necessary to define the input data for the equation’s progression first. Figure 4 gives an example for a bridge superstructure. The used input data as well as the progression of structural deterioration can be seen in Figure 4.

5.2 Example 2: Prognosis and Probable Impact of Remaining Service Life

The starting point for the prognosis on remaining service life is represented by the rating from the latest visual inspection – having been transformed into a health index. As the first year of Life Cycle Calculations will mostly not correspond to the year when the visual inspection was carried out, Visual Inspection Indicator (i.e. health index) is to be adapted before using it as a starting point for lifetime prognosis. This process differs from the service life expectancy process as it incorporates trigger mechanisms regarding structural retrofit and preventive maintenance. In Figure 5 these

effects can be seen.

The lifting in the calculational annual-analysis-variable results from interventions, where certain treatments were applied, and consequently the condition was improved. The extent of the lift depends

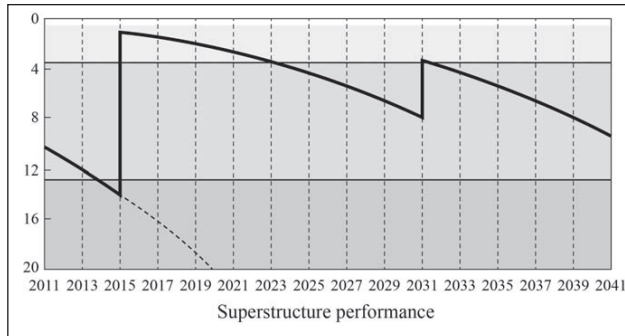


Figure 5 – Prognosis and probable impact of remaining service life

on the type of intervention and on the incorporated structural member.

Analyses like the one described in the present example are the basis for long-term maintenance planning for highway infrastructure. Depending on the underlying strategy, minimize cost or maximize

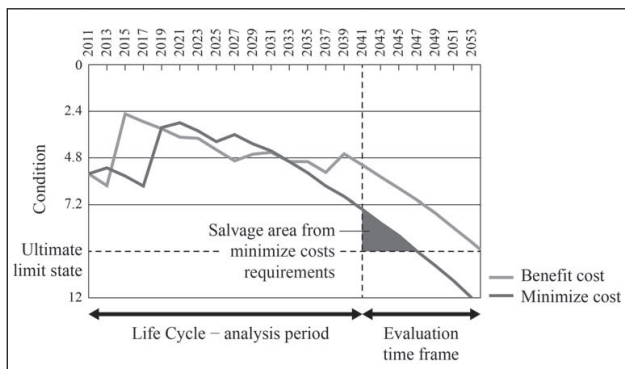


Figure 6 - Minimize cost strategy

benefit considerations can be the driving boundary conditions for Life Cycle Analysis of single structures or structural networks (see Figures 6 and 7).

6. Benchmark Values on Service Life in Bridge Components

In [4] input data for lifeline calculations are available. It underlines the consistency between benchmark data available in literature and in an already existing guideline. The unrestricted ageing case (do-nothing strategy) is represented as well as the corresponding service lifetimes including preventive maintenance. The latter leads to ranges of total service life which are achieved in the course of calculational lifetime prognosis presented in chapter 4.

References

1. Veit-Egerer R. and Widmann M., 2010, "Life Cycle Methodology & Durability Analysis with Regard to Relevant Heavy-Maintenance Instructions. VCE-WD 220; IRIS (Integrated European Industrial Risk Reduction System - IP: SP3 & 7); European Commission FP7; Project No.: FP7-NMP-2007-LARGE-1.
2. IAEA Safety Glossary - Terminology used in Nuclear Safety and Radiation Protection, 2007.
3. MIYAMOTO A., ISHIDA J., 2008 "Bridge maintenance strategy based on life-cycle cost and rebuild cost stabilization, Bridge Maintenance, Safety, Management, Health Monitoring and Informatics" - Koh&Frangopol (eds), Taylor & Francis Group, London, ISBN 978-0-415-46844-2.
4. prCWA 63:2012 (E)2012, "Ageing Behaviour of Structural Components with regard to Integrated Lifetime Assessment and Subsequent Asset Management of Constructed Facilities", CEN Enquiry (TC), ON Secretariat, June 2012.
5. EN 206-1, 2000 Concrete - Specification, performance and conformity.
6. EN 1990 to 1999, 2002-2007 Eurocode, all parts.
7. EN 15331, 2008, Criteria for design, management and control of maintenance services for buildings.
8. EN 31010, 2008, Risk management - Risk assessment techniques (IEC 56/1268/CDV).
9. ISO 13822, 2009, Bases for design of structures - Assessment of existing structures (Revision of ISO 13822:2001).
10. ISO 13823, 2008, General principles on the design of structures for durability.
11. ISO 13824, 2008, Bases for design of structures - General principles on risk assessment of systems involving structures.
12. ISO 14040, 2008, Environmental management - Life cycle assessment - Principles and Framework.
13. ISO 14044, 2006, Environmental management - Life cycle assessment - Requirements and guidelines.
14. ISO 14963, 2003, Mechanical vibration and shock - Guidelines for dynamic tests and investigations on bridges and viaducts.
15. ISO 15686-1, 2008, Buildings and constructed assets - Service life planning - General principles and framework.
16. ISO 15686-2, 2001, Buildings and constructed assets - Service life planning - Service life prediction procedures.
17. ISO 15686-7, 2006, Buildings and constructed assets Service life planning - Performance evaluation for feedback.
18. ISO 15686-8, 2008, Buildings and constructed assets - Service-life planning - Reference service life and service-life estimation.
19. ISO 15686-10, 2008, Buildings and constructed assets - Service-life planning - When to assess functional performance.
20. ISO 16587, 2004, Mechanical vibration and shock - Performance parameters for condition monitoring of structures.
21. ISO 18649, 2004, Mechanical vibration - Evaluation of measurement results from dynamic tests and investigations on bridges.
22. ISO 31000, 2008, Risk management - Principles and guidelines.

An Approach for Reliability Based Control of Post-Tensioned Containment Structure

Alexander ILIEV, Marin KOSTOV, Anton ANDONOV

Risk Engineering Ltd, Sofia, Bulgaria
Alexander.Iliev@RiskEng.bg

Abstract

Structural elements like the post-tensioning of a containment structure of a nuclear power plant are currently reviewed on 30 year old partly destructive approaches. A reliability based control approach is desired. The feasibility of applying the IRIS Risk Paradigm to establish a consistent approach for reliability based control of post-tensioned containment structures has been demonstrated.

Keywords : Condition assessment, health index, degradation over time

1. Introduction

The world's nuclear power plants are, on average, 25 years old [1] (Figure 1) and most plants are believed to be able to operate for 60 years or more. The design lifetime of a nuclear power plant is typically 30 to 40 years. This may be extended by 10 to 20 years or more provided that the plant operator can demonstrate by analysis, trending, equipment and system upgrades, increased vigilance, testing, ageing management and other means that licence renewal or permission to continue operation based on the original licence poses no threat to public health, safety or the environment.

Special emphasis should be put on the assessment of the aged status and ageing management of those safety-related systems, structures and components that limit the operating lifetime of the plant, i.e. those that cannot be replaced or readily reconstructed, such as the reactor pressure vessel and containment.

An essential component of the nuclear power plant safety is the structural capacity of the containment structure. The containment has to prevent the reactor installation from external impacts, as well as to provide a tight physical barrier against release of radioactive materials in case of severe internal accidents. Therefore, the containment structures are designed to resist to internal pressure and temperature loadings. Common practice is to use post-tensioned concrete for NPP containment structures. The design post-tensioning force is selected in such a way that the produced equivalent external pressure overlaps the expected internal pressure caused by Design Basis Accident (DBA) and thus provides elastic response of the containment structure. The containment ultimate capacity itself is a complex parameter and cannot be considered as a constant value. Generally it depends on a series of variables, e.g. the material properties of the concrete, the liner, the reinforcement and the tendons respectively, as well as the structural

composition - the structural system, the arrangement of the post-tensioning tendon system, the presence of penetrations and openings and the measures to mitigate the stress concentrations caused thereof, the arrangement of the liner welding and anchors, etc. In addition, for the case of non-grouted tendons, the actual post-tensioning force can be considered as variable rather than constant; it can be influenced by many time-

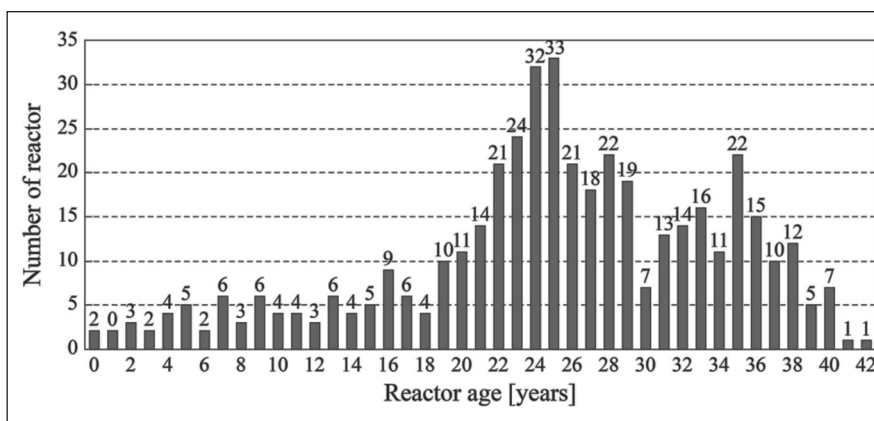


Figure 1: Number of Reactors in Operation by Age (as of 31 Dec. 2009)

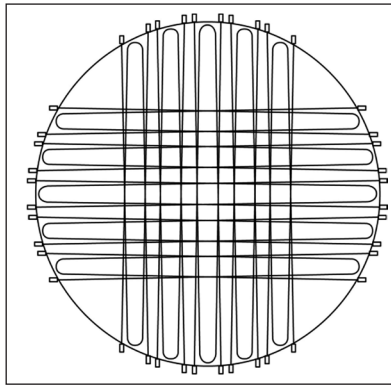


Figure 4: Arrangement of the Prestressing Tendons in the Dome Part

used at both ends of each tendon consisting of ear / koush / anchor screw and nut with pads.

The area of the cross section of one cable is 140 mm². High strength cables are made from cold drawn wire technology in low temperature under pressure, which achieves high physical and mechanical characteristics. The tendon 55 Ø15.2B7 has an area of 7700 mm², ultimate force of 14300 kN and design post-tensioning force of 9810 kN.

The anchoring device includes an anchor block, 55 pcs three-part wedges, anchor screw and nut with pad. The anchor block is a new element representing a steel plate with a thickness of 200 mm with an external threaded bearing S45 °360x16. Each anchor block has 55 pcs. concentric holes with a diameter 20 in which the post-tensioning cables are passing. The outer edge of opening is shaped in a manner to accommodate a three-part anchor bolt.

3. Motivation for the Current Approach

In case of post-tensioned containments, the control and maintenance of post-tensioning systems is necessary for the safe operation of the nuclear power plant (NPP). Development of non-destructive examination (NDE) and monitoring techniques and methodologies is essential, especially for the control of the ageing process at the non-accessible locations and hidden defects (for example liners in hidden places, reinforcement in massive structures, etc.).

Continuous monitoring is implemented at the start of the nuclear power plant's operation and will end when final shutdown takes place. It gives an accurate picture, throughout the lifetime of the structure, firstly of the phenomena which affect the tension of prestressing cables, and therefore the

residual compression prevailing in the structure and, secondly, of the overall and relative settlement of the reactor building.

There are basically two current approaches widely used for inspection/monitoring of the tendon post-tensioning force. The first one is based on lift-up tests. During the lift-up process, the pressure in the test press is continuously increased and recorded until the anchor is released, i.e. lifted from the supporting block. The post-tensioning force is derived from the pressure.

Another widely used monitoring approach is constant measurement of the tendon force on the anchor by strain gauge or pressure cell installed between the anchor and the supporting block. Alternatively, the tendon force can be monitored by measuring the force in few tendon cables and after that estimating the total tendon force, as shown in Figure 5.

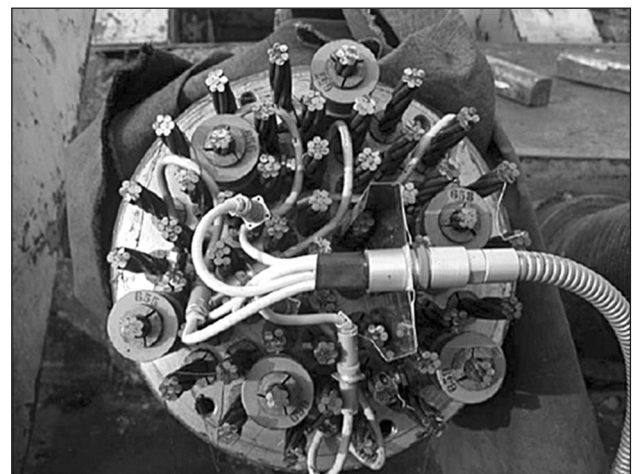


Figure 5: Monitoring of the Tendon Force by Measurement of the Cable Forces at Selected Cables

Limitations of the Currently Used Methods

The current monitoring approaches mentioned above have a number of limitations. The sensors embedded in the concrete are subjected to ageing processes which affect their reliability and they cannot be replaced. Therefore, it is not expected from such monitoring systems to be operable during the entire reactor building life.

One of the main limitations of the lift-up tests is that the test can be performed only during an outage that is usually once a year. Additionally, the lift-up test is considered relatively subjective, due to the uncertainties during detection of the anchor lift. Also,

the lift-up tests are demonstrated in the practice to have negative influence on the tendon and anchor durability.

The direct measurement of the post-tensioning force at the anchor is considered the most advanced method from those mentioned above. The disadvantage is that the installation or the replacement of the sensors requires dismantling the tendon where the sensors will be installed. Having in mind that the expected life of such sensors will be significantly shorter than that of the reactor building, such operations should be expected. However they could be performed only in an outage.

The described methods for post-tensioning force monitoring have one common disadvantage, that is measurement of the tendon force only at the anchor and that they do not take into account the tendon force distribution along the tendon length. Typical distribution of the tendon force at one regular and one irregular (around an opening) tendon is presented in Figure 6.

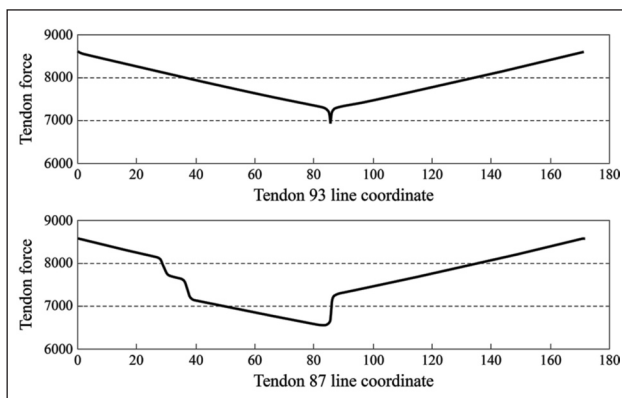


Figure 6: Distribution of the Prestressing Force along the Tendon Length

The equivalent external pressure as produced by the post-tensioning system and the containment confinement is a function rather of the average tendon force than the tendon force at the anchor. Therefore, the monitoring of the stress state of the containment structure should be based on the global tendon state, as tendon monitoring based only on anchor force readings might produce misleading conclusions.

Currently, there are many NPPs applying for license extension or already licensed to year 2030. Therefore, it is necessary to develop long-term solutions for containment monitoring procedures, which would overcome the above mentioned limitations of the current approaches. One possible solution is monitoring based on ambient vibrations

of the structure that is successfully applied to a large number of bridges [2].

4. Methodology of the Current Approach

The proposed approach, applied on NPP reactor building structure can improve the control on the overall stress state of the structure, outline particular areas of the structure with altered stress state and improve the understanding of the structural global and local behaviour. The main idea behind the proposed approach is to monitor the effects of the post-tensioning and thus indirectly the containment capacity and the overall NPP safety instead of directly measuring the post-tensioning forces in the tendons. The current approach is based on a permanent vibration monitoring system on the NPP reactor building structure, registering the ambient vibrations in different locations on the structure. Eventual changes in the stress state of the containment structure or eventual damage formations will be detected and indicated through alterations in the spectral distribution function.

The method of studying the stress state of a structure, considering alterations in the vibration amplitudes and subsequently in the spectral distribution function, is proposed by Vienna Consulting Engineers ZT GmbH (VCE) [3]. The basis of this method is that any change in the energy distribution function is related to a particular change in the stress or damaged state of a location of the studied structure. Based on a permanent vibration monitoring it is possible to follow every potential change in the frequency or the amplitudes, which will subsequently affect the energy distribution function. When isolating only the influence of the prestressing force on the structural vibrations it will be possible to evaluate the general stressed state of the structure, depending on the ambient vibrations recorded.

The proposed structural health monitoring approach is based on temporary and permanent ambient vibration measurements and finite element analyses. Firstly, numerical simulations should be executed for initial assessment of the structural modal characteristics. Attention should be paid when investigating the higher local modes of the dome and the cylinder because they are likely to be strongly affected by the stress state of the structure. Secondly, additional numerical analyses should be performed for studying the influence of the post-tensioning level on the modal behaviour of the main structural parts – dome and cylinder. The analytically obtained modal

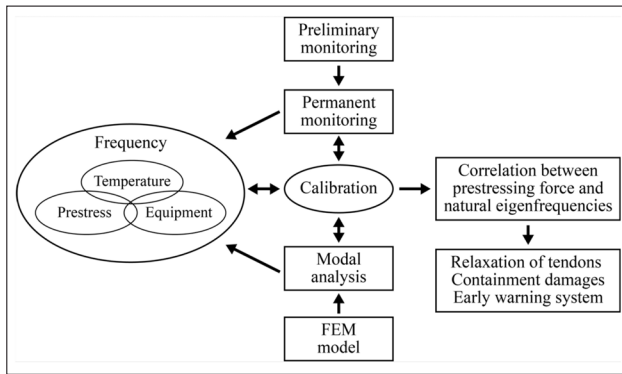


Figure 7: Methodology of the Current SHM Approach

response is compared with the response obtained experimentally through ambient vibration monitoring and if needed the numerical model will be updated through a consecutive process of finite element model updating. This procedure is based on a mathematical optimization problem: the difference between the numerical and experimental data should be minimized through iterative modal analyses. The entire process should be finalized with specific thresholds and finally implemented into an early warning system. A general methodology scheme is presented in Figure 7.

The influence of the post-tensioning force on the containment dynamic response will be studied numerically. The level of post-tensioning is expected to affect mainly the higher modes of a structure, while the global modes should remain practically unchanged [2]. The amplitude changes increase predominantly in the high frequencies with increasing the post-tensioning force of the tendons (Figure 8). These amplitude changes will affect the energy distribution function and a further step in the investigation will be to study the influence of the other factors, influencing the ambient vibrations, in order to isolate the influence of the post-tensioning force itself.

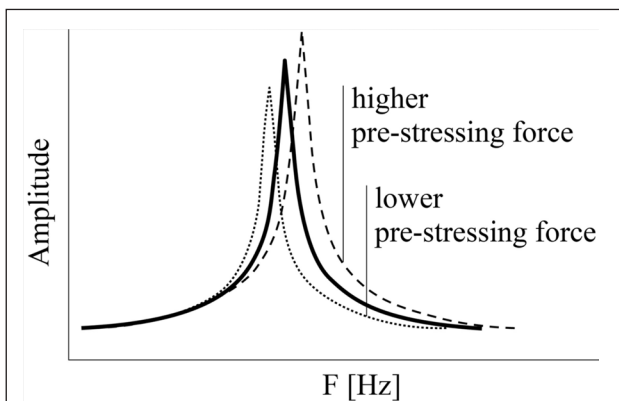


Figure 8: Influence on the Prestressing Force (Stressed State) on the Modal Behaviour of a Structure

An important step of the analysis is the comparison of the monitoring data and the results of the numerical simulations, where essential conclusions will be obtained regarding the structural mode shapes of the reactor building and the expected frequency and amplitude changes due to the factors indicated above. It is expected that the different temperature zones on the internal and external surface of the structure will affect the structural higher modes characteristics (amplitudes and/or frequencies) and thus the spectral distribution function.

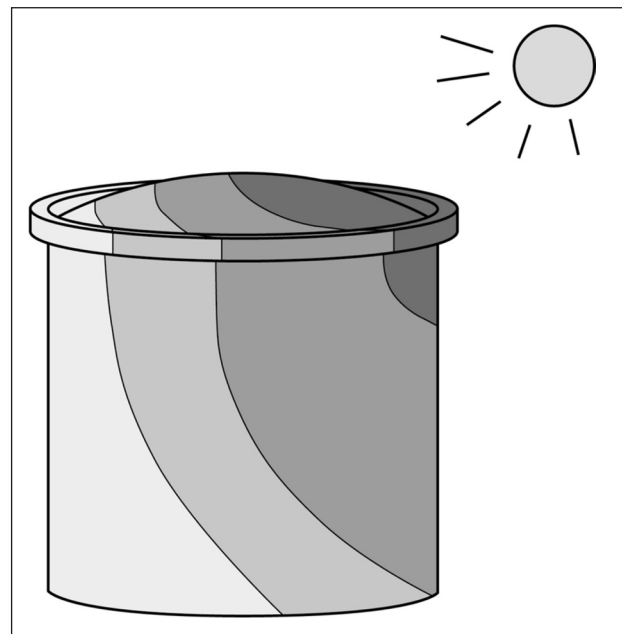


Figure 9: Zones with Different Temperatures at the Structure due to Sun Radiation

The alteration in the energy distribution function will be independently investigated for each factor affecting it, by numerical analyses. The main tool for studying the influence of the various factors on the structural dynamic response will be the complex-harmonic analyses. They will be performed for different stress states and the resulted frequency spectra in different locations of the structure will be the base for studying the correlation between the stressed state and the structural vibration behaviour.

Another main tool used in the current study will be the spectral density function. This function reveals more clearly the fraction of energy transferred to different frequency ranges, resulting in the change of its pattern. The definition of the spectral density function is presented and explained in [3] and is defined as:

$$E_i(f) = \sum_{k=0}^f F_i(k) \Delta k, \text{ where} \quad (1)$$

$$F_i(f) = \frac{G_i(f)}{\sigma_i^2} \text{ is normalized Spectral Density}$$

Function and (2)

$$\sigma_i^2 = \sum_f G_i(f) \Delta f \text{ is Spectral Distribution}$$

Function (3)

$G_i(f)$ is the acceleration spectrum, calculated by a conventional FFT routine.

The spectral density function $E_i(f)$ varies from 0 to 1 and the observed tendencies in its pattern of the function will be used to indicate the alterations in the stress state [3]. Vibration investigations should be carried out for all disturbances from the external environment acting on the structure and affecting its stressed state.

4.1 Expected Advantages of the Proposed Approach:

One of the main advantages is that the method offers continuous real-time monitoring of the containment, which in combination with appropriate thresholds and implemented into an intelligent warning system, could provide continuous information about the containment condition capability to serve as ultimate barrier. The estimated stress state could be used for subsequent containment damage detection potential in case of different accidents. Another advantage is that the proposed approach is totally non-destructive and delicate with respect to the containment structure, as far as the accelerometers can be installed and/or replaced at any time, without depending on, or disturbing the NPP operation. Furthermore, the proposed approach is based on measurement of the global effect of the post-tensioning system on the containment, rather than post-tensioning force at the anchor head, thus avoiding misleading conclusions.

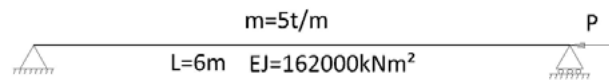
4.2 Summarizing the Main Goals of the Current Approach for SHM for the Containment Structure Are:

- i) Control of the containment stressed state;
- ii) Identification of relaxation in tendons;
- iii) Location of existing damaged or relaxed tendon;
- iv) Better understanding of the structural global and local behaviour.

4.3 Change of Dynamic Behaviour, because of Compression Stress

Considering the geometric non-linearity of the structure (second order effects) could be noted basically in the following form: $[k] = [k_{ph}] + [k_g]$, total stiffness of a given structure is a sum of its physical and geometric stiffness. Geometric stiffness is in direct relation with internal (axial) forces of the system. In an elastic non-rigid body significant compressive forces decrease the total stiffness ($k_{geom} < 0$), and significant tensile forces increase the total stiffness.

When loss of stability (buckling) is to occur $k_g \rightarrow -k_{ph}$ and the total stiffness is close to 0. This is shown with a simple example:



The equation for calculation of natural frequency of a beam subjected to axial forces (continuous model with neglected shear forces) is:

$$f_i = \frac{\lambda_i^2}{2\pi L^2} \sqrt{\frac{EJ}{m}} \quad ; \quad (4)$$

$$\lambda_i = i^2 \pi^2 \sqrt{1 + \frac{PL^2}{EJi^2 \pi^2}} \quad [4]$$

In Table 1 the first three natural frequencies are given for $P=0$; $P=0.1P_{cr}$; $P=0.25P_{cr}$; $P=0.50P_{cr}$, and $P=0.95P_{cr}$, where $P_{cr}=41123$ kN is the critical force (Euler buckling) of the beam.

Table 1: Natural Frequencies of Prestressed Simply-Supported Beam

Mode No	P=0	P=0.1Pcr	P=0.25Pcr	P=0.5Pcr	P=0.95Pcr
	Frequency [Hz]				
1	7.7543	7.3459	6.6869	5.4129	1.2463
2	63.221	62.793	62.145	61.049	59.024
3	152.07	151.59	150.85	149.62	147.38

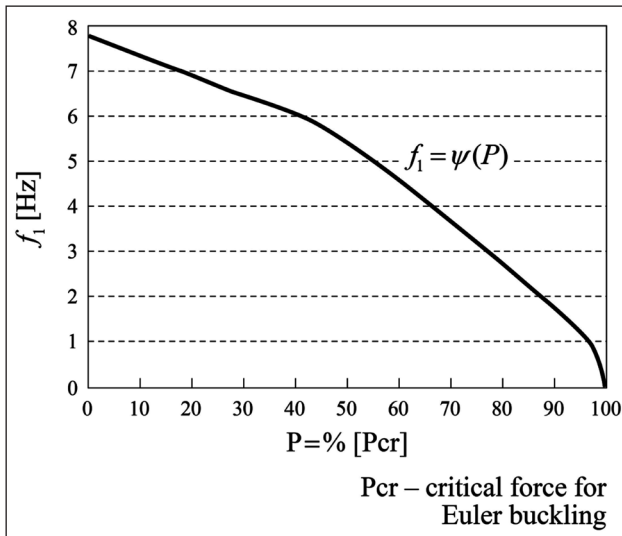


Figure 10: Relation between Compressive Force and Fundamental Frequency

The relation $f_1 = \Psi(P)$ is shown in Figure 10. There are analogical predictions for tendencies in eigenmodes of the containment for $f < 20\text{Hz}$. Modes with $f > 20\text{Hz}$ for spatial vibrations of a relatively stiff structure are of greater interest because they are difficult to predict with simple models. The concrete stresses due to post-tensioning are less than $0.1\sigma_{CR}$.

4.4 Development of FE Model with SOLVIA

4.4.1 Cylindrical Wall

The cylindrical wall is modelled with 4-node rectangular shell elements. The wall is meshed in such way that the tendon's path passes through existing nodes (Figure 11). Openings and penetrations are neglected.

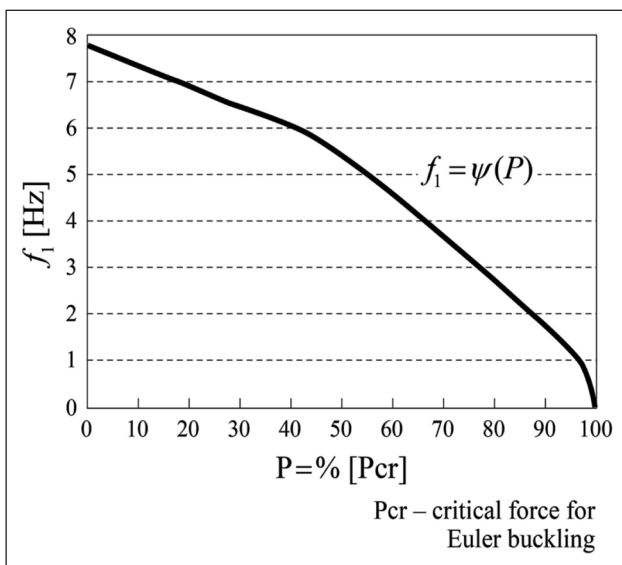


Figure 11: Placement of Elements and Nodes in the Cylinder [m]

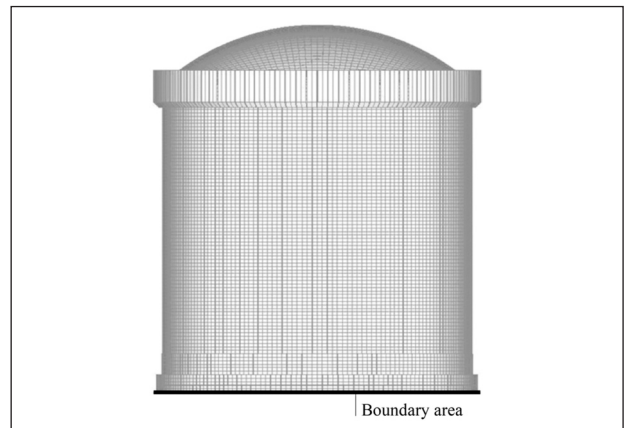


Figure 12: Boundary Condition of the Structure

5. Results and Progress beyond the Current Practice

5.1 Dynamic Analyses of the Structure

5.1.1 Complex-Harmonic Analysis

Analysis of frequencies from 0 to 60 Hz, increment step 0.05 Hz.

Acceleration load $a = a_0 \cdot \sin \theta t$, where $a_0 = 0.15g$.

Various types of complex-harmonic analyses are performed, considering different levels of post-tensioning and thus different stress states of the structure:

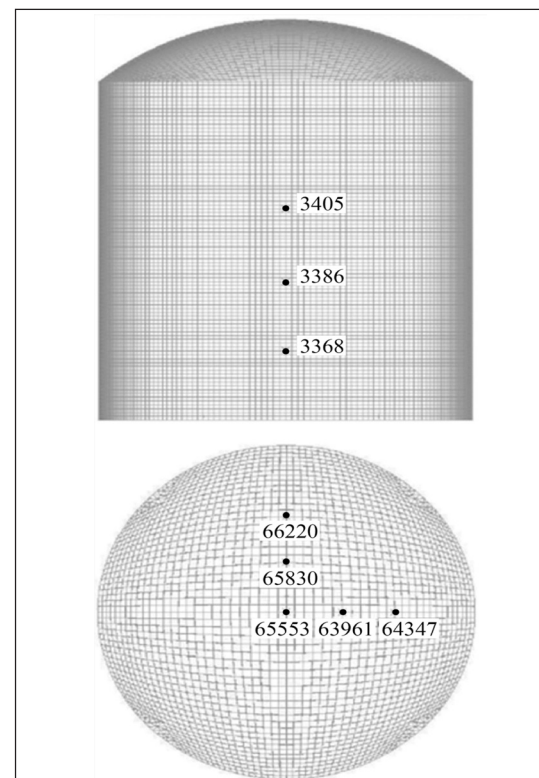


Figure 13: Placement of Controlled Nodes

- Analysis of the containment structure without post-tensioning;
- Analysis of the containment with design post-tensioning;
- Analysis of the containment with post-tensioning 80% from the design (long-term loss of stress during exploitation).

Frequency response spectra are created for displacement [m], velocity [m/s] and accelerations [m/s²] for some nodes of interest with respect to frequency [Hz]. The controlled nodes are shown in Figure 13.

5.2 Analysis of Results

As the permanent vibration monitoring system at the reactor building structure is installed only at the dome part, main attention will be given to this structural part. The significant local modes in the dome part are demonstrated by comparison of the frequency response functions from two dome locations – top of the dome and base of the dome (ring beam). In Figure 14 the frequency response spectra are presented for displacements in vertical direction. The analysis is performed with design values of the post-tensioning force. The peaks in the frequency response spectrum appear exclusively at the top dome location, therefore all of them represent local modes of the dome structure. The range of the local mode frequencies at the dome start at approximately 14Hz.

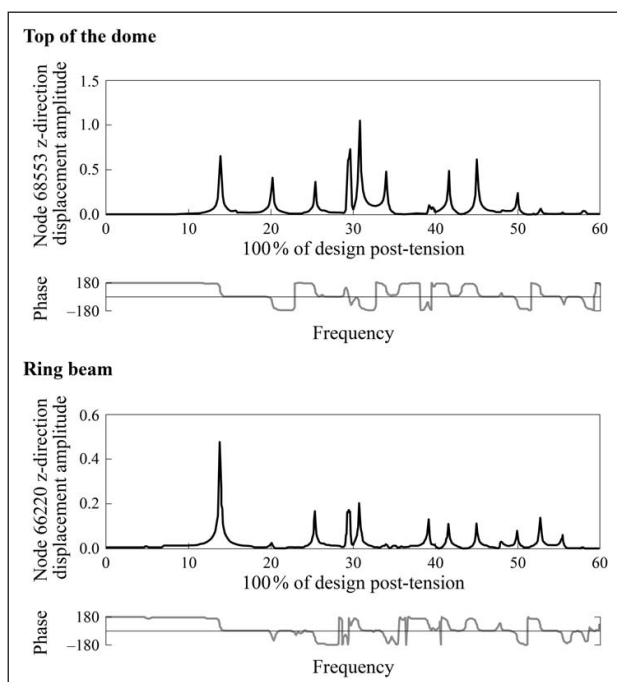


Figure 14: Displacement Spectrum in Vertical Direction: Top of the Dome (Above) and Ring Beam (Below)

The local modes of the dome part of the structure are presented in Figure 15. The modes at 13.9Hz and 20.25Hz can be classified as first local modes of the dome. The rest of the observed local modes are of higher order – 25.5Hz, 29.7Hz and 34.1Hz.

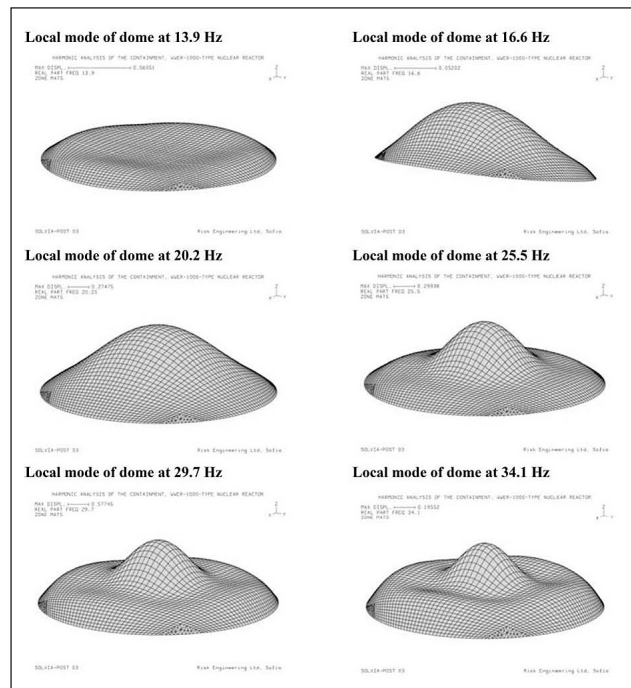


Figure 15: Local Modes of Dome

After the series of complex-harmonic analyses with different post-tensioning force, the obtained general results could be summarized as follows:

- Change in deformed shapes of vibration of the structure due to post-tensioning;
- Shift of natural frequencies of the structure for different states of post-tensioning;
- Excitation of additional natural frequencies in post-tensioned state;
- Amplitude change of the structural response for different states of post-tensioning;
- Change of normalized spectral density function $\psi(f)$.

The complex-harmonic analyses of the containment structure are performed for design post-tensioning load, 80% of the design post-tensioning load and for a case without post-tensioning load.

Change in Deformed Shapes of Vibration of the Structure due to Post-Tensioning

Deformed shapes at design post-tensioning and close levels (80%) differ from low post-tensioning

Table 2: Natural Frequencies

Number of modes	Natural frequency[Hz]			Deviation [%]
	Complex harmonic 0%	Complex harmonic 80%	Complex harmonic 100%	
1	5.2500	5.2500	5.2500	-
12	13.950	13.950	13.950	-
13	16.600	16.600	16.600	-
26	20.300	20.300	20.300	-
38	25.450	25.500	25.500	0.20
56	29.300	29.450	29.450	0.51
163	58.170	58.185	58.185	0.02

levels. In case of the cylindrical part the reason is the shape of the tensioned containment – the cylindrical wall changes shape to rotational hyperboloid. In case of the dome part – the deformed dome has less curvature. In addition there are local effects from post-tensioning, particularly in the dome. This is clearly observed at frequency 5.25 Hz – in the 0% level the deformed shape is global translational in horizontal direction. At levels close to design post-tensioning in the dome symmetrical vertical displacements appear. For the rest of the natural frequencies up to 60 Hz clear secondary effects in the dome do not appear because vertical displacements prevail.

Shift of Natural Frequencies of the Structure for Different States of Post-Tensioning

Table 2 shows all matching natural modes and their frequencies.

At frequencies up to 20 Hz the deviation is smaller than accuracy of analysis $\epsilon=0.05$ Hz (the increment step in the complex-harmonic analyses). At frequencies higher than 25 Hz, an increase of natural frequencies due to post-tensioning is observed, also mentioned in [2]. The absolute value of deviations is close to the accuracy of the analysis. The reasons for the small deviations are the significant spatial stiffness of the containment structure and the fact that it is linear elastic. The current results show that frequency shifts due to different post-tensioning forces are insignificant for the containment structure.

Excitation of Additional Natural Frequencies in Post-Tensioned State

In complex-harmonic analyses with post-tensioning additional natural frequencies are excited. They are related to local vibration modes, typical for the changed geometry of the post-tensioning containment and there is also relation to secondary effects from the post-tensioning. The additionally

excited natural frequencies are higher than 30Hz (high-frequency range) and they could be an appropriate base for studying the influence of the post-tensioning force and the overall stress state on the local modes characteristics.

Amplitude Change of the Structural Response for Different States of Post-Tensioning

The increase of post-tensioning force in the tendons changes the shape of the cylindrical and dome part of the structure and as a consequence its geometrical stiffness is increased. This leads to changes in the amplitudes of the natural vibrations at lower and higher frequencies. The following effects are observed:

For frequencies up to 20 Hz in horizontal direction (vibrations in the cylindrical part) the amplitude values are lower for the post-tensioning structure. The reason is the increased geometrical stiffness of the structure mentioned above. The affected vibration modes are global – with significant mass excitations.

For frequencies over 20 Hz in horizontal direction (vibrations in the cylindrical part) and over 10 Hz in vertical direction (vibrations in the dome part) the amplitude values are higher for the post-tensioned structure. The affected vibration modes are mainly local high-frequency modes. The comparison between the amplitude values for 80% and 100% post-tensioning shows that an increase of 20% in the post-tensioning force results in amplitude increase of 10 to 20% in the higher order modes. In some cases the amplitude increase is higher for the higher frequency modes, as it is for the dome part of the structure.

Change of Normalized Spectral Density Function $E(f)$

The increase of post-tensioning alters the shape of the normalized distribution function $E(f)$. The relative

participation of frequencies less than 20Hz, in the formation of the spectral density function, decreases. For structures without post-tensioning, these frequencies (less than 20 Hz) have the main influence (80%) of the integral value for $E(f)$. As a conclusion the spectral density function is negligibly affected by the post-tensioning force for frequencies up to 20Hz, for both structural parts – cylinder and dome.

With increase of post-tensioning forces the participation of the lower modes in $E(f)$ decreases and the main weight comes from frequencies in the range of 20 to 45 Hz, where post-tensioning effects on the higher frequency modes are stronger. The alterations in the spectral density function vary from 2% to 10% depending on the location of the observed location. Locations in the cylindrical part of the structure demonstrate higher increase of $E(f)$ than locations in the dome part of the structure. The values of $E(f)$ for full post-tensioning are higher than values of $E(f)$ for 80% post-tensioning.

For frequencies over 50 Hz, particularly in acceleration spectra, there is a reverse effect – higher amplitudes for the post-tensioning structure at lower frequencies.

5.3 Comparison of the Results Obtained by Ambient Vibration Monitoring with the Results from the Finite Element Model

The basic measurements with BRIMOS® on the dome were taken in May 2010 by a team of VCE [5]. For the dynamic assessment of the structure itself five sensors have been placed. The main idea of BRIMOS® is rather simple. The dynamic characteristic of a structure is recorded by acceleration sensors and the signal in time range is changed into a frequency response by use of an FFT (Fast Fourier Transformation). In doing so the results of this calculation are the natural frequencies of the structure represented in the ANPSD and the raw-spectrum.

Since the methodology of the current approach uses the results from the complex-harmonic analyses in this comparison the obtained eigenmodes and eigenvalues are used.

The following conclusions could be done:

- i) There is general compatibility between the deformed shapes obtained by the ambient vibration monitoring and the finite element analyses.
- ii) The frequencies obtained through the finite element model are generally higher. This could

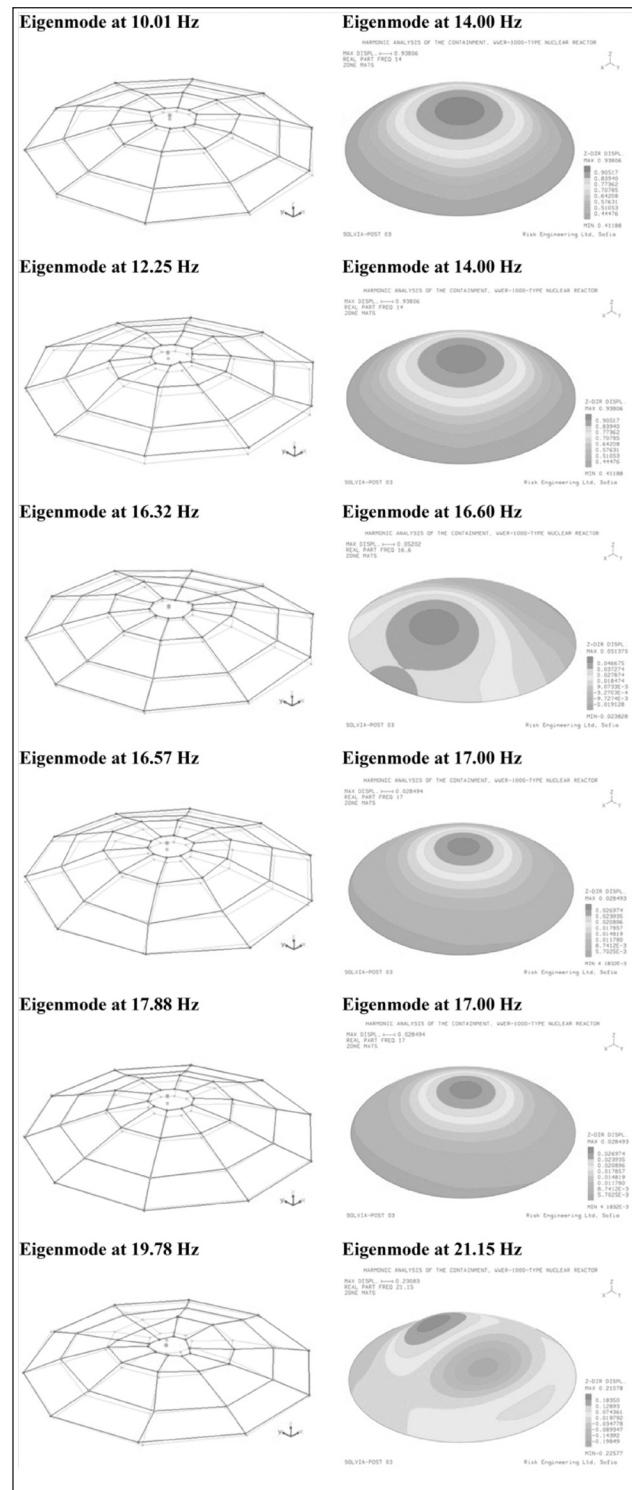


Figure 16: Eigenmodes Obtained through Ambient Vibration Monitoring (Left) and Eigenmodes Obtained through Finite Element Model (Right)

be due to overestimation of the stiffness in the computational model or due to other effects that have not been considered in the numerical simulation.

Table 3: Comparison of Natural Frequencies

Natural Frequencies Ambient Vibration Monitoring [Hz]	Natural Frequencies Finite Element Model [Hz]
10.01	14.00
12.25	14.00
16.32	16.60
16.57	17.00
18.76	20.25
19.78	21.15

5.4 Conclusions and Possibilities for Future Development of the Investigation

The current study puts the basic steps and reveals tendencies in the structural vibration behaviour of the post-tensioned containment of a WWER-1000 type nuclear reactor that should be more deeply investigated. The tendencies of the spectral density function should be further studied and special emphasis should be given to specific structural locations, higher variety of post-tensioning force and assumption of specific limited with decreased post-tensioning force.

The comparison of the numerical results and the monitored data showed very close proximity of the results. Outlining the essential structural local modes of both parts of the structure - dome and cylinder, allows the further development of the study by focusing on these particular structural modes of interest. Their behaviour and their influence on the spectral density function should be studied again by both manners - numerically and experimentally.

To obtain statistically stable numerical results further analyses are required – a wider set of output data to summarize, reduce simplifications, include openings and penetrations, where local effects are expected. In a further study these should be included because of the non-regularity of the tendon trajectories and the concrete wall around them.

Another further step should be assessment of the effects of other factors influencing the vibration behaviour: equipment forced vibration, containment temperature and environmental conditions. An FE model with solid elements could be used for analysing the influence of non-uniform solar heating on the dynamic behaviour.

The limited amount of the study allows rough numerical evaluation of the changes, and focuses on the directions of the spectral density curve shifts. The obtained results are very close to the theoretical, which is an indication for the correct assumptions in the model and the analyses. Improvement of NPP safety is a main issue for the nuclear industry. With 20 WWER-1000 type reactors across the world and a number of reactors to be designed and built (of modern technological generation but with similar building structures) spending time and resources for a better understanding of their behaviour is justified.

With rapid improvements of monitoring instrumentation it is possible to apply systems, monitoring permanently the condition of the building structure and based on specific thresholds to evaluate the current state of the structure. In areas with limited access (for example the tendons of the containment) these systems could be used for warnings about internal malfunctions (relaxation or tendons, deterioration of material properties due to ageing etc.) These systems will effectively serve as permanent monitoring tool, presenting the current stress state of the structure and as a warning system, alerting when the structural safety is in risk.

References

1. IAEA, Nuclear Power Reactors in the World, 2010.
2. Wenzel, H. (2009). "Health Monitoring of Bridges". John Wiley & Sons Ltd.
3. Tanaka, H., Höllrigl-Binder, M., Allmer, H., (2009). "Structural Health Monitoring by Spectral Analysis". VCE Internal Report.
4. Blevins, Robert D., "Formulas for Natural Frequency and Mode Shape", Van Nostrand Reinhold Company, 1979.
5. VCE, "Monitoring of Kozloduy NPP. Structural Monitoring with BRIMOS", Internal report, 2010.

Time Dependent PSA of Nuclear Power Plants Under Seismic Events

M. Hari Prasad, P. N. Dubey, Gopika Vinod, G. R. Reddy and R. K. Singh

Reactor Safety Division, Bhabha Atomic Research Centre,
Trombay, Mumbai, INDIA.
Email: hari_m@barc.gov.in

Abstract

Probabilistic Safety Assessment (PSA) is an analytical technique for assessing the risk of Nuclear Power Plant (NPP). Risk can be defined as the product of the likelihood of occurrence of an accident and the consequences from that accident. The main objective of seismic PSA is determination of frequency of occurrence of an accident due to seismic event and the corresponding consequences. In static PSA analysis the frequency of an accident does not change with time. Where as in actual practice failure probabilities of the systems changes with time due to random loading and aging phenomenon. Hence, one should consider time dependency of the accident frequency. This leads to the implementation of stochastic failure probabilities of the safety systems into the seismic PSA analysis. In this paper stochastic reliability concepts have been utilized to estimate the time dependent failure probabilities of safety systems and have been utilized in finding out the time dependent accident frequency arising from a seismic event.

Key words: External events, PSA, hazard, seismic fragility, fault trees, event trees, accident sequence, Core damage frequency, Random process.

1. Introduction

Generally the load application on a component or structure is random in nature. It could be either discrete in nature or continuous in nature. Also the loading can be time invariant or time variant. If the loading action on a component is varying with time the probability of failure of the component should also change with time and in estimating this one should utilize the concepts of stochastic process. In general, the plant consists of normally operating and emergency standby systems and components. The failure of systems during an earthquake will lead to a change in the state of the plant and various scenarios can follow depending on the initiating event and the status of other subsystems. In this case, the earthquake is the external initiating event (IE), which in turn can initiate other internal events as listed below:

- Loss of Offsite Power
- Loss of Coolant Accident (LOCA)
- Process Water System Failure
- End Shield Cooling System Failure
- Moderator Cooling System Failure
- Service Water System Failure
- Many other Internal IEs

In this paper failure probability has been estimated by using stochastic reliability concepts and is explained with a case study and the results are utilized in estimating the time dependent accident frequency due to seismic event. The present analysis is based on seismic PSA procedure [1] [2]. Seismic PSA evaluation process can be divided into seismic hazard evaluation, seismic fragility evaluation and accident sequence analysis and are explained in the following subsections.

2. Seismic Hazard Evaluation

The seismic hazard analysis refers to the estimation of the annual frequency of a hazard parameter such as the Peak Ground Acceleration (PGA), which characterizes the ground motion at a nuclear power plant site [3] [4] [5]. The seismic hazard model takes into account the seismic history of the region, potential sources of seismic activity, rates of occurrence of earthquakes from these sources, maximum magnitudes, and attenuation of earthquake ground motion from the source to the site. The effects of all the earthquakes of different sizes, occurring at different locations in different earthquake sources at different probabilities of occurrence are integrated into one curve that shows the probability of exceeding different levels of

ground motion levels at the site for a given period of time. The annual frequency of exceedance can be expressed as

$$v(z) = \sum_{i=1}^N v_i(m_0) \int_{m_0}^{m_u} \int_{m_0}^{r_0} f_M(m) f_R(r) P[Z > z/m \geq m_0, r] dr dm \tag{1}$$

in which

$v(m_0)$ = the annual frequency of occurrence of earthquakes on seismic source 'n' whose magnitudes are greater than m_0 and below the maximum event size, m_u .

$P(R=r_j | m_i) = f_R(r) =$ the probability of an earthquake of magnitude m_i on source 'n' occurring at a certain distance r_j from the site

$P(M=m_i) = f_M(m_i) =$ the occurrence probability of an earthquake of magnitude m_i on source 'n'

$P(Z > z | m_i, r_j) =$ the probability that ground motion level z will be exceeded, given n earthquake of magnitude m_i at a distance of r_j from the site.

The hazard curve of the site under study [6] is shown in Figure 1.

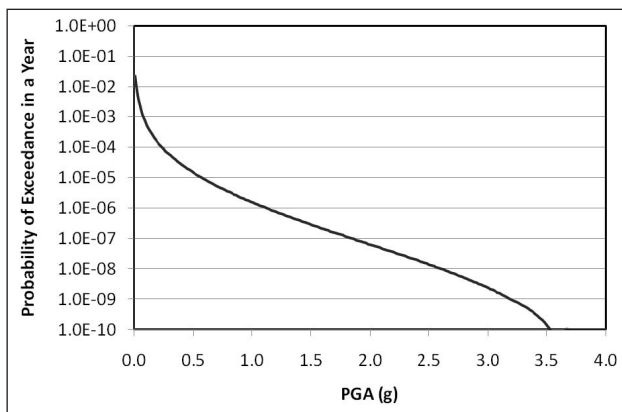


Figure 1: Hazard Curve for a typical NPP Site

3. Seismic Fragility Evaluation

The seismic fragility of a structure or equipment component is defined as the conditional probability of its failure for a given level of seismic input parameter, typically the peak ground acceleration (PGA). In the fragility evaluation, the conditional probability of component failure is determined by considering the capacities of the components in various failure modes. Seismic-induced fragility data is generally unavailable for components and structures. Thus, fragility curves must be developed primarily from analysis combined heavily with engineering judgment supported by very

limited test data. Such fragility curves will contain a great deal of uncertainty.

The uncertainty can be of aleatory or epistemic in nature. The aleatory uncertainty can be represented with the help of probability distributions and the uncertainty in the parameters of the distributions is of epistemic in nature. The fragility curve for any component can be defined with the help of its median ground acceleration capacity, A_m and the corresponding uncertainties β_R (aleatory) and β_U (epistemic). Hence, the probability of failure (P_f) at a non exceedance probability (Q) can be expressed as [7] [8]:

$$P_F(a) = \Phi \left[\frac{\ln\left(\frac{a}{A_m}\right) + \beta_u \phi^{-1}(Q)}{\beta_R} \right] \tag{2}$$

If both the uncertainties are combined together then the probability of failure can be given as follows:

$$P_F(a) = \Phi \left[\frac{\ln\left(\frac{a}{A_m}\right)}{\beta_C} \right] \tag{3}$$

where

$$\beta_C = \sqrt{\beta_R^2 + \beta_U^2}$$

in which parameter 'a' is PGA and $\Phi(\cdot)$ is the standard Gaussian cumulative function. The above procedure will be helpful in finding out the time invariant failure probability of the structure as a function of PGA value. The stochastic reliability concept is explained in the following section to estimate the time dependent failure probability of the structure.

4. Stochastic Reliability Analysis

Consider the loading action on a component is random sequence of point loadings. In this case the question arises how to implement this type of loading in estimation of probability of failure of structure. This problem can be solved with the help of extreme value theory. Suppose that the loading is taking place n times over a period of time t , then the component or structure under these loadings will survive if it doesn't fail under the maximum among these loadings. One can find out the maximum load distribution based on the extreme value theory. According to this

the cumulative distribution function (CDF) of the maximum load can be expressed as follows:

$$P(L_{\max} < l) = P(L_1 < l \cap L_2 < l \cap L_3 < l \dots \cap L_n < l) \quad (4)$$

$$F_x(x) = [F_L(l)]^n$$

The probability density function (PDF) of the maximum load can be derived as follows:

$$f_x(x) = n[F_L(x)]^{n-1} f_L(x) \quad (5)$$

Where $f_L(l)$ is the PDF of the loading. For example if a random load is applied at different point of times the maximum load distribution for different number of times is shown in the Figure 2. From the figure one can observe that as the number of times the loading action increases the variance of the maximum load distribution reduces and the mean value reaches the actual value. At the same time the interference area between the load and resistance curves increases, in effect the probability of failure also increases.

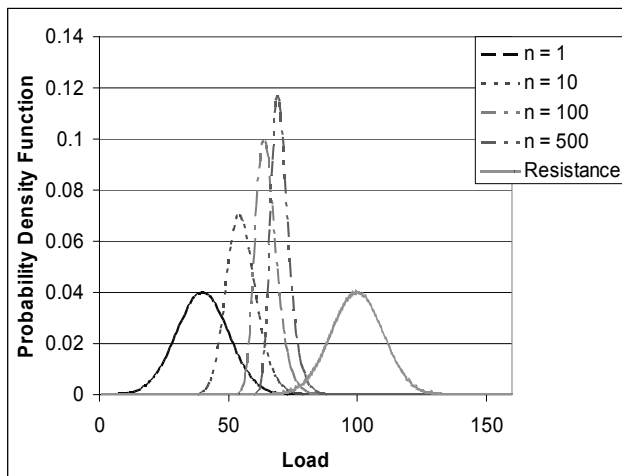


Figure 2: PDF curves for maximum load for different number of loadings

If one considers that the arrival rate of the loading is constant then as the time increases the number of times the loading occurrence also increases. Hence the failure probability also increases. One can calculate the survival probability (reliability) or probability of failure as follows [9]:

$$S(t) = \int_{-\infty}^{\infty} \int_{-\infty}^r f_R(r) f_x(x) dx dr \quad (6)$$

If one substitutes the PDF of maximum load distribution the above equation becomes

$$S(t) = \int_{-\infty}^{\infty} \int_{-\infty}^r f_R(r) n [F_L(x)]^{n-1} f_L(x) dx dr \quad (7)$$

From the above equation one can calculate the reliability when the loading occurs at arbitrary times.

5. Accident Sequence Analysis

Seismic events are treated as initiating events that can cause adverse impacts on support systems, front line systems and structural integrity. The method of dealing with these various challenges is to use a single event tree for many of the consequential seismic events [6]. The initiating event for the seismic event trees is the occurrence of seismic event and whenever seismic event occurs it will in turn initiate other internal events like loss of offsite power, LOCA, loss of process water systems etc. Hence, event trees should be generated for all the initiating events and dominating accident sequences should be identified for the Core Damage Frequency (CDF) estimation.

5.1. Seismic Event Trees

As discussed above in seismic event trees, seismic event is the initiating event and the other internal initiating events are due to seismic event. As a case study event tree for seismically induced Class IV power supply failure has been developed and is shown in the Figure 3. Upon failure of Class IV power, reactor trips on 'No Primary Coolant Pump running'. High primary heat transport (PHT) Pressure trip will follow if the first trip parameter fails. This leads to the actuation of Reactor Protection System (RPS), initially with Shutdown System (SDS-1) and with SDS-2, if SDS-1 fails. Emergency power supply (EPS) i.e., Class III is 6.6 KV system with 4 DG sets. If Class III is available and there is no failure in PHT System, the mode of decay heat removal and long term reactivity control will be same as normally followed with decay heat removal systems (DHRS) such as Secondary Steam Relief System (SSR), Auxiliary Boiler Feed Water System (ABFWS) and Shut down Cooling System (SDCS). If there is a failure in decay heat removal systems, core cooling will be achieved through valving in of fire water system (FWS). Class IV failure followed with complete loss of Class III failure leads to a Station Blackout scenario. During station black out scenario core cooling will be achieved through valving in of Fire water system.

The dominating accident sequences, in terms of consequences, are given below. However, in the present analysis station blackout with failure of FWS is considered while evaluating time dependent accident frequency due to seismic event.

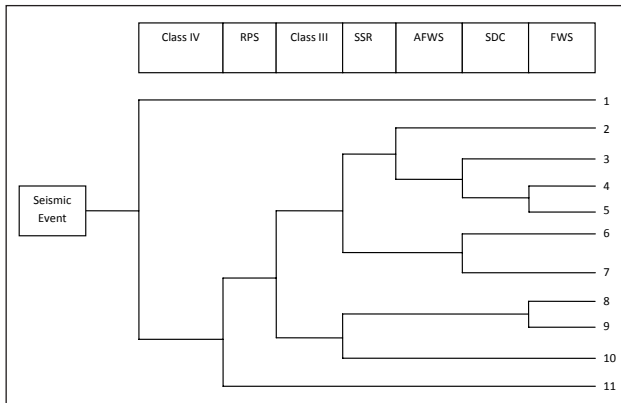


Figure 3: Seismic Event tree of Class IV failure

- Seismic-Class IV-RPS
- Seismic-Class IV-SSR-SDC
- Seismic-Class IV-AFWS-SDC-FWS
- Seismic-Class IV-Class III-SSR
- Seismic-Class IV-Class III-FWS

5.2 Seismic Fault Trees

In evaluating the accident sequence frequency from the seismic event trees one should have the information about the initiating event frequency and the seismically induced failure probabilities of process systems and safety systems. Initiating event frequency (frequency of occurrence of seismic events) can be derived from hazard curve analysis as explained in the previous sections and the seismically induced failure probabilities of systems can be evaluated by developing seismic fault trees. Unlike the traditional fault trees, these fault trees will consist of component failures mainly from structures point of view. The fault trees are developed based on the assumption that components of a similar design, located at the same elevation and with the same orientation will fail in a given seismic event if one of these groups fails and are considered as a single component. Once the seismic fault trees are developed, next step is to develop component fragilities depending on their seismic capacities as explained in the previous section. In finding out the seismic capacities of the components one has to perform seismic response analysis. The system fragility curve can be generated from the component fragilities depending on the system configuration and its failure criteria. This can be well represented with the seismic fault trees. Seismic fragilities of Class-IV power supply system, RPS, Class-III power supply system are generated based on the procedure explained in section 3 and are shown in the Figures 4, 5 and 6 respectively. However,

the fragility curves of FWS are generated based on the stochastic reliability concept which is further discussed in the following subsection.

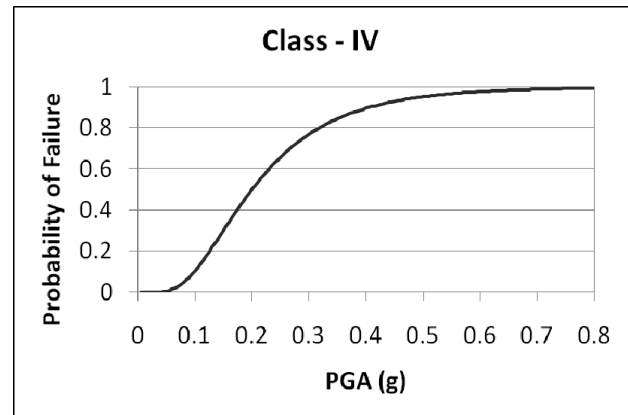


Figure 4: Fragility Curve of Class IV Power Supply System

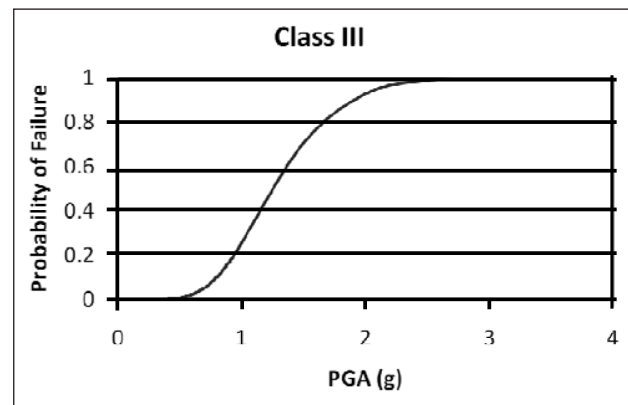


Figure 5: Fragility Curve of Class III Power Supply System

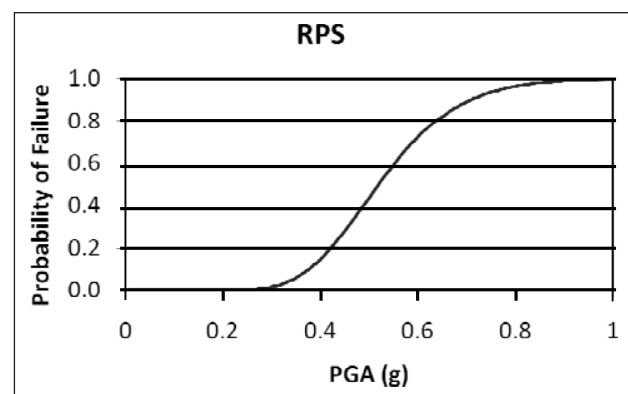


Figure 6: Fragility Curve of RPS

5.2.1 Fire Water System

Fire water system is very important for a Nuclear Power Plant from viewpoint of safety. The main objective of fire water system is to ensure availability of water for fire fighting under normal operating conditions and anticipated operational occurrences

[6]. Depending up on the type of equipment to be protected, either hydrant system or automatic or non-automatic high velocity sprinkler system has been adopted. The system has been designed to be available under safe shutdown earthquake condition for firefighting of related equipment or system. Fire water system comprises constantly pressurized hydrant system and the sprinkler systems. The source of fire water is from the cooling water tunnels connected with fire water pump house. The quantity of fire water is same as that of condenser cooling water. Fire water system helps the safety system to perform their safety function in case of emergency such as total power failure (station blackout) condition. Fire water system mainly consists of pumps, piping, valves and diesel engines. In finding out the fragility of the piping system both static and dynamic seismic analysis has been carried out and failure probability of the system as a function of time has been estimated by using stochastic reliability analysis as discussed in the previous section.

For the stochastic analysis it is important to find the stresses that act on the piping system. The piping system has been analyzed for pressure, dead weight, thermal and earthquake loads. Finite element model of the piping systems and the corresponding floor response spectra used in the analysis is shown in the Figures 7 and 8 respectively. Maximum stress obtained for OBE loading is 270 MPa. Due to the uncertainty in the various parameters the loading is considered as random variable and it is assumed to follow normal distribution with coefficient of variation as 0.1.

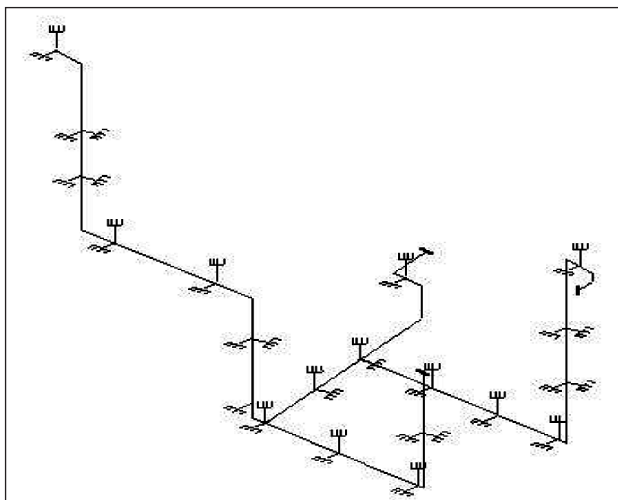


Figure 7: Finite element Model of Steam Generator Piping System

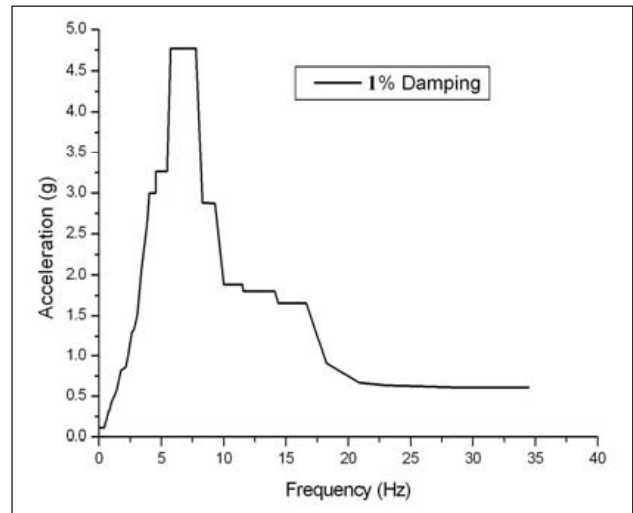


Figure 8: Floor Response Spectra Corresponding to Steam Generator Line

Based on the number of occurrences of earthquake for a given period of time the loading distribution also varies as explained earlier. From this exercise one can obtain the failure probability of the structure as a function of time and PGA value. The fragility of the fire water piping system for different time periods as a function of PGA is shown in the Figure 9.

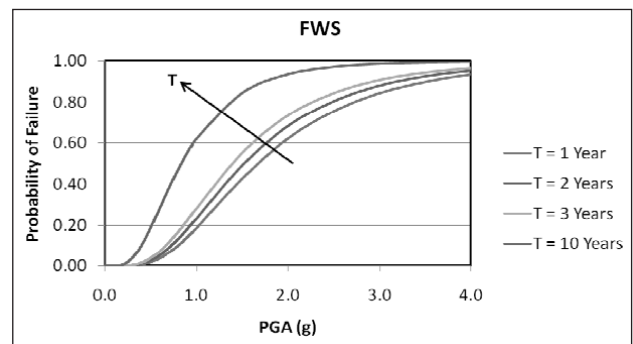


Figure 9: Fragility Curve of FWS Piping System

5.3 Accident Sequence Evaluation

In this step accident sequence frequency is calculated by convoluting both seismic hazard curves and the fragilities of the corresponding systems as given in equation 8.

$$P_F = \int_0^{\infty} \left(\frac{dH}{da} \right) P_F(a) da \quad (8)$$

Where H is Hazard curve, a is PGA level, $P_F(a)$ is conditional failure probability at a given PGA level and P_F is the total failure frequency. From the seismic event tree of Clas IV power supply failure one can identify different dominating accident sequences.

Table 1: Calculation of CDF with respect to Time

a	a + Δa	ΔH	P _f (a)				CDF (T=1 yr)	CDF (T=10 yrs)
			Class IV	Class III	FWS (T=1 yr)	FWS (T=10 yrs)		
0.010	0.030	1.73E-02	2.564E-08	1.038E-22	2.983E-19	7.398E-15	1.374E-50	3.408E-46
0.030	0.050	2.90E-03	2.779E-04	1.013E-15	1.392E-12	3.628E-09	1.134E-33	2.958E-30
0.050	0.070	9.98E-04	5.799E-03	6.111E-13	5.238E-10	4.826E-07	1.851E-27	1.706E-24
0.070	0.090	4.58E-04	2.790E-02	2.848E-11	1.714E-08	7.991E-06	6.237E-24	2.909E-21
0.090	0.110	2.47E-04	7.271E-02	4.136E-10	1.868E-07	5.255E-05	1.385E-21	3.895E-19
0.110	0.130	1.47E-04	1.376E-01	3.110E-09	1.103E-06	2.076E-04	6.941E-20	1.307E-17
0.130	0.150	9.44E-05	2.155E-01	1.539E-08	4.422E-06	5.971E-04	1.384E-18	1.869E-16
0.150	0.170	6.39E-05	2.990E-01	5.715E-08	1.363E-05	1.386E-03	1.489E-17	1.515E-15
0.170	0.190	4.52E-05	3.822E-01	1.723E-07	3.475E-05	2.763E-03	1.034E-16	8.219E-15
0.190	0.210	3.30E-05	4.611E-01	4.441E-07	7.688E-05	4.918E-03	5.189E-16	3.320E-14
						Σ CDF	3.630E-09	1.650E-08

However, in the present analysis station blackout with failure of Fire Water System has been analysed from core damage point of view. The dominating accident sequence frequency is evaluated by convoluting the seismic hazard of the site under consideration and the corresponding system fragilities that are presented in the sequence. The dominating sequence under consideration is

- Seismic-Class IV-Class III-FWS

In the above sequence the seismic event frequency is obtained from the hazard curve of the site and the failure probabilities of the systems are taken from the fragility curves of the corresponding systems. The fragility curves considered for Class IV and Class III systems are time independent curves where as for FWS time dependant curves are considered. In finding out the seismic event frequency from hazard curve the PGA range is divided into small intervals and the corresponding values and the calculations are given

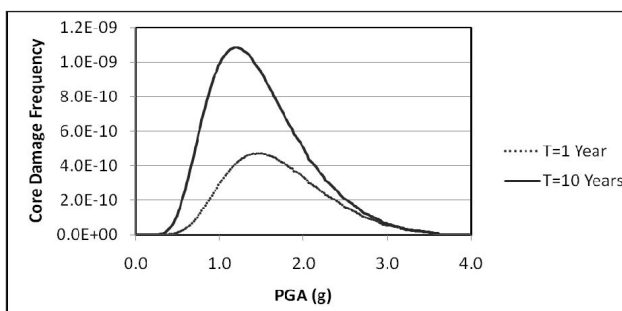


Figure 10: Graph between PGA Vs CDF

in Table 1. In the Table 1 the range of PGA is given only up to 0.21g. However in the actual calculation it is taken up to 4g. A graph between PGA vs CDF is shown in the Figure 1. The CDF from the seismically induced station black out with failure of FWS for 1 year is estimated as 3.63×10^{-9} /yr. Whereas, for 10 years it is estimated as 1.65×10^{-8} /yr.

6. Conclusions

A general procedure for implementing stochastic reliability concepts in seismic PSA has been explained. A case study on seismically induced LOOP along with failure of Class III power supply and FWS has been analyzed. Seismic event tree for the same has been developed. Seismic hazard curves have been developed for a given site which gives the frequency of occurrence of particular level of PGA. In finding out the system failure probabilities seismic fragilities at component level later at system level has been developed based on the corresponding seismic fault trees. In case of FWS piping system the fragility curves have been generated based on stochastic reliability concepts and the failure probability is estimated as a function of time. Finally, the accident sequence frequency as a function of time has been calculated by convoluting both seismic hazard curves and the fragilities of the corresponding systems. The core damage frequency due to simultaneous occurrence of seismic event followed by station blackout event and failure of FWS has been estimated with respect to time.

References

1. Kennedy, R. P., Cornell, C.A., Campbell, R.D., Kaplan, S., Perla, H. F. (1980) "Probabilistic seismic safety study of an existing Nuclear Power Plant", Nuclear Engineering and Design, 59, 315-338.
2. IAEA-TECDOC-724 (1993), "Probabilistic Safety Assessment for seismic events", IAEA, Vienna.
3. Steven L. Kramer (2003). Geotechnical Earthquake Engineering, University of Washington, Prentice-Hall International Series in Civil Engineering and Engineering Mechanics.
4. McGuire R.K (1995). Probabilistic seismic hazard analysis and design earthquakes: Closing the loop. Bull. Seism. Soc. America, Vol. 85 (5), 1275-1284.
5. Paolo Bazzurro, Allin Cornell C (1999). Disaggregation of seismic hazard. Bull. Seism. Soc. America, Vol. 89 (2), 501-520.
6. M. Hari Prasad, P.N. Dubey, G. R. Reddy, R.K.Saraf and A.K. Ghosh (2006), "Seismic PSA of Nuclear Power Plants- A Case Study", BARC external report, BARC/2006/E/015, July, 2006.
7. Kennedy, R. P., and Ravindra, M. K. (1984), "Seismic fragilities for Nuclear power Plant risk studies", Nuclear Engineering and Design, 79, pp. 47-68.
8. Kennedy, R. P., Campbell, R. D., and Kassawara, R. P. (1988), "A seismic margin assessment procedure", Nuclear Engineering and Design, 107, pp. 61-75.
9. M. Hari Prasad, G. Rami Reddy, A. Srividya and A. K. Verma (2010), "Time Variant Reliability Analysis Under Random Loads", International Conference on Reliability Safety and Hazards - 2010, Dec 14-16, Mumbai, India.

Probabilistic Failure Assessment of PWR Nuclear Power Plant Piping Components against Erosion-Corrosion

Jiboy Jose¹, K. Balaji Rao², M. B. Anoop², Gopika Vinod³, H. S. Kushwaha⁴

¹Former Junior Research Fellow, ²Scientist, CSIR-SERC, CSIR Campus, Taramani, Chennai

³Scientist-Engineer at BARC, Assoc. Professor at Homi Bhabha National Institute, Mumbai

⁴Raja Ramanna Fellow at Department of Atomic Energy, Mumbai

Email: anoop@serc.res.in

Abstract:

Erosion-corrosion (EC) is one of the important and complex degradation mechanisms in the nuclear power plant piping systems. Depending on the nature of piping material, piping geometry and operating conditions, different components of piping system are susceptible to EC to different degrees. Due to variations in operating conditions and inherent uncertainty associated with the prediction models, EC is to be treated as a random phenomenon. The effect of randomness should be considered in the design of piping components. In this paper, an attempt is made to apply system reliability concept to determine the reliability of an elbow against EC at different times. The application of system reliability concept helps in taking into account : (i) there are a number of sections within a given piping component that are vulnerable to undergo EC - reflecting the complexity of EC mechanism, and, (ii) the safety margins of these sections within a component, connected in series, are positively correlated. The usefulness of the model developed in estimation of reliability of elbows at different times is demonstrated through two example problems. A flowchart that can be used for reliability-based design of piping components against EC (in conjunction with ASME design procedure) is also presented.

Keywords: Erosion-Corrosion; Power Plant Piping Systems; Failure Assessment; System Reliability; Reliability-based Design

1. Introduction

Erosion-Corrosion is one of the major causes of material degradation of carbon steel piping systems carrying water (single phase) or wet steam (two-phase) in Pressurized Heavy Water (PWR) Nuclear Power Plants as observed from various high risk piping failures listed in Tables 1- 3. The piping systems susceptible to erosion-corrosion damage include feedwater, condensate, extraction steam, turbine exhaust, and, feedwater heater and moisture separator, reheater vents and drains [1]. Significant degradation of pipe wall thickness has been reported in a number of operating nuclear power plants resulting in fatal accidents, and costly repairs. The severe piping rupture at Surry nuclear plant in 1986 prompted nuclear regulatory authorities for a plant-specific monitoring program to prevent the failure of piping by erosion-corrosion [2]. Hence, an assessment of the resistance degradation based on a suitable wear rate model is essential to predict the life of the piping components against erosion-corrosion damage. The selection of the model for estimation of erosion-corrosion rate should, amongst other factors, be based

on its range of applicability and ease of application. Use of such models would help in evolving better strategies of inspection which may be carried out using high precision inspection methods such as radiography, thermography and ultrasonic testing to check the safety of the piping components and replace the susceptible piping components or to carry out the necessary maintenance in time.

Erosion-Corrosion (EC) is an accelerated form of corrosion caused by the relative motion between corrosive medium (with or without suspended particles) and metal surface leading to loss of material [3]. Modeling erosion-corrosion phenomenon is complex as it is affected by a number of variables such as pH, dissolved oxygen content, temperature, quality of flowing fluid, quality of oxide layer on inner surface of the pipe, chemical composition of the steel pipe and particle impact angle [4-6]. Many researchers have made attempts to develop models for estimation of erosion-corrosion rate and to formulate service life models for piping components subjected to erosion-corrosion degradation mechanism. Stack and co-workers developed a mathematical model

for estimating erosion-corrosion in mild steel pipes carrying aqueous solution containing alumina particles based on detailed laboratory studies [3-6]. They assumed the erosion-corrosion process to be purely additive, i.e., sum of erosion and corrosion effects. The model is admittedly applicable for low particle impact angles (impact angles < 4°), low flow velocities (flow velocities < 2 m/s), constant temperature and constant pH (pH=9.0) of flowing fluid. Abdulsalam [7] developed a steady state model to account for the steady hydrogen flux through metal and has established that erosion-corrosion is dependent on the kinetic rate of metal oxide film dissolution at lower temperatures and on mass transfer limited rate at higher temperatures. Ting and Ma [1] developed an erosion-corrosion model based on phenomenological considerations and statistical data of pipe wall thickness obtained from Taiwan PWR nuclear power plants for different piping components subject to various operating conditions. The model proposed by Ting and Ma [1] can be used to estimate EC rate both in steady and unsteady state regimes. In the present investigation, this model is used for estimating the EC rate. All the three models discussed till now are deterministic.

For a given type of piping component (viz. Elbow, Tee) and operating conditions, the EC rate is observed to vary [1]. The phenomenon of EC being complex, modeling errors also need to be considered. So, the wear rate predicted and modeling error associated with the prediction should be treated as random variables. The uncertainties arising from the inherent variations in the phenomenon of EC and the modeling error can be handled by probability theory. Using system reliability concepts and assuming a correlation coefficient between safety margins of various sections (potential of undergoing erosion-corrosion damage), values of reliabilities and failure probabilities of a piping component during its service life are determined after formulating a safety margin equation involving relevant random variables. A flowchart that can be used for reliability based design of piping components against EC (in conjunction with ASME design procedure) is also presented in this paper.

2. Comparative Study of Erosion-Corrosion Models

A comparative study to select a suitable model to estimate erosion-corrosion rate for Nuclear Power Plant piping components under operating conditions was undertaken at CSIR-SERC, Chennai.

For this purpose, a piping component of 16-inch outer diameter is considered [1]. The other details required for estimation of EC are obtained from Ting and Ma [1] as follows: Flow parameters: Flow velocity - 5.28 m/s, pH - 9.0, Temperature - 370°F; Pipe parameters: Nominal thickness of pipe - 25 mm, Minimum measured thickness - 22 mm, Outer diameter - 406 mm.

The wear rate estimated using the model proposed by Stack *et al.* [3] for these flow conditions is 0.41 mm/year with erosion dominating over corrosion. Using Ting and Ma model a wear rate of 0.59 mm/year was computed for the same flow conditions in the unsteady region (Fig. 8 of Ting and Ma [1]). It is noted that Abdulsalam model [7] can be used only for predicting the steady state wear for higher temperatures and so was not included in the comparative study. For the two models, service life predictions based on the respective wear rates has also been computed. The results of the comparative study are presented in Table 4 [8]. These results indicate that Ting and Ma [1] erosion-corrosion model could be used to evaluate the erosion-corrosion rate in Nuclear power plants. Its range of applicability (presented in the next section) and ease of application makes it a suitable one for estimation of wear rate and hence in the determination of service life.

2.1 Ting and Ma Model for Wear Rate Estimation

Ting and Ma [1] proposed an analytical method to evaluate the potential risk of erosion-corrosion in carbon steel piping using the erosion-corrosion model proposed by Berge [9]. It assumes that the soluble iron species production and mass transfer affect erosion-corrosion rate. According to their studies, the total wear rate due to erosion-corrosion is given by,

$$W_r = \frac{K_1 K_2}{K_1 + K_2} (C_{EQ} - C_\infty) \quad (1)$$

where K_1 is the reaction constant which depends on fluid velocity and water temperature, and K_2 is the mass transfer coefficient, which depends on Sherwood Number ($S_h = \alpha_1 R_e \alpha_2 S_c \alpha_3$), R_e is the Reynolds number of flow, S_c is the Schmidt number used in mass transfer calculations ($S_c = \nu / (\rho \times D_v)$), ν is the kinematic viscosity of the fluid, ρ is the density of fluid and D_v is the molecular diffusability; α_1, α_2 , and α_3 are the constants, which depend on pipe component geometry, C_∞ is the soluble ferrous iron concentration in bulk water, and C_{EQ} is the equilibrium soluble ferrous iron

concentration at the oxide layer, depending on pH value and coolant temperature it is given by,

$$C_{EQ} = \alpha_4 \exp\left[-\frac{(T - \alpha_5)^2}{\alpha_6}\right] + \alpha_7 \quad (2)$$

where α_4 , α_5 , α_6 and α_7 are constants depending on pH value, and T is the temperature.

2.1.1 Range of Applicability of the Model [1]

1. Applicable for a wide range of temperatures, i. e., from 90°F to 570°F.
2. Applicable for pH values from 9 to 10.
3. Applicable for a wide range of fluid velocities, i. e., from 1 m/s to 35 m/s.

2.1.2 Susceptible Piping Components

The decision concerning the rank-ordering of various classes of components such as elbows, tees, bends, etc based on susceptibility to erosion-corrosion is very complicated [10]. It depends on the interaction of several variables with weighting factors applied to each of the variables. If one knows about a given system, it might be possible to use engineering judgment to select the rank ordering; however, because of the complexity, computer codes are usually the choice. According to Ting and Ma [1], the susceptible piping components in a nuclear power plant are 90° elbow, 45° elbow, reducer, tee and straight pipes. Based on the measured data during inspection, Ting and Ma [1] made observations about the locations of the most occurrences of thinnest pipe wall thickness for the piping components (Table 5).

Based on a statistical analysis of measured thinnest portions of the 90° and 45° elbows Ting and Ma [1] presented the results in the form of histograms for various sections. The relative weights computed using these histograms are presented in Tables 6 and 7, respectively. These values are to be used for a suitable prediction of wear rates for different sections.

3. Estimation of Erosion-Corrosion Rate

Values of wear rate for different temperatures ranging from 180°F to 420°F (the range of temperature in which wear rate changes with change in flow velocity) were read from plots (Figs. 8 and 9 of Ting and Ma [1]) and best fitting curves were plotted for predicting the wear rate for different velocities. The predictions of wear rates in the unsteady state regime were found to be satisfactory [8]. However, the discrepancies observed in the transition stage could be attributed to the absence of an efficient model to

predict the wear rate in this range. The fitted wear rate equations for fluids with pH = 9.0, for different temperatures, lying in the unsteady and steady states, are presented in Tables 8 and 9, respectively.

4. Life Prediction of the Piping Component

If statistical data on pipe thinning are available (which could be based upon the in-service inspection reports or by pooling suitable relevant data from similar power plants), the life of a piping component can be predicted using the model by Ting and Ma [1]. While estimating the remaining life, the lowest thickness of the pipeline should be used to account for the wide variations in measured thickness in a particular piping component. However, such data may not be always available, especially, in the initial stages of commissioning of the plant or when a new type of plant is being built. In such cases, a probabilistic analysis of wall thinning has to be carried out to determine the reliability of a component or to assess the safety of the component against erosion-corrosion.

5. Probabilistic Failure Assessment

In order to take into account the variations in the EC rate, the predicted wear rate and the modeling error associated with the prediction should be treated as random variables. The uncertainties arising out of random variations in wear rate and modeling error can be handled by probability theory [11]. Hence, in this study, wear rate and modeling error are treated as random variables with nominal computed value as mean and by assuming suitable values for coefficients of variation (reflecting the complexity of the phenomenon). An attempt has been made here to demonstrate the use of reliability analysis in failure life assessment of piping components at the design stage itself. The deterministic design procedure for the design of piping components is followed to arrive at the preliminary dimensions of piping components needed for reliability studies.

5.1 Determination of Preliminary Dimensions of Piping Components

Knowing the operating conditions and noting that hoop stress is going to govern the design [12], relevant equations from ASME Boiler and Pressure Vessel code 1998, Section III-Division 1 Subsection NC-Class 2 components [13] is used to determine minimum wall thickness of pipes. The minimum thickness (t_{min}) of the pipe is accordingly given by,

$$t_{min} = \left(\frac{PD_0}{2(S + Py)} + A \right) \times F \quad (3)$$

where P is the operating pressure, S is the maximum allowable stress at the design temperature, D_0 is the outer diameter, y is a coefficient from ASME codes for determining pipe wall thickness, A is allowance for thread, groove depth and mechanical strength and F is a factor depending on the radius of the bend. The notations are also shown in Fig. 1.

Assuming the life of the pipe (T'), the design thickness of the pipe is given by

$$t_0 = t_{min} + \text{Allowance for erosion-corrosion} \quad (4)$$

Then the thickness at any time, T (where $T < T'$) is given by, $t_T = t_0 - A_i R T$, where R is the predicted erosion-corrosion rate using equations of Tables 8 and Table 9 and, A_i is the modeling error.

5.2 Application of Reliability Concepts

Reliability is the probability of a structure or structural component performing satisfactorily during its lifetime. Generally reliability index, β , is used to get a measure of structural safety. Using the first order second moment method, β is defined as the ratio of mean of safety margin ($\langle Z \rangle$) to the standard deviation (σ) of the safety margin [14]. Hence,

$$\text{Reliability index } \beta = \frac{\langle Z \rangle}{\sigma} \quad (5)$$

For the problem considered, safety margin at any time T is formulated as follows

$$Z = \left(\frac{t_T - t_{min}}{t_{min}} \right) \quad (6)$$

where t_{min} is the minimum wall thickness determined using Eq. 3.

While the thickness of the pipe is assumed deterministic (because good quality control is maintained in their manufacture), from Eq. 4, due to randomness in R and A_i , t_T and hence Z is a random variable. The region $Z \leq 0$ represents the failure domain while $Z > 0$ represents safe domain.

Reliability index is related to notional failure probability (P_f) of the structure or structural component by the relation,

$$P_f = \Phi(-\beta) \quad (7)$$

where $\Phi(\cdot)$ is the cumulative distribution function of standard normal variable.

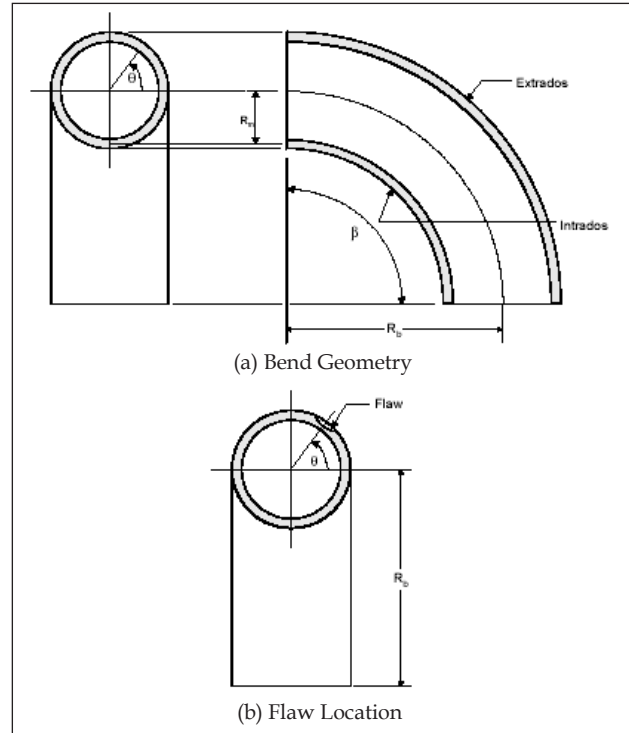


Figure 1: Dimensions of an elbow

The computed failure probability (Eq. 7) is exact when Z follows a normal distribution. For the present problem, the failure probability represents the probability of wall thickness at any time becoming less than the minimum required wall thickness (Eq. 3).

The expected value of the safety margin at any time T is

$$\langle Z \rangle = \left\langle \frac{t_T - t_{min}}{t_{min}} \right\rangle = \left[\frac{(t_0 - t_{min}) - \langle A_i \times R \times T \rangle}{t_{min}} \right] \quad (8)$$

The following equation gives the standard deviation (σ_T) of the safety margin equation at various times during service life.

$$\text{Var}(Z) = \left(\frac{T^2}{t_{min}^2} \right) \times \left(\text{Var}(A_i) \times \langle R \rangle^2 + \text{Var}(R) \times \langle A_i \rangle^2 \right) = \sigma_T^2 \quad (9)$$

where the variances are given by

$$\text{Var}(A_i) = [\text{COV}(A_i) \times \mu(A_i)]^2 \quad (10)$$

$$\text{Var}(R) = [\text{COV}(R) \times \mu(R)]^2 \quad (11)$$

where $\text{COV}(A_i)$ and $\mu(A_i)$ are respectively the coefficient of variation and nominal computed mean value of modeling error A_i whereas $\text{COV}(R)$ and $\mu(R)$

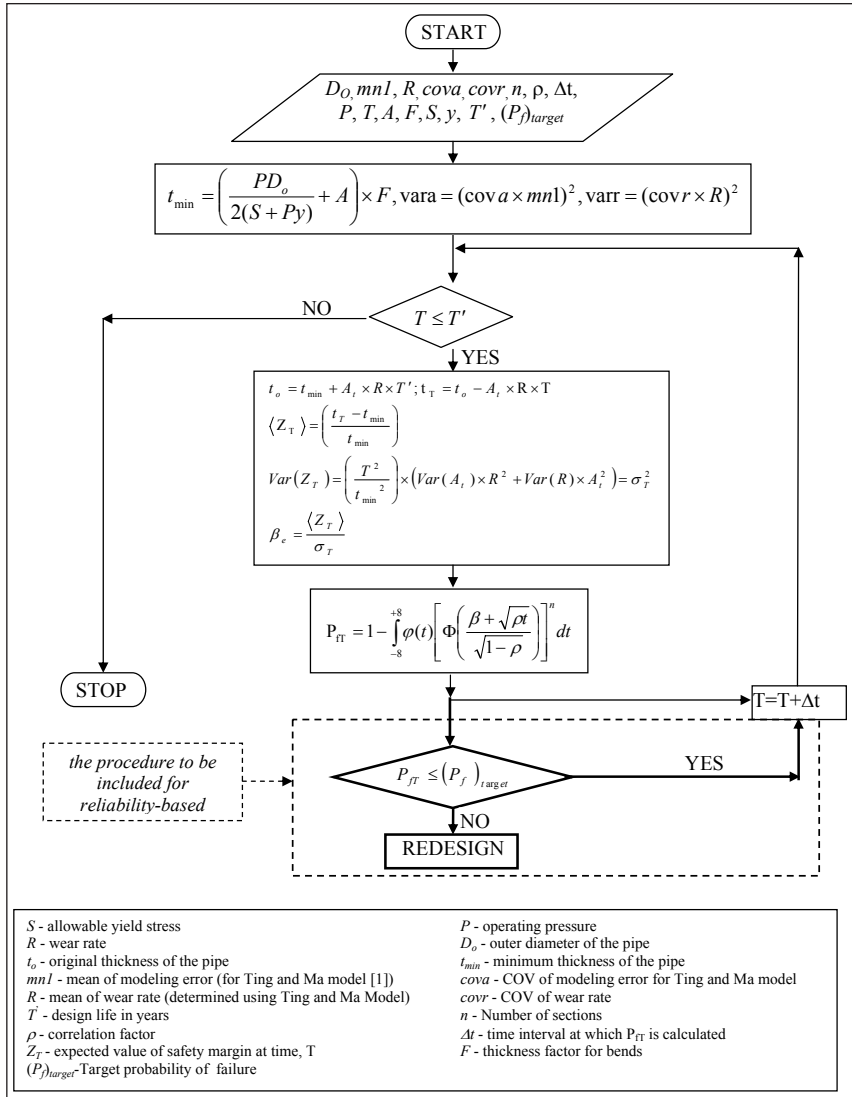


Figure 2: Flow Chart for reliability-based design of piping components

are the coefficient of variation and nominal computed mean value of wear rate R .

The failure probabilities so computed (Eq. 7) give the probability of failure of the piping component at a section at any time T due to EC. However, as noted by Ting and Ma [1], even for a given piping geometry, there are several sections within a component which are vulnerable to undergo wall thinning. This observation can be handled within the reliability framework by developing a series system model, the details of which are presented in the next section.

5.3 Reliability of Series System

The concept of component and system depends on the level of modeling adopted in reliability analysis. There are different methods for determination of system reliability. The available methods for

system reliability analysis can be broadly classified into analytical and simulation methods. The usefulness of system reliability analysis using analytical method is demonstrated in Ref. 15.

In the present paper, FOSM (First Order Second Moment method) is used to find reliability indices at different times. The mean and the standard deviation of the safety margin equation, required for computing reliability, are determined using first order approximation.

As indicated earlier, there are different sections within a given piping component which are vulnerable to undergo erosion-corrosion damage (Tables 6 and 7). This observation is taken into account in the present investigation by considering all the potential locations of EC damage connected in series. If there are ' n ' such locations within a piping segment, the failure of the piping segment occurs when the thickness at any location is $\leq t_{min}$ at any time (weakest link hypothesis).

For a series system having equally correlated elements with normal distributed linear safety margins, the probability of failure for the given system, P_{fs} is given by [16],

$$P_{fs} = 1 - \int_{-\infty}^{+\infty} \varphi(t) \prod_{i=1}^n \left[\Phi \left(\frac{\beta_i + \sqrt{\rho}t}{\sqrt{1-\rho}} \right) \right]^n dt \quad (12)$$

where $\varphi()$ and $\Phi()$ are respectively the density and distribution function of the standard normal variable, ρ is the correlation coefficient between safety margins of elements, and β_i is the reliability index of the i^{th} element determined using Eq. 5.

Assuming further that $\beta_i = \beta_e$ for $i = 1, \dots, n$, the failure probability of the system is given by,

$$P_{fs} = 1 - \int_{-\infty}^{+\infty} \varphi(t) \left[\Phi \left(\frac{\beta_e + \sqrt{\rho}t}{\sqrt{1-\rho}} \right) \right]^n dt \quad (13)$$

Applying these concepts for the nuclear power plant piping component undergoing degradation due to erosion-corrosion, probability of failure at any time T is calculated using the modified equation as

$$P_{fT} = 1 - \int_{-\infty}^{+\infty} \varphi(t) \left[\Phi \left(\frac{\beta + \sqrt{\rho t}}{\sqrt{1 - \rho}} \right) \right]^n dt \quad (14)$$

Numerical integration is carried out with small step size to find the probability of failure for different correlation coefficients ($\rho = 0.0, 0.5$ and 0.95). The flow chart of the computer program developed is given in Figure 2.

6. Validation Study

To validate the proposed reliability model, a 90° elbow reported by Ting and Ma [1] is considered. The details of the elbow are as follows: The outer diameter is 406 mm, original thickness (t_o) of 12.7 mm and a minimum thickness (t_{min}) of 11.09 mm with an estimated life of four years. The wear rate according to Ting and Ma [1] with an operating temperature of 188°C and a flow velocity of 5.28 m/s is 0.399 mm/year.

The thickness of the pipe after 1 year with erosion-corrosion allowance is computed as

$$t_1 = t_o - A_t \times R \times T = 12.7 - 1 \times 0.399 \times 1 = 12.3 \text{ mm}$$

The statistical properties of the random variables R and A_t are assumed as

$$\text{Mean}(R) = 0.399 \text{ mm/year, COV}(R) = 0.2$$

$$\text{Mean}(A_t) = 1.0, \text{COV}(A_t) = 0.25$$

Using first order approximation of Z_{T_1} , the mean and standard variation of Z_{T_1} at the end of one year are determined as,

$$\begin{aligned} \langle Z_1 \rangle &= \left(\frac{t_1 - t_{min}}{t_{min}} \right) = \left[\frac{(t_o - t_{min}) - \langle A_t \times R \times T \rangle}{t_{min}} \right] \\ &= \left[\frac{(12.7 - 11.09) - (1.0 \times 0.399 \times 1)}{11.09} \right] = 0.1091 \end{aligned}$$

The variances of the random variables are

$$\text{Var}(A_t) = (1.0 \times 0.25)^2 = 0.0625$$

$$\text{Var}(R) = (0.399 \times 0.2)^2 = 0.006368$$

$$\begin{aligned} \text{Var}(Z_1) &= \left(\frac{T^2}{t_{min}^2} \right) \times (\text{Var}(A_t) \times \langle R \rangle^2 + \text{Var}(R) \times \langle A_t \rangle^2) = \sigma_1^2 \\ &= \left(\frac{1^2}{11.09^2} \right) \times (0.0625 \times 0.399^2 + 0.006368 \times 1.0^2) = 1.326 \times 10^{-4} \\ \sigma_1 &= \sqrt{1.326 \times 10^{-4}} = 1.15 \times 10^{-2} \end{aligned}$$

The reliability index,

$$\beta_1 = \frac{\langle Z_1 \rangle}{\sigma_1} = \frac{0.1091}{1.15 \times 10^{-2}} = 9.487$$

Since there are 9 sections connected in series, the system (elbow) failure probability is given by

$$P_f = P \left[\bigcup_{i=1}^9 Z_i \leq 0.0 \right].$$

The reliabilities and the failure probabilities for the piping component are numerically computed at the end of each year for four years and the results are shown in Figure 3.

It is observed from Figure 3 that the failure probability of the piping component undergoing EC damage, though increases with time decreases with an increase in the value of correlation coefficient between safety margins of elements. The values of predicted failure probabilities are realistic, since at the end of about four years the piping component seems to have been replaced according to Table 2.2 (replacement records of the pipe components during each outage) of Ting and Ma [1]. Also, from Figure 3, it is noted that a conservative value of failure probability can be obtained using $\rho=0.0$. The correlation of resistance/safety margin among the various sections, where possible erosion-corrosion may take place, should be considered in the reliability analysis. This is justified in view of two reasons: (i) in-service inspection data on elbows have clearly shown that there are different sections which have potential to undergo erosion-corrosion (Tables 6 and 7), and (ii) the phenomenon of erosion-corrosion is complex and the occurrence of an event at one section may affect the vulnerability of other sections in a given component. These reasons along with the fact that the system is in series suggests that a positive correlation coefficient between safety margins needs to be considered in safety assessment of piping components.

The usefulness of the proposed method in integrating the deterministic ASME design approach with failure probability assessment is demonstrated below through examples.

7 Illustrative examples

Example 1

A typical 90° elbow of a feedwater heater extraction piping component of outer diameter 406 mm is considered. The details of the piping component are as follows. Operating pressure (P) = 6.35 MPa [17], Allowable stress (S) 117.8 MPa for high carbon steel

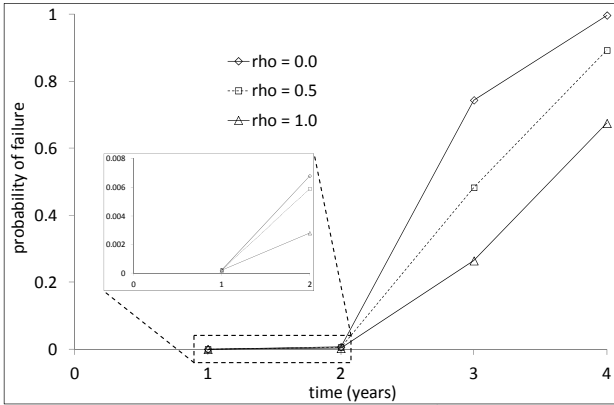


Figure 4: Variation of probability of failure with time for 90 elbow considered in validation study

[18], Assumed service life =15 years. The wear rate according to the predicted equations (Table 8) for an operating temperature of 188°C and a flow velocity of 5.28 m/s is 0.59 mm/year.

From ASME Boiler and Pressure Vessel code [13] (see Appendix I), the minimum thickness (t_{min}) is,

$$t_{min} = \left(\frac{PD_o}{2(S + Py)} + A \right) \times F$$

$$t_{min} = \left(\frac{6.35 \times 406}{2(117.8 + 6.35 \times 0.4)} + \left(\frac{t_{min} + 5}{4} \right) + 0.3968 \right) \times 1.06$$

$$= 17.9 \text{ mm}$$

$$= 17.9 \text{ mm}$$

Here 1.06 is the factor for thickness for an assumed radius of bend of 6D (Table 11). Assuming the service life of the pipe (T) to be 15 years, the design thickness of the pipe (t_o) with erosion-corrosion allowance,

$$t_o = 17.9 + 15 \times 0.59 = 26.8 \text{ mm}$$

The reliabilities and the failure probabilities for the piping component are numerically computed at the end of every year for 15 years with different correlation coefficients. The results are plotted in Figure 4. Though the computed failure probabilities seem to be on the higher side, the actual performance of these components has shown that these values are realistic (viz. [19]).

It is observed from the Figure 4 that failure probability decreases with an increase in correlation coefficient as noted earlier. Thus, for probability of failure assessments of the pipe at the design stage, it is safe to assume a value of $\rho = 0.0$.

Example 2

A 90° elbow of a primary heat transport system piping component of inner diameter 400 mm with a design thickness of 34.5 mm is considered. The details of the pipe are: operating pressure (P) = 11.25 MPa [8], allowable stress (S) = 117.5 MPa [18] for high carbon steel (SA 333 Grade 6), assumed life = 15 years [20]. The wear rate according to the predicted equation with a temperature of 230°C and a flow velocity of 2.718 m/s is 0.077 mm/year. The statistical properties are the same as in the previous example.

The minimum thickness of the pipe as per ASME formula with suitable groove depth and mechanical allowance is 33.25 mm. The mean and standard deviation of Z_T are calculated and the reliability indices are obtained as in the previous example. The reliabilities and failure probabilities for the pipe are computed at the end of every year for a life of 15 years and are plotted (Figure 5) for different correlation coefficients.

As noted in the previous example, probability of failure decreases with increase in value of the correlation coefficient. The results of this example also reinforce the fact that system reliability concepts can be used in the probabilistic failure assessment of piping components. Based on these observations and the validation study reported, an attempt is made in the next section to propose a procedure for reliability-based design of piping component.

8. Reliability-Based Design of Piping Components subjected to Erosion-Corrosion

The failure probability assessment procedure proposed in this paper can be used in reliability-based design of piping components subjected to erosion-corrosion to meet the needs of specified target probability of failure at specified age. A detailed code calibration could result in partial safety factors that can be used in the design to arrive at uniform implied reliability at component level. However, if the interest centers around the exact determination of reliability of a piping component at different times, reliability analysis has to be carried out taking into account the actual variation in operating conditions and the member has to be proportioned in such a way that the target reliability is achieved at different times. The flowchart that can be used for such a design is shown in Figure 2.

Table 1 Degradation mechanism with its attributes and the susceptible regions [1]

Mechanism	Attributes	Susceptible regions
Erosion-Corrosion	Turbulent Flow at Sharp Radius Elbows and Tees Proximity to Pumps, Valves and Orifices Material: Chromium content Fluid pH Oxygen Temperature	Evaluated in accordance with plant conditions

Table 2 Cases of piping failures due to erosion-corrosion [17]

Sl. No	Details of the plant	Reason
1.	Name: Trojan Nuclear Plant, Aug 4,1987 Component, Material: Feedwater Lines in secondary piping inside containment, A-106 Gr. B Details: Temperature-235°C, Pressure-920 psi (6.35 MPa), Outer Diameter-14 inch (356 mm), Nominal Wall Thickness-0.593 inch (15 mm), Minimum Wall Thickness-0.510 inch (12.9 mm), Oxygen content-4 ppb, pH-9.0, Flow velocity-22.6 feet/s (6.8 m/s). Nature of Failure: Thinning of Class 2 feedwater lines	Less than optimum values for material, oxygen, pH and flow velocity. Temperatures promoting high unsteady wear rate. Single phase erosion-corrosion thinning.
2.	Name: Virginia Surry Nuclear Plant, Dec 9, 1986 Component, Material: 90° elbow Feedwater Condensate Line, Plain carbon steel piping Details: Length 18 inch (457 mm) Nature of Failure: Blowing up of a section of the pipe by about two or three feet resulting in complete separation.	Thinning to below one-tenth of an inch due to single-phase erosion-corrosion, use of pickled piping

Table 3 Degradation Mechanism Category [8]

Large Pipe Break Potential	Conditions	Degradation Category	Degradation Mechanism
High	Degradation mechanism likely to cause a large break (>50 GPM)	Large Break	Erosion-Corrosion
Medium	Degradation mechanism likely to cause a small break	Small break	Thermal Fatigue, Erosion-Cavitation, Corrosion, Stress Corrosion Cracking
Small	No degradation mechanism present	None	n/a

Table 4 Comparison of predicted wear rates and the useful life

Approach	Wear rate (mm/year)	Predicted Life (years)
Stack [3]	0.41	7.2
Ting [1]	0.59	5.1

Note: Flow parameters: Flow velocity - 5.28 m/s, pH - 9.0, Temperature - 370°F Pipe parameters: Nominal thickness of pipe - 25 mm, Minimum measured thickness - 22 mm, Outer diameter - 406 mm

Table 5 The susceptible piping components with locations of maximum thinning [1]

Susceptible piping component	Location of maximum thinning of pipe
90° elbow	Outward bend of elbow
45° elbow	Outward bend of elbow
Reducer	At the two ends
Tee	Uniform
Straight pipe	Inlet position

Table 6 Sections on a 90° elbow with their vulnerabilities to erosion-corrosion [1]

Section	Weightage [1]
B1	0.61
B2	0.55
B3	0.58
B4	0.91
B5	1.00
B6	0.73
B7	0.67
B8	0.55
B9	0.73

Table 7 Sections on a 45° elbow with their vulnerabilities to erosion-corrosion [1]

Section	Weightage [1]
B1	0.76
B2	0.73
B3	1.00
B4	0.91
B5	0.47

Table 8 Wear rate prediction regression equations for Ting and Ma model [1]

Temperature (°F)	Wear rate equation, $y = f(x)$ (wear rate in mm/100000 hours; R - coefficient of determination)
180	$y = 0.0279x^2 - 0.0058x + 0.1842$ ($R^2 = 0.9946$)
240	$y = 0.0945x^2 + 0.2518x + 0.3361$ ($R^2 = 0.9988$)
270	$y = 0.1934x^2 + 0.1943x + 0.7214$ ($R^2 = 0.9994$)
300	$y = 0.2525x^2 + 0.1793x + 0.9349$ ($R^2 = 0.9996$)
330	$y = 0.2483x^2 + 0.1663x + 0.9478$ ($R^2 = 0.9995$)
360	$y = 0.1882x^2 + 0.1269x + 0.8100$ ($R^2 = 0.9992$)
420	$y = 0.0327x^2 + 0.0960x + 0.3513$ ($R^2 = 0.9994$)

(Notes: 1. x is velocity of heavy water in the nuclear power plant pipe in m/s; 2. Conversion from Degree Fahrenheit (°F) to Degree Celsius (°C) $C = \frac{5}{9}(F - 32)$)

Table 9 Wear rate at low and high temperatures for Ting and Ma model [1]

Temperature (°F)	Wear rate (in mm/100000 hours)
90	$y = 0.02$
120	$y = 0.02$
510	$y = 0.05$
540	$y = 0.02$
570	$y = 0.01$

(Notes: Conversion from Degree Fahrenheit (°F) to Degree Celsius (°C) $C = \frac{5}{9}(F - 32)$)

Table 10 Threading and grooving allowance [18]

Type of pipe	A (inches)
Threaded steels and nonferrous pipe:	
¼ inch nominal and smaller	0.065
1 inch nominal and larger	Depth of thread
Grooved steel and nonferrous pipe:	Depth of groove +1/64 inches

Table 11 Minimum thickness for bending [18]

Radius of Bends	Minimum Thickness Recommended Prior to Bending
6 pipe diameters or greater	$1.06 t_{min}$
5 pipe diameters	$1.08 t_{min}$
4 pipe diameters	$1.16 t_{min}$
3 pipe diameters	$1.25 t_{min}$

Note: t_{min} - Minimum thickness determined for straight pipes

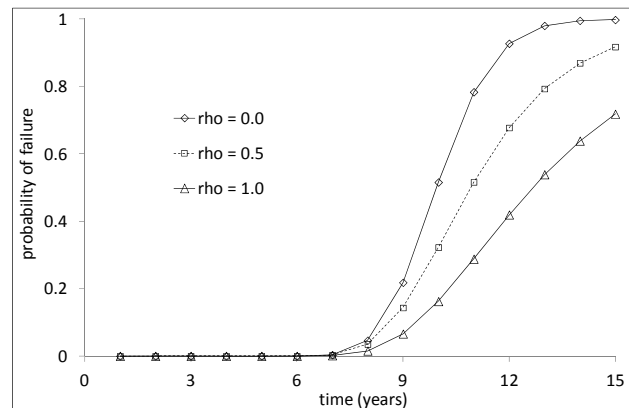


Figure 4: Variation of probability of failure with time for the piping component considered in Example 1

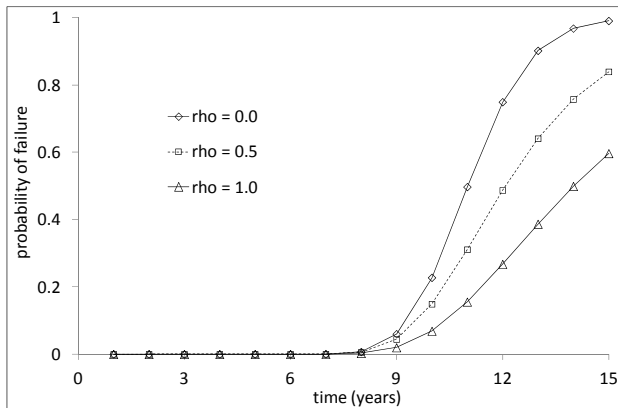


Figure 5: Variation of probability of failure with time for a typical Primary Heat Transport System piping component considered in Example 2

9. Summary and Conclusions

From comparative studies presented, it is found that Ting and Ma [1] model is useful in predicting the deterministic EC rate. In this study, the wear rate equations in the unsteady region were proposed based on the regression analysis of the results presented by Ting and Ma [1]. The best fitting curve plotted from the data given [1] was found to predict the wear rate satisfactorily in the range of temperatures considered.

The validation of the proposed probabilistic failure assessment procedure of nuclear power plant piping components was done by determining the probability of failure of a piping component and then comparing with the predicted deterministic failure time by Ting and Ma [1]. The results indicate that the proposed methodology of determining failure probability is scientific and rational and series system modeling is to be used in the failure assessment of a piping component subjected to EC degradation. The usefulness of the proposed probability of failure assessment methodology in the reliability-based design of piping component is also indicated (Figure 2).

From studies reported in this paper, the following conclusions are drawn.

1. The results of the failure probability assessment procedure presented can be used to develop inspection and maintenance schedule at the design stage itself. The methodology also integrates the probabilistic theory with the deterministic design procedures to make engineering design decisions more rational.
2. The flowchart presented in Figure 2 can be used in the reliability-based design of piping components.

For the purpose of design of pipelines to be on the conservative side, a value of $\rho=0.0$ can be used.

In the probabilistic failure assessment, the various elements connected in series in a given elbow system are assumed to have equal reliabilities. However, a more realistic modeling would involve weighing the element reliabilities with their respective vulnerabilities to undergo EC.

Acknowledgements

The paper is being published with the kind permission of Director, CSIR-Structural Engineering Research Centre, Chennai. K. Balaji Rao and M.B. Anoop are thankful to Dr T.V.S.R. Appa Rao and Dr N. Lakshmanan, Former Directors, CSIR-SERC, Chennai, for their support and guidance. The authors are thankful to Board of Research in Nuclear Sciences for partially funding the work (Sanction no. 2000/36/13/BRNS).

References

1. Ting, K. and Ma, Y. P., "The evaluation of erosion/corrosion problems of carbon steel piping in Taiwan PWR nuclear power plants", Nuclear Engineering and Design, 191(2), 1999, pp. 231-243.
2. Wu, P.C., "Erosion/Corrosion-Induced Pipe Wall Thinning in U.S. Nuclear Power Plants", NUREG-1344, April 1989.
3. Stack, M., Corlett, N. and Turgoose, S., "Some recent advances in the development of theoretical approaches for the construction of erosion-corrosion maps", Wear, 233-235, 1999, pp. 535-541.
4. Stack, M., Corlett, N. and Zhou, S., "Impact angle effects on the transition boundaries of the aqueous erosion-corrosion map", Wear, 225-229, 1999, pp.190-198.
5. Stack, M., Corlett, N. and Zhou, S., "Some thoughts on the effect of elastic rebounds on the boundaries of erosion-corrosion map", Wear, 214, 1998, pp. 175-185.
6. Stack, M., Corlett, N. and Zhou, S., "A methodology for the construction of the erosion-corrosion map in aqueous environments", Wear, 203-204, 1997, pp. 474-488.
7. Abdulsalam, M. and Stanley, J., "Steady-state model for erosion-corrosion of feedwater piping", Corrosion, 48 (7), 1992, pp. 587-593.
8. Balaji Rao, K., Anoop, M. B., Jiboy Jose, Lakshmanan, N., Mishra, A., Gopika Vinod, Babar, A. K. and Kushwaha, H. S., "A Report on the Evaluation of Erosion/Corrosion Problems in Carbon Steel Piping of Pressurized Heavy Water Reactor (PWR) Nuclear Power Plants", SERC, Chennai, 2003.
9. Berge, J. P., "Effect of chemistry on corrosion-erosion of steels in water and wet steam", Proceeding of 2nd Conference on Water Chemistry, BNES, 1980.
10. Bridgeman, J. and Shankar, R., "Erosion/corrosion data handling for reliable NDE", Nuclear Engineering and Design, 131, 1991, pp. 285-297.
11. Pandey, M., "Probabilistic models for condition assessment of oil and gas pipelines", NDT&E International, 31(5), 1998, pp. 349-358.

12. Balaji Rao, K., Anoop, M. B., Priya, C., Lakshmanan, N., Gopika Vinod, Saraf, R.K. and Kushwaha, H. S., "A Report on Finite Element Based Reliability Analysis of Pipe Works in Nuclear Power Plants", GAP 01241, July 2003.
13. ASME Boiler and Pressure Vessel Code Section III-Division 1 Subsection NC Class 2 components Rules for Construction of Nuclear Power Plant Components, The American Society for Mechanical Engineers, New York 1998.
14. Christensen, P.T. and Baker, M. J., "Structural Reliability theory and its Applications", Springer-Verlag, 1982.
15. Ang, A.H-S. and Tang, W. H., "Probability Concepts in Engineering Planning and Design", Vol II, Decision Risk and Reliability, John Wiley and Sons, 1984.
16. Grigoriu, M. and Turkstra, C., "Safety of structural systems with correlated resistances", Applied Mathematical Modelling, Vol. 3, No. 2, 1979, pp. 130-136.
17. Bush, S., "The effects of erosion-corrosion on power plant piping", Proceedings of National Board Classic Series 59th general meeting. Tennessee: National Board Classic Series, 1990.
18. ASME Boiler and Pressure Vessel Code Section II Part D Properties, New York: The American Society of Mechanical Engineers, 1998.
19. Moolayil, T.M., "Mitigation of degradation of high energy secondary cycle piping due to flow assisted corrosion (FAC) and life management of high energy piping in Indian nuclear power plants", Proceedings of Second International Symposium on Nuclear Power Plant Life management, IAEA-CN-155-050, 2007 (CD-ROM).
20. Takoma, M., "Japan's policy on NPP life management", IAEA Scientific Forum, 2002.

APPENDIX I:

Pressure Design of Piping Products: ASME Boiler and Pressure Vessel Code [13]

Straight Pipe under Internal Pressure

The equations for determining the preliminary pipe wall thickness as per ASME are as follows.

$$t_m = \frac{PD_o}{2(S + Py)} + A \quad (A-1)$$

where

t_m = minimum required wall thickness, inches,

P = internal Design Pressure, psi

D_o = outside diameter of pipe, inches.

S = maximum allowable stress for the material at the Design temperature, psi (Section II, Part D, Subpart 1, Tables 1 A and 1 B)

A = additional thickness provided, inches.

(a) to compensate for material removed or wall thinning due to threading or grooving, required to make a mechanical joint. The values of A listed in Table 11 are minimum values of material removed in threading.

(b) to provide for corrosion or erosion. Since corrosion and erosion vary widely from installation to installation, it is the responsibility of designers to determine the proper amounts which must be added to either or both of these conditions.

y = a coefficient having a value of 0.4, except that, for pipe with a D_o / t_m ratio less than 6, the value of y shall be taken as $y = \frac{d}{d + D_o}$, where d is the inner diameter of the pipe.

The thickness of pipes at bends should be multiplied by an appropriate factor depending on the radius of bend (Table 11).



SRESA JOURNAL SUBSCRIPTION FORM

Subscriber Information (Individual)

Title

First Name

Middle Name

Last Name

Street Address Line 1

Street Address line 2

City

State/Province

Postal Code

Country

Work Phone

Home Phone

E-mail address

Subscriber Information (Institution)

Name of Institution/ Library

Name and Designation of Authority for Correspondence

Address of the Institution/Library

Subscription Rates

	Subscription Quantity	Rate	Total
Annual Subscription (in India)	_____	Rs. 15,000	_____
(Abroad)	_____	\$ 500	_____
	_____		_____
	_____		_____

Payment mode (please mark)

Cheque Credit Card Master Card Visa Online Banking Cash De mand Draft

Credit card Number

Credit Card Holders Name

Credit Card Holde

Guidelines for Preparing the Manuscript

A softcopy of the complete manuscript should be sent to the Chief-Editors by email at the address: editor@sresa.org.in. The manuscript should be prepared using 'Times New Roman' 12 font size in double spacing, on an A-4 size paper. The illustrations and tables should not be embedded in the text. Only the location of the illustrations and tables should be indicated in the text by giving the illustration / table number and caption.

The broad structure of the paper should be as follows: a) Title of the paper – preferably crisp and such that it can be accommodated in one or maximum two lines with font size of 14 b) Name and affiliation of the author(s), an abstract of the paper in ~ 100 words giving brief overview of the paper and d) Five key words which indicates broad subject category of the paper. The second page of the paper should start with the title followed by the Introduction

A complete postal address should be given for all the authors along with their email addresses. By default the first author will be assumed to be the corresponding author. However, if the first author is not the corresponding author it will be indicated specifically by putting a star superscript at the end of surname of the author.

The authors should note that the final manuscript will be having double column formatting, hence, the size of the illustration, mathematical equations and figures should be prepared accordingly.

All the figures and tables should be supplied in separate files along with the manuscript giving the figure / table captions. The figure and table should be legible and should have minimum formatting. The text used in the figures and tables should be such that after 30% reduction also it should be legible and should not reduced to less than font 9.

Last section of the paper should be on list of references. The reference should be quoted in the text using square bracket like '[1]' in a chronological order. The reference style should be as follow:

1. Pecht M., Das D, and Varde P.V., "Physics-of-Failure Method for Reliability Prediction of Electronic Components", Reliability Engineering and System Safety, Vol 35, No. 2, pp. 232- 234, 2011.

After submitting the manuscript, it is expected that reviews will take about three months; hence, no communication is necessary to check the status of the manuscript during this period. Once, the review work is completed, comments, will be communicated to the author.

After receipt of the revised manuscript the author will be communicated of the final decision regarding final acceptance. For the accepted manuscript the author will be required to fill the copy right form. The copy right form and other support documents can be down loaded from the SRESA website: <http://www.sresa.org.in>

Authors interested in submitting the manuscript for publication in the journal may send their manuscripts to the following address:

Society for Reliability and Safety
RN 68, Dhruva Complex
Bhabha Atomic Research Centre,
Mumbai - 400 085 (India)
e-mail : editor@sresa.org.in

The Journal is published on quarterly basis, i.e. Four Issues per annum. Annual Institutional Subscription Rate for SAARC countries is Indian Rupees Ten Thousand (Rs. 10,000/-) inclusive of all taxes. Price includes postage and insurance and subject to change without notice. For All other countries the annual subscription rate is US dollar 500 (\$500). This includes all taxes, insurance and postage.

Subscription Request can be sent to SRESA Secretariat (please visit the SRESA website for details)

SRESA's International Journal of
**Life Cycle Reliability
and Safety Engineering**

Contents

Vol.3

Issue No.1

Jan-March 2014

ISSN - 2250 0820

- Optimal Design of Monitoring Systems for Life Cycle Benefits:
Application to an Offshore Wind Turbine Support Structure
Sebastian Thöns, Michael Haubro Faber, Werner Rücker (Denmark)..... 1
- Massive Shear Wall Testing for Nuclear Industry
Adrian Bekö, Helmut Wenzel, Peter Rosko (Austria) 11
- Ageing Behaviour of Structural Components for Integrated Lifetime
Assessment and Asset Management
Robert Veit-Egerer, Helmut Wenzel, Rui Lima (Austria) 22
- An Approach for Reliability Based Control of Post-Tensioned
Containment Structure
Alexander ILIEV, Marin KOSTOV, Anton ANDONOV (Bulgaria) 29
- Time Dependent PSA of Nuclear Power Plants Under Seismic Events
*M. Hari Prasad, P. N. Dubey, Gopika Vinod, G. R. Reddy and
R.K. Singh (India)..... 40*
- Probabilistic Failure Assessment of PWR Nuclear Power Plant Piping
Components against Erosion-Corrosion
Jiboy Jose, K. Balaji Rao, M. B. Anoop, Gopika Vinod, H. S. Kushwaha (India) 47
-